2023

The dynamic relationship between permafrost and landcover in northwestern Canada's discontinuous permafrost zone

Olivia Carpino
carp6500@mylaurier.ca

The dynamic relationship between permafrost and landcover in northwestern Canada's discontinuous permafrost zone

by:

Olivia Alexandra Carpino

M.Sc. Geography, University of Guelph, 2017

B.Sc. Honours Environmental Geoscience and Geomatics, University of Guelph, 2015

DISSERTATION

Submitted to the Department of Geography and Environmental Studies

in partial fulfillment of the requirements for

Doctor of Philosophy in Geography

Wilfrid Laurier University

Declaration of Co-Authorship/Previous Publication

I declare that I am the principal author of this thesis and the research is the product of my own work. Any co-authors listed were collaborators for the chapters in which they were involved. Chapters 2, 3, and 4 represent the main body of the thesis. Chapter 2 is comprised of work that has been published in Hydrology and Earth Systems Sciences. Chapter 3 and Chapter 4 have not yet been submitted for publication.

Abstract

Northwestern Canada's subarctic is among the most impacted regions in the world as it is experiencing rapid climatic and environmental change. As a result, northwestern Canada has been experiencing region-wide permafrost thaw and disappearance, both of which are also occurring at unprecedented rates. Permafrost temperatures in the Taiga Plains have been warming steadily over the last several decades, which has been particularly detrimental across its lower latitudes of the discontinuous permafrost zone where the permafrost is already relatively thin and warm. These factors indicate that permafrost in the southern Taiga Plains may be in a state of disequilibrium with the current climate.

Permafrost degradation has important implications for wide-ranging boreal peatland landscapes and the associated local hydrology and ecology. Decreases in the area underlain by permafrost in these peatland complexes has resulted in a transformation from permafrost and forest-dominated landscapes to those that are wetland dominated. However, permafrost-free forested areas have also been observed following the loss of permafrost and the gradual drying and succession of the previously treeless bog landscape. This research first seeks to explore the trajectory of peatland landcover change following permafrost thaw by identifying unique landcovers that represent different thaw stages. Next, this research works to monitor peatland-dominated environments across the southernmost portion of the Taiga Plains by using near-annual imagery to quantify landcover changes that may be representative of permafrost thaw. Finally, this research aims to encapsulate the factors that contribute to permafrost presence or absence by proposing a permafrost index map across the southern Taiga Plains.

Keywords: permafrost thaw, landscape transition, climate change, boreal forest, wetland, Taiga Plains, discontinuous permafrost, peatland

Acknowledgements

First and foremost, I would like to thank my advisor Dr. William Quinton for his guidance and insight throughout this research. I am incredibly grateful for his enthusiasm, flexibility, and willingness to share his expertise and answer questions over the course of this program. I would also like to thank my committee members Dr. James Craig, Dr. Steve Kokelj, and Dr. Laura Chasmer for their assistance and support during this research.

I would like to thank Dr. Kristine Haynes for her encouragement and reassurance during her time at Laurier. I am incredibly thankful to have worked with her and her help was truly invaluable. I would also like to thank Dr. Ryan Connon and Dr. Stephanie Wright for sharing their insights and wealth of knowledge while developing this dissertation. I would similarly like to thank the other members of the Scotty Creek Research Station team for all their help over the years, particularly Brenden Disher and Mason Dominico. Finally, I would like to thank my wonderful family and friends for their endless support.

Statement of Originality

I declare that this dissertation is an original document and the result of my own research, methodologies, and findings, except as acknowledged or appropriately cited. This work has not been submitted, in part, or in whole, for a degree at Wilfrid Laurier University or any other university.

Table of Contents

List of Tables

List of Figures

CHAPTER 1: General Introduction

1.1 Introduction & Background

Up to 80% of the world's boreal forests are located in environments underlain by permafrost (Helbig, Pappas, et al., 2016; Olefeldt et al., 2016). Permafrost temperatures have risen by over 4ºC since the Little Ice Age (*i.e.* the cold period spanning approximately the 16th-19th centuries) (Jorgenson & Osterkamp, 2005) and permafrost thaw has been exacerbated by further anthropogenic climate change, forest fire, and industrial development (Camill, 2000; Gibson et al., 2018). Permafrost is an important component of many northern environments, which not only characteristically supports the ground surface, but also influences vegetation distribution, soil properties, and hydrology (Pellerin & Lavoie, 2000; Shur & Jorgenson, 2007). Generally, any ice-rich terrain (*i.e.* when ice exceeds the pore space of soil) can be vulnerable to drastic permafrost-thaw induced changes where the amount of change is directly related to the amount and type of ice that is found in the ground (Jorgenson & Osterkamp, 2005). Beyond that general principle, permafrost-thaw induced change is also related to factors such as slope, aspect, soil texture, vegetation, and hydrology (Shur & Jorgenson, 2007). These properties make studying permafrost environments challenging but also highlight that the mode of permafrost degradation and the associated visible changes on the landscape can be attributed back to such factors.

Peatlands with discontinuous permafrost are of particular note as they make up a large portion of the southern Taiga Plains and as such are the focus of many research studies. While permafrost presence is obviously determined by climate, peat is a dominant control allowing permafrost to exist in areas with mean annual air temperatures warmer than 1ºC (Smith et al., 2005; Smith & Riseborough, 2010). Contrastingly, permafrost is typically unable to persist in mineral soils with temperatures above –2ºC (Camill, 2000, 2005). Plateau-wetland complexes

contain permafrost plateaus, also referred to as peat plateaus, which are essentially forested mounds that remain perennially frozen. They are distinguishable from the surrounding environment as they typically rise one to two metres above the water table and thus, the surrounding collapse scar and fen wetland features as well (Quinton et al., 2003; Robinson & Moore, 2000).

During summer months, dry peat insulates permafrost from ground heating due to a low thermal conductivity. However, during winter months, peat that was formerly dry becomes saturated and icy with a higher associated thermal conductivity that promotes ground cooling (Camill, 1999; Quinton & Baltzer, 2013; Woo, 2012). Permafrost in discontinuous permafrost peatlands is therefore largely restricted to peat plateaus as only these features contain enough unsaturated peat to insulate and thereby maintain permafrost (Hayashi et al., 2004; Quinton et al., 2009; Zoltai & Tarnocai, 1975). The insulating properties and low thermal conductivity of peat along with the vegetation canopy minimizes surface warming allowing frost bulbs to develop and permafrost to propagate (Beilman et al., 2001; Beilman & Robinson, 2003; Robinson & Moore, 2000). Additionally, permafrost presence supports certain ecosystem features including the presence of black spruce (*Picea mariana*) on plateaus (Baltzer et al., 2014; Haynes et al., 2020; Iwata et al., 2012; Lieffers & Rothwell, 1987).

Despite the advantageous thermal properties of dry peat, permafrost areal coverage has significantly decreased across the region due to increasing temperatures (Robinson & Moore, 2000; Wright et al., 2009). One example of pronounced permafrost thaw in the Taiga Plains is across its lower latitudes, where the permafrost is relatively thin and warm, often already at or near the thaw point temperature (Biskaborn et al., 2019). Increasing thaw leads to the collapse of peat plateaus and formation of collapse scar wetlands, which can range from small, defined depressions within a plateau, to spanning hundreds of metres and even connecting with other

wetland features, including fens (Quinton et al., 2009). This permafrost degradation also impacts the ability for *P. mariana* to persist due to waterlogging and plateau inundation (Quinton et al., 2011). Consequently, this has resulted in a shift towards more wetland-dominated landscapes as the areal coverage of both collapse scars and fens increase, which are not only permafrost-free features but are also largely tree-free (Quinton et al., 2011; Robinson & Moore, 2000; Thie, 1974; Zoltai, 1993; Zoltai & Tarnocai, 1975). Permafrost thaw-induced changes to peatlands are an increasingly apparent consequence of climate change in the discontinuous permafrost zone, and because of the direct connection between permafrost and landcover, remotely sensed landcover change observations can be used to monitor underlying permafrost thaw.

Previously, peatlands had evolved and undergone landscape transition through a series of long-term periods of permafrost aggradation and degradation (Tarnocai, 2009; Turetsky et al., 2007). This cyclical permafrost development and thaw has been described as a process where permafrost evolves from small, perennial ice bulbs that form below *Sphagnum* hummocks in permafrost-free wetlands (Zoltai, 1993). Overtime these small, isolated frozen hummocks expand and merge into plateaus, which with time, foster *P. mariana*. However, when the *P. mariana* canopy experiences a disturbance, a collapse scar forms, initiating the transition to a permafrost-free wetland again (Zoltai, 1993). In a stable climate, the transition between permafrost and permafrost-free landcovers is ongoing but the proportions of each remain relatively consistent on the scale of hundreds (Zoltai, 1993) to even thousands of years (Treat & Jones, 2018). However, warming-induced permafrost thaw appears to have halted the cycle, disrupting the balance between permafrost aggradation and degradation (Beilman et al., 2001; Jorgenson et al., 2010; Schuur & Abbott, 2011). Today, permafrost degradation is favoured and the timescales previously described do not appear to account for the current rates and patterns of thaw-induced landscape evolution.

Present permafrost thaw and degradation can be attributed to a combination of processes that can be generalized regardless of the feature or landscape. Most clearly, rapid increases in temperature can lead to accelerated permafrost thaw (Camill & Clark, 1998; Tarnocai, 2009). Warming temperatures are particularly detrimental for permafrost as ground temperatures are already as much as 4ºC warmer than air temperatures (Osterkamp, 2003). Furthermore, permafrost temperatures throughout much of the discontinuous permafrost zone are already rapidly approaching 0ºC, meaning permafrost is vulnerable to irreversible thaw (Biskaborn et al., 2019; Osterkamp & Romanovsky, 1999). Both unusually warm summers and deep, insulating snowpacks during cold winter months can be responsible for warming and thawing permafrost (Camill, 2000; Jorgenson & Osterkamp, 2005).

In addition to warming temperatures that can affect permafrost on very large scales, more local conditions can also come into play. For example, soil texture and ice content are important factors controlling the impacts of permafrost thaw. Fine-grained textures, such as silts, typically have high ice contents that are exhibited in a wide range of ice structures including segregated forms of ice (Jorgenson & Osterkamp, 2005). In contrast, very coarse soils and gravels typically have very low ice content in the form of pore ice or crustal ice (Jorgenson & Osterkamp, 2005). Gravelly soil deposits typically have a maximum ice content of 40% compared to the segregated ice forms found in finer soil deposits, where ice contents can be as high as 80%, though this is more common in more northern permafrost regions (Shur & Jorgenson, 2007). Degradation of these varying soil textures and ice structures is very closely related to the different permafrost environments and landforms that result from permafrost thaw. While permafrost degradation in all areas can result in changes to the environment, lowland and peatland areas are particularly susceptible to some of the most dramatic modes of permafrost degradation in the southern Taiga

Plains, including collapse-scar wetlands in plateau-wetland complexes (Jorgenson & Osterkamp, 2005).

Insolation also leads to greater permafrost degradation on south-facing slopes, which not only applies to mountain and hill environments but also to lowland permafrost landforms including plateaus (Shur & Jorgenson, 2007). Additionally, when a disturbance (*e.g.* fire, disease, insect, etc.) removes or thins vegetation cover, these changes can increase insolation at the ground surface, which leads to thaw depressions (Wright et al., 2009). Such areas of preferential thaw therefore develop elevated soil moisture contents, and since soil thermal conductivity increases with its moisture content, the preferential thaw process is reinforced (Quinton et al., 2019). Any impounded water at the surface increases the heat flux, furthering a positive feedback that accelerates permafrost degradation (Chasmer & Hopkinson, 2017; Devoie et al., 2019). The lateral flow of water, at both the surface and subsurface, can also drastically increase thaw in neighbouring permafrost landforms (Devoie et al., 2019; Walvoord & Kurylyk, 2016). Additionally, surface water decreases the albedo of the landscape (Helbig, Wischnewski, et al., 2016).

Even localized decreases to tree canopy density can increase insolation to the ground at that small area, which in turn leads to preferential ground thaw (Wright et al., 2009). These areas of preferential thaw appear as thaw depressions, which cause water to flow towards and collect in these areas, increasing soil moisture. As soil thermal conductivity increases with increasing moisture, a positive feedback is initiated and the preferential permafrost thaw is reinforced (Quinton et al., 2019; Wright et al., 2009). These areas of preferential thaw can lead to the formation of taliks and, with time, collapse scars, when thaw extends below to the base of the active layer (Chasmer & Hopkinson, 2017; Connon et al., 2018). As permafrost thaw and talik development continues, the previously isolated collapse scars expand and become interconnected

with surrounding wetlands (Connon et al., 2015; Devoie et al., 2019). By this time, the permafrost barriers are largely absent (Haynes et al., 2018) and runoff is maximized due to the areal expansion of runoff contributing area and greater hydrological connectivity (Connon et al., 2014, 2015). Decreases in wetness over time are well-attributed to increases in connectivity. As wetland continue to drain and dry, *Sphagnum* hummocks begin to form in permafrost-free wetlands (Zoltai, 1993). Over time, individual hummocks grow vertically due to the vertical growth pattern of the hummock-forming *Sphagnum* species (Zoltai, 1993). Hummocks also begin to expand horizontally, a process accelerated by the coalescing of individual hummocks to form larger, compound hummocks, which become sufficiently large and well-drained to support individual trees (*P. mariana*) (Camill, 1999). The growth process culminates in a tree-covered wetland, with hydrological and ecological features that are in many ways intermediary to that of collapse scars and forested peat plateaus (Disher et al., 2021). While permafrost is unlikely to return to these newly forested areas, seasonal ice bulbs have been observed (Disher et al., 2021), indicating that previous cyclical findings may still have some applicability in these environments even though thaw is favoured (Camill, 1999; Zoltai, 1993; Zoltai & Tarnocai, 1975).

The Taiga Plains has undergone dramatic changes due to the cumulative impacts of climate change and human disturbances, particularly because of the permafrost thaw that results from these changes. Many forested areas have collapsed into wetland and lake features while other regions are now experiencing forest re-establishment. Permafrost degradation, whether initiated by climate change, wildfire, or increasing development, can alter an environment's thermal properties as well as its hydrology and ecology. Insights into incremental land cover changes initiated by permafrost thaw have emerged from a range of remote sensing and field-based studies across peatland environments (Beilman & Robinson, 2003; Carpino et al., 2018; Chasmer & Hopkinson, 2017; Gibson et al., 2021; Gibson et al., 2018; Quinton et al., 2011).

1.2 Research Objectives

While an average annual air temperature ≤0°C is an approximate indicator of the presence of permafrost, the discontinuous permafrost zone is also inherently defined by variability in permafrost presence or absence across the landscape due to more localized factors. However, this variability in permafrost distribution throughout northwestern Canada's discontinuous permafrost zone is not well understood due to the remoteness and size of the region, its spatial and temporal heterogeneity, limited data availability, and sparse monitoring networks. Each of these elements introduces challenges but they also provide strong justification for studying how climate warming might impact permafrost environments. As northwestern Canada's discontinuous permafrost zone is currently experiencing rapid climatic and environmental change, there has been unparalleled permafrost degradation, which has important implications for wide-ranging peatland-dominated landscapes and the associated local hydrology and ecology. Determining permafrost distribution and monitoring the state of such permafrost are common themes throughout this research with the goal of furthering the understanding of the relationship climate change has on accelerating permafrost thaw and the resultant changes to the overlying landscape. This research will explore the following objectives:

1) Develop an improved understanding of permafrost distribution across northwestern Canada's discontinuous permafrost zone;
2) Identify permafrost and permafrost-free areas within peatland-dominated regions and the characteristics that distinguish them;
3) Present a conceptual model detailing the impacts of permafrost thaw on land cover change in peatland-dominated regions;
4) Determine the future landcover trajectory across permafrost areas under climate change

1.3 Dissertation Summary

1.3.1 Chapter 2 Outline

Carpino, O., Haynes, K., Connon, R., Craig, J., Devoie, É., and Quinton, W.: Long-term climate-influenced land cover change in discontinuous permafrost peatland complexes, Hydrol. Earth Syst. Sci., 25, 3301–3317, https://doi.org/10.5194/hess-25-3301-2021, 2021.

The discontinuous permafrost zone is undergoing rapid transformation as a result of unprecedented permafrost thaw brought on by circumpolar climate warming. Rapid warming over recent decades has significantly decreased the area underlain by permafrost in peatland complexes. It has catalysed extensive landscape transitions in the Taiga Plains of northwestern Canada, transforming forest-dominated landscapes to those that are wetland dominated. However, the advanced stages of this landscape transition, and the hydrological and thermal mechanisms and feedbacks governing these environments, are unclear. This study explores the current trajectory of land cover change across a 300 000 km^2 region of northwestern Canada's discontinuous permafrost zone by presenting a north–south space-for-time substitution that capitalizes on the region's 600 km latitudinal span. We combine extensive geomatics data across the Taiga Plains with ground-based hydrometeorological measurements collected in the Scotty Creek basin, Northwest Territories, Canada, which is located in the medial latitudes of the Taiga Plains and is undergoing rapid landscape change. These data are used to inform a new conceptual framework of landscape evolution that accounts for the observed patterns of permafrost thaw-induced land cover change and provides a basis for predicting future changes. Permafrost thaw-induced changes in hydrology promote partial drainage and drying of collapse scar wetlands, leading to areas of afforestation forming treed wetlands without underlying permafrost. Across the north–south latitudinal gradient spanning the Taiga Plains, relatively undisturbed forested plateau–wetland complexes dominate the region's higher latitudes, forest–wetland patchworks

are most prevalent at the medial latitudes, and forested peatlands are increasingly present across lower latitudes. This trend reflects the progression of wetland transition occurring locally in the plateau–wetland complexes of the Scotty Creek basin and informs our understanding of the anticipated trajectory of change in the discontinuous permafrost zone.

1.3.2 Chapter 3 Outline

Carpino, O., Guo, J., Wright, S., van der Sluijs, J., Connon, R., & Quinton, W.: Detecting forest-wetland changes in northwestern Canada's discontinuous permafrost region using Landsat trend analysis.

Rapid circumpolar warming has led to accelerated permafrost thaw, which has induced extensive landscape change in northwestern Canada. Here, forest-dominated peatland landscapes, which were initially largely underlain by permafrost, are transitioning to treeless, wetland-dominated landscapes that are permafrost-free. This study explores permafrost thaw-induced landscape transition in boreal peatlands across northwestern Canada's discontinuous permafrost zone. Previous studies that have focused on changes to boreal peatlands over time have largely used aerial photographs and/or high-resolution satellite images acquired only at end nodes or decadal intervals across each study's time frame. This study uses a dense near-annual resolution of mosaicked Landsat imagery to detect changes to peatland landscapes across a 37-year timeframe for 10 study sites across a latitudinal transect through the southern Northwest Territories and northern British Columbia, Canada. Specifically, Tasseled Cap transformations (brightness, greenness, and wetness) are applied to the Landsat imagery, to visually assess the impacts of permafrost thaw. Tasseled Cap pixel trends as well as time series are analyzed for peat plateaus, collapse scar wetlands, and channel fens. This study demonstrates that individual landcovers within peatlands have differing brightness, greenness, and wetness trajectories.

1.3.3 Chapter 4 Outline

Carpino, O., Wright, S., Connon, R., Kokelj, S., Daly, S., Gingras-Hill, T., & Quinton, W.: Permafrost distribution in northwestern Canada's sporadic discontinuous permafrost zone.

Permafrost maps are important for northern communities who depend on them for development and infrastructure planning, resource management, and climate change adaptation. However, existing products are typically at national or circumpolar scales and are of limited use to local communities and governments. This paper documents the development of a permafrost map in northwestern Canada's discontinuous permafrost zone, specifically the Hay-Slave Lowlands, the southernmost ecoprovince of the Taiga Plains. The permafrost map presented here increases the understanding of the factors that determine the presence of permafrost, while producing a high-resolution product that is more suited for these purposes than the current suite of coarsely resolved permafrost maps. This map of the Hay-Slave Lowlands is of relatively high-resolution (100 x 100 m grid cells) and created using an additive index of factors known to influence the distribution of permafrost in this region. These include factors related to air temperature, soil type, landcover, terrain, and elevation, which are all publicly available datasets in Canada. This created a ~230,000 km^2 permafrost map covering a maximum latitudinal span of approximately 57º N to 63º N. The initial results presented here indicate that peatland-dominated areas across the region's lowlands as well as the elevated terrain features such as the Cameron Hills and the Caribou Mountains are most likely to be underlain by permafrost. The additive index, especially using broadly available datasets aims to be an accessible method that could be applied to other areas across Canada and throughout the circumpolar region.

CHAPTER 2: Long-term climate-influenced land cover change in discontinuous permafrost peatland complexes

2.1 Introduction

Northwestern Canada is one of the most rapidly warming regions on Earth (Box et al., 2019; Vincent et al., 2015) and it is transitioning to a warmer state at a rate that appears to have no analogue in the historical record (Porter et al., 2019). This transition includes region-wide thaw and disappearance of permafrost at unprecedented rates (Rowland et al., 2010). The Taiga Plains ecoregion of northwestern Canada extends from 55º to 68º N and as such, encompasses the spectrum of permafrost cover, from continuous to sporadic. Permafrost thaw in the Taiga Plains ecoregion is especially pronounced in its lower latitudes where the permafrost is relatively thin and warm, often already at the thaw-point temperature (Biskaborn et al., 2019), indicating a state of disequilibrium with the current climate (Helbig, Pappas, et al., 2016). For example, Kwong & Gan (1994) repeated the permafrost surveys of Brown (1964) in northern Alberta and the southern Northwest Territories (NWT) and found that the southern limit of permafrost occurrence had migrated northward by about 120 km over a period of 26 years. Beilman & Robinson (2003) estimated that 30-65% of the permafrost has disappeared from the southern Taiga Plains in the preceding 150 years, most of which disappeared in the latter 50 years. The accelerated rates of permafrost warming and thaw observed in recent decades throughout the circumpolar region (Biskaborn et al., 2019), including all of northwestern Canada (Holloway & Lewkowicz, 2020; Kokelj et al., 2017), have dramatically transformed land covers in the southern Taiga Plains (Chasmer & Hopkinson, 2017).

Much of the southern Taiga Plains is occupied by peatland-dominated lowlands, a landscape of raised, black spruce (*Picea mariana*) tree-covered peat plateaus overlying thin (<10 m), ice-rich permafrost interspersed with permafrost-free, treeless wetlands. These permafrost-free wetlands are predominantly classified as channel fens and collapse scar wetlands, the latter of which are developed from thermokarst erosion of the plateaus (Robinson & Moore, 2000). Peat plateaus and collapse scar wetlands are typically arranged into distinct "plateau-wetland complexes," which are separated by channel fens. Each of these major land cover types in the lowlands of the southern Taiga Plains, have contrasting hydrological functions (Hayshi et al., 2004) and therefore changes to their relative proportions on the landscape can affect water flux and storage at the basin scale (Quinton et al., 2011). Permafrost thaw underlying plateaus is driven by horizontal conduction and advection from adjacent wetlands, and vertical heat flows from the ground surface (Walvoord & Kurylyk, 2016). As this permafrost thaws, the overlying plateau ground surface subsides and is engulfed by the surrounding wetlands (Beilman et al., 2001; Helbig, Pappas, et al., 2016; Quinton et al., 2011). As such, permafrost thaw in this environment transforms forests to treeless, permafrost-free wetlands (Robinson & Moore, 2000). In the process, this also changes the hydrological function of the transformed land cover, in part due to a change in surface water-groundwater interactions (McKenzie & Voss, 2013). Such a transformation can profoundly affect local drainage processes and pathways (Connon et al., 2014; 2015) with implications to regional hydrology (St. Jacques & Sauchyn, 2009; Korosi et al., 2017; Connon et al., 2018), ecology (Beilman, 2001) biogeochemical processes (Gordon et al., 2016) and carbon cycling (Helbig, Pappas, et al., 2016; Vonk et al., 2019).

Zoltai (1993) described a perpetual cycle of permafrost development and thaw in which permafrost evolves from perennial ice bulbs that form below *Sphagnum* hummocks in permafrost-free treeless wetlands (*i.e.* collapse scars). Such hummocks expand and coalesce eventually forming tree-covered plateaus. However, over time plateaus experience a disturbance (*e.g.* fire, disease) that initiates the development of collapse scars and as a result, the plateau or portions of it revert to a permafrost-free wetland. In a stable climate, the permafrost and permafrost-free fractions of a landscape are assumed to remain relatively consistent. Zoltai (1993) estimated that the time required to complete this cycle is approximately 600 years. Treat and Jones (2018) indicated time scales for forest recovery following permafrost thaw in the range of 450 to 1500 years. However, there is growing evidence throughout the southern Taiga Plains that the climate warming of recent decades has disrupted the cycle of permafrost thaw and redevelopment such that the rates of permafrost loss greatly exceed those of permafrost development (*e.g.* Halsey et al., 1995; Robinson & Moore, 2002; Quinton et al., 2011).

The accelerated rates of permafrost thaw and resulting land cover change described above call into question the utility of existing concepts (*e.g.* Zoltai, 1993) as a means to estimate the current trajectory of land cover change since such concepts were developed from analyses of geological sediments (*e.g.* peat cores) which generally lack the resolution needed to identify land cover change sequences over relatively short (*i.e.* decadal) periods. Moreover, it is uncertain whether the current rates of climate warming are represented in the sediment record. As a result, there remains considerable uncertainty on the trajectory of permafrost thaw-induced land cover change in this region, including possible end-members and intermediate stages. Because of the close connection between land cover type and hydrological function in this region, the

uncertainty related to possible land cover change trajectories also raises new uncertainties in regards to the region's water resources.

In addition to unprecedented climate warming in the North, accelerated permafrost thaw is also driven by positive feedbacks including increased fragmentation of forested peat plateaus with increasing thaw (Chasmer et al., 2011), a process which increases the length of interface between permafrost and permafrost-free terrain, and therefore also increases the overall flux of energy into the remaining permafrost bodies (Kurylyk et al., 2016). Connon et al. (2018) demonstrated that talik layers situated between the active layer and underlying permafrost are widespread in thawing peatland-dominated terrains and their occurrence increases with increasing permafrost thaw. Devoie et al. (2019) demonstrated that once a talik forms, the rate of permafrost thaw can increase tenfold.

Since the permafrost table beneath peat plateaus rises above the water surface of the adjacent wetlands, plateaus function as "permafrost dams" that prevent wetlands from draining. Permafrost thaw therefore removes this effect and enables previously impounded wetlands to partially drain until the hydraulic gradient driving their partial drainage reaches an equilibrium state (Haynes et al., 2020). The slow release of water from the long-term storage of wetlands no longer impounded by permafrost changes the physical and ecological characteristics and hydrological function of these wetlands (Haynes et al., 2020). Such drainage transforms the uniformly wet *Sphagnum* lawns that characterise impounded wetlands, into hummocky surfaces that provide a wider range of near surface moisture conditions including those sufficiently dry to support the re-growth of trees (Haynes et al., 2020). There is also evidence that when *P. mariana* forest is lost due to permafrost thaw and plateau inundation, forest regeneration does not depend

on the regeneration of permafrost (Haynes et al., 2020; Chasmer & Hopkinson 2017). For example, treeless collapse scars have transformed into *P. mariana*-dominated forest within two to three decades after the permafrost dams disappear (Haynes et al., 2018).

In addition to the transient drainage process described above that may occur following the removal of the impounding permafrost (Haynes et al., 2018), such removal also increases the hydrological connectivity of basins through the incorporation of wetlands that were previously impounded and therefore hydrologically isolated from the basin drainage network (Connon et al., 2015). This process of "wetland capture" expands the runoff contributing areas of basins, a process that increases their runoff potential. Connon et al. (2018) attributed the trends of increasing runoff ratio (*i.e.* fraction of basin runoff per unit input of precipitation) in basins throughout the Taiga Plains to this permafrost thaw-induced process of runoff contributing area expansion.

The transition of one type of ground cover to another as a result of permafrost thaw or a subsequent process such as partial wetland drainage and re-establishment of forest also results in a change of surface energy balance (Kurylyk et al., 2016; Devoie et al., 2019). Insight into the nature of such changes can be obtained through comparing the energy regimes of the existing suite of land covers including the end-members of land cover change. For example, the incoming solar radiation measured at a height of 2 m above the ground surface is highest in the treeless wetlands and lowest in areas of peat plateaus with dense forest (Haynes et al., 2019). The average shortwave radiation flux density of treeless wetlands is approximately twice of that measured below dense forest (Haynes et al., 2019). Plateau areas with moderate or sparse tree canopies have incoming solar radiation values intermediate between these two end members

(Chasmer et al., 2011). The ground surface albedo varies over the narrow range of 0.15 to 0.19 (Hayashi et al., 2007) among the ground surface types discussed here, the exception being the late snowmelt period while plateau ground surfaces are still snow covered and the treeless wetlands are snow-free (Disher et al., 2021; Connon et al., Submitted).

The nature of changes to a land cover's surface energy balance is governed by the properties of its subsurface, ground surface, and the overlying tree canopy, all of which change as one land cover type transitions to another (Helbig, Wischnewski, et al., 2016). The reduction in the areal cover of forested plateaus and concomitant increase in the coverage of treeless wetlands indicates that in the first instance, permafrost thaw increases the incoming shortwave flux to the transformed land cover (Kurylyk et al., 2016; Devoie et al., 2019). Chasmer et al. (2011) found that this thaw-induced transition and associated increase of incoming shortwave radiation occurs over several years as tree mortality decreases the density of tree canopies. However, the forests that subsequently re-establish in partially drained wetlands may have an energy balance that shares some characteristics of the forested peat plateaus, where insolation is relatively low, and the low albedo (and therefore high energy adsorption) of trunks, branches and stems result in relatively high long-wave and sensible heat compared to the treeless wetland surfaces (Helbig, Wischnewski, et al., 2016).

Unprecedented climate warming and the feedbacks to thaw and land cover change are new factors not accounted for in current theories on permafrost degradation-aggregation cycles based on the analysis of peat cores. As a result, the time scales for land cover transformations derived from such theories cannot account for the current rates and patterns of all thaw-induced land cover change. This study examines peat plateau-wetland complexes along a latitudinal gradient

through the Taiga Plains to improve the understanding of permafrost thaw-driven land cover change in this region as well as to advance the ability to predict land cover changes over the coming decades. This overall objective will be accomplished by: (1) delineating the current extent of peatlands and forest distribution along the latitudinal span of discontinuous permafrost; (2) characterising the end-members and intervening stages of land cover transition; (3) providing an interpretation of the hydrological and ground surface energy balance regimes for each stage of land cover transition based on twenty years of field studies at the Scotty Creek Research Station; and (4) presenting a conceptual framework of peatland transition during and following permafrost thaw.

2.2 Study Site

2.2.1 The Taiga Plains Ecozone

Much of northwestern Canada's boreal region is located within the discontinuous permafrost zone, which ranges latitudinally from extensive-discontinuous (50-90% areal permafrost coverage) in the north to sporadic-discontinuous (10-50%) in the south. Within this region, the Taiga Plains ecozone contains a patchwork of mineral and organic terrain. This study examines the peat plateau-collapse scar wetland complexes that dominate the lowlands of this ecoregion (Helbig, Pappas, et al., 2016; Wright et al., 2009). While air temperature is the predominant control on permafrost, relatively dry peat at the ground surface can allow permafrost to exist where mean annual air temperatures (MAATs) are at or even above 0°C due to thermal insulation (Vitt et al., 1994; Camill & Clark 1998). Permafrost is therefore largely restricted to below peat plateaus since only these features contain unsaturated layers sufficiently developed to insulate permafrost (Zoltai & Tarnocai 1975; Hayashi et al., 2004; Quinton et al.,

2009). The areal coverage of permafrost in the discontinuous zone has significantly decreased in recent decades due to increasing MAATs and has resulted in a shift towards more wetland-dominated landscapes (Thie, 1974; Robinson & Moore, 2000; Wright et al., 2009; Quinton et al., 2011; Olefeldt et al., 2016).

The discontinuous permafrost zone of the Taiga Plains ecozone covers 312,000 km^2 and, for the purposes of this study, is divided into the areas of extensive-discontinuous permafrost (151,000 km^2) and sporadic-discontinuous permafrost (161,000 km^2) (Brown et al., 2002; Figure 2-1). The Taiga Plains, bounded by the Taiga Cordillera to the west and Taiga Shield to the east, has a dry continental climate with short summers and long, cold winters with MAATs ranging from -5.5°C to -1.5°C (Vincent et al., 2012). MAATs have increased across the Taiga Plains over the past 50 years (1970 – 2019) (Vincent et al., 2012) in a manner consistent with panarctic warming (Box et al., 2019). This is largely due to increases in average winter and spring temperatures of approximately 3°C over this period (Vincent et al., 2012). However, there has been no consistent trend in mean annual precipitation over this period in the Taiga Plains (Mekis & Vincent, 2011).

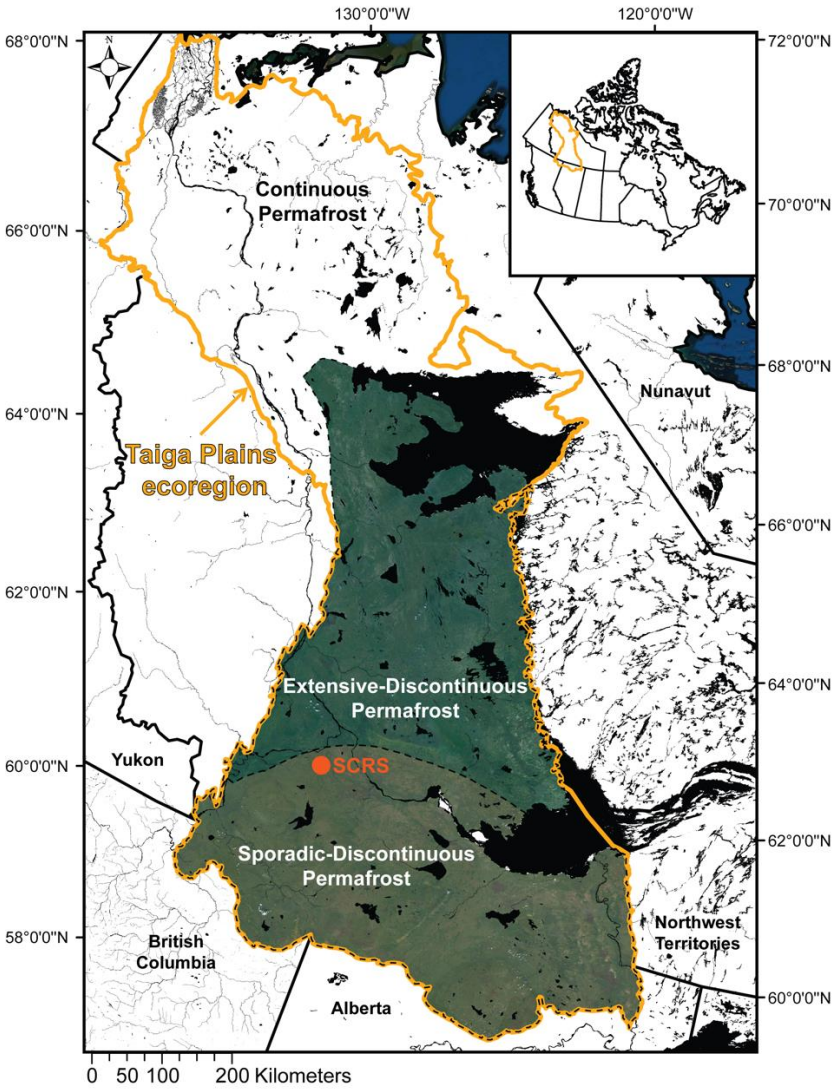

Figure 2-1: The Taiga Plains ecoregion with the discontinuous permafrost zones (coloured) defining the study region (Brown et al., 2002). The location of Scotty Creek Research Station (SCRS) is also indicated. Contains information licensed under the Open Government Licence – Canada.

2.2.2 Scotty Creek, Northwest Territories

Scotty Creek (61.3ºN, 121.3ºW) has been the focus of field studies and monitoring since the mid-1990s and as such, the long-term and detailed data archive at Scotty Creek (Haynes et

al., 2019) provide a unique opportunity to evaluate land cover changes over a period that coincides with rapid climate warming. Scotty Creek therefore also provides a reference to interpret land cover changes for terrains that are also present throughout the region. Scotty Creek is located approximately 50 km south of Fort Simpson, Northwest Territories (Figure 2-1) where the MAAT (1970-2015) is -2.6°C and the mean annual precipitation (1970-2015) is 400 mm, of which 150 mm falls as snow (Environment and Climate Change Canada, 2019). Data collected by Environment and Climate Change Canada at the Fort Simpson A climate station show that MAAT has increased by approximately 0.05°C/year since 1950, with warming most pronounced during the winter. Scotty Creek drains a 152 km^2 area dominated by peatlands with peat accumulations ranging between 2 and 8 m overlying a clay and silt rich glacial till (McClymont et al., 2013). The Scotty Creek drainage basin occupies one of many peatland-dominated lowlands of the Taiga Plains, and as such its landscape is dominated by complexes containing tree-covered peat plateaus overlying permafrost alongside treeless and permafrost-free collapse scar wetlands. Such plateau-wetland complexes are separated by channel fens that collectively function as the basin drainage network (Hayashi et al., 2004; Quinton et al., 2009). This type of land cover not only dominates the lowlands of the Taiga Plains but is also found extensively throughout northwestern Canada and across the circumpolar subarctic (Olefeldt et al., 2016).

2.3 Methods

2.3.1 Geomatics Methods

To place Scotty Creek into a regional context, geomatics methods were applied to both zones of discontinuous permafrost within the Taiga Plains to quantify the areas occupied by each of the major land covers of all areas identified as peatland-dominated lowland. Multispectral

Landsat 8 imagery (30 m resolution; Figure 2-2a) was acquired across an area of over 300,000 km^2 totalling 70 Landsat scenes. Of these, 59 scenes were used to construct the base of the mosaic and 11 were used as secondary data to patch and minimize cloud cover. The 59 primary scenes were acquired in 2017 and 2018 while the 11 secondary scenes were acquired between 2013 and 2016 as data of suitable quality was unavailable during the preferred time period. Acquiring imagery during the snow-free season was prioritized and as such, all 70 Landsat tiles were acquired in June, July, or August, rendering the coniferous forest cover seasonally comparable and allowing for a more streamlined mosaicking process. A colour infrared mosaic (Landsat 8 bands 5, 4, 3 displayed as R, G, B; Figure 2-2b) was created across the study region in ArcGIS (ESRI, Redlands, California) using a Lambert Conformal Conic projection. The mosaic dataset was colour balanced and the boundary was amended to the Taiga Plains ecozone including the delineations dividing the sporadic and extensive discontinuous zones (Brown et al., 2002).

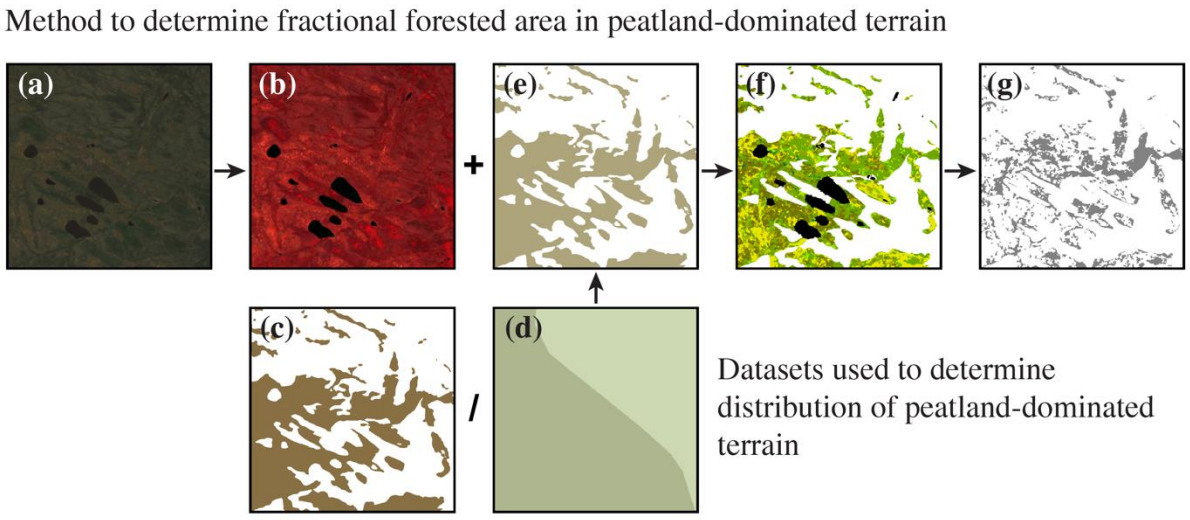

Figure 2-2: A summary of the regional geomatics methods used over a 2 km x 2 km sample area. Two main workflows are highlighted: the datasets used to map probable

peatland-dominated terrain and the methods used to determine fractional forested area within those peatland-dominated areas. (a) Multispectral Landsat 8 imagery; (b) false-colour infrared Landsat 8 imagery; (c) Natural Resources Canada saturated soils dataset; (d) Northern Circumpolar Soil Carbon Database (NCSCD) fractional area of organic soils; (e) probable peatland-dominated terrain; (f) unsupervised classification identifying land covers within peatland-dominated terrain; (g) coniferous forest cover within peatland-dominated terrain.

To determine the current distribution of the peatland-dominated lowlands that contain the same type of terrain as observed at Scotty Creek (*i.e.* plateau-wetland complexes separated by channel fens), two complementary products were used in the ArcGIS suite of programs. First, a Natural Resources Canada saturated soils dataset (Figure 2-2c; Natural Resources Canada 2017) was selected to isolate areas that were wetland-dominated and likely representative of the plateau-wetland complexes targeted in this study. Next, the Northern Circumpolar Soil Carbon Database (NCSCD) (Figure 2-2d; Bolin Centre for Climate Research 2013) was selected to determine whether the highlighted wetland-dominated areas are also likely to represent peatland-dominated areas.

The saturated soils dataset is part of a larger digital cartographical project of Natural Resources Canada, CanVec. The CanVec dataset is a vector format dataset, which can be downloaded by province/territory or Canada-wide and includes over 60 features organized into 8 themes, including land features. Land features in this dataset, such as the distribution of saturated soils, were originally digitized at a scale of 1:50000 (Natural Resources Canada 2017). The NCSCD is also a polygon database developed by the Bolin Centre for Climate Research through synthesizing data from numerous regional and national soil maps alongside field-data collected across Canada, USA, Russia, and the European Union. The NCSCD includes data on the fractional coverage of different soil types and stored soil organic carbon (Hugelius, Bockheim, et

al., 2013; Hugelius, Tarnocai, et al., 2013). In the present study, the layer containing information on the fractional coverage of soil types was used. While the original format of the NCSCD is a vector of delineated zones, gridded data is also available at resolutions varying from 0.012° to 1° (Hugelius, Tarnocai, et al., 2013). The NCSCD is comprised of a circumarctic dataset as well as country-wide and regional datasets, including one of Canada (Hugelius, Tarnocai, et al., 2013).

The NCSCD is a widely used dataset (Gibson et al., 2018; Olefeldt et al., 2014; Stofferahn et al., 2019) but the zones do not map specific locations of peatland-dominated terrain (Figure 2-2d). The locations of peatlands are helpful for work in regions such as the Taiga Plains, where the landscape is a patchwork of both organic and mineral terrain. The saturated soils dataset and the NCSCD were then both masked to the Taiga Plains boundaries in ArcGIS, where over 26,000 saturated soil polygons and 572 NCSCD zones were contained within the study region. The saturated soils dataset was mapped to display probable peatland terrain across the study region (Figure 2-2c). The areas of each saturated soil polygon were calculated alongside the areas for each NCSCD zone using the boundaries in the dataset. As the fractional coverage product from the NCSCD was used in this study, the fractional area of probable peatland terrain within the same NCSCD zone was calculated. The fractional areas of organic soils reported in the NCSCD were then compared to the fractional areas of probable peatland terrain from the saturated soils dataset within the same NCSCD zone boundary (Figure 2-2e).

The Landsat mosaic dataset (Figure 2-2b) was then combined with the resultant product displaying peatland terrain (Figure 2-2e). An unsupervised land cover classification was subsequently completed on the Landsat mosaic across the areas identified by the saturated soils and NCSCD datasets to identify and classify the land covers within these peat plateau-wetland

complexes (Figure 2-2f). The first iteration of the unsupervised classification (Iso Cluster classification approach) targeted 50-75 classes (72 created). The original 72 classes were then aggregated into 12 final classes within the peatland terrain outlined across the Taiga Plains study region. The final 12 aggregated classes include: coniferous (dense and sparse), mixed (dense and sparse), and broad leaf forests stands (dense and sparse), collapse scar, fen, open water, bare ground, cloud, and cloud shadow.

Forested peatlands are particularly indicative of landscape change in this region (Quinton et al., 2010; Baltzer et al., 2014; Chasmer & Hopkinson 2017) and as such, identifying the forested areas within the already identified peatland-dominated terrain was the focus of the Landsat classification. Specifically, the proportion of coniferous forested area within the total peatland area was quantified across the region's latitudinal span (Figure 2-2g). Fractional coniferous forested area was selected rather than total forested area to account for the observed spatial differences in peatland distribution across the Taiga Plains. For each degree of latitude, a bin was created for fractional forested area and the median was calculated alongside upper (*i.e.* 75^{th} percentile) and lower (*i.e.* 25^{th} percentile) quartiles. This data was plotted as a function of latitude across the Taiga Plains ecozone. This generated a dataset of forest cover across the peatland-dominated regions of interest that was subsequently complemented by field data collected in the Scotty Creek basin to guide the proposed conceptual framework.

2.3.2 Scotty Creek Imagery

To help capture examples of the stages of the transitioning landscape, imagery was collected using a Remotely Piloted Aircraft System (RPAS) across the Scotty Creek basin to represent how each of these illustrated trajectory stages manifests on the landscape in a peat

plateau and collapse scar wetland-dominated environment. The RPAS imagery (0.5 m resolution) was collected in the summer of 2018 using an eBee Plus equipped with a senseFly SODA 3D mapping camera and all image processing was completed in Pix4DMapper.

Imagery for Scotty Creek, including aerial photographs from 1947, 1970, and 1977, IKONOS satellite imagery from 2000, and Worldview satellite imagery from 2010 and 2018 were used to quantify the area occupied by peat plateaus, collapse scar wetlands and channel fens in each of these years. The aerial photographs (0.5-1.2 m resolution) and IKONOS imagery (4 m resolution) were previously classified and the results were presented in Quinton et al. (2011). Carpino et al. (2018) completed the land cover classifications for the 2010 Worldview imagery and Disher (2020) classified the 2018 Worldview imagery. Collectively, these images document the land cover change at the Scotty Creek basin over the period 1947 to 2018.

2.3.3 Hydrological Data

A comprehensive archive of hydrometeorological measurements was used in this study to examine the temporal variation in hydrological characteristics as land cover transition from one stage to another. The form and hydrological function of the major land cover types of permafrost plateau, collapse scar, and channel fen are well understood from numerous studies at Scotty Creek since the 1990s (Quinton et al., 2019). Field studies and monitoring at Scotty Creek over this period have also provided firsthand accounts of how permafrost thaw changes land covers (Quinton et al., 2019). In the present study, we examined how runoff, evapotranspiration, and water storage are affected as land cover changes. In addition, we examined the precipitation data collected from 2008 to 2019 (Geonor, Model T200B) in relation to the three hydrological components listed above to gain insights into how changes in land cover affect the water balance

for each stage in the land cover transition. These stages will be presented in detail in section 4.2. The Geonor precipitation data include both rain and snow measurements logged at 30 minute intervals (Table 2-1). Monitoring of discharge from Scotty Creek by the Water Survey of Canada began in 1996. For this study, annual basin runoff (mm $year^{-1}$) between 1996 and 2015 was calculated and used in the basin runoff component of the conceptual framework (Table 2-1) (Connon et al., 2014; Haynes et al., 2018). Given that this period of discharge monitoring coincided with a period of considerable climate warming and documented land cover change at Scotty Creek, the trend in calculated runoff over the period of record reflects a shift from a permafrost plateau-dominated landscape to one increasingly influenced by hydrologically-connected wetlands. Therefore, the temporal trend of runoff from the Scotty Creek basin is driven by permafrost thaw-induced land cover change (Connon et al., 2014; Haynes et al., 2018).

Table 2-1: Annual precipitation (2008-2019), basin runoff (1996-2015; Connon et al., 2014; Haynes et al., 2018), evapotranspiration (2013-2016; Warren et al., 2018), and residual storage values are presented (mm $year^{-1}$) for two distinct transitional landscape stages at Scotty Creek: a landscape dominated by forest and a patchwork landscape of near-equal forest and treeless wetland land covers.

	FOREST > WETLAND	FOREST ≈ WETLAND
PRECIPITATION	493	493
RUNOFF	149	215
EVAPOTRANSPIRATION	206	255
RESIDUAL STORAGE	138	23

Recent work by Warren et al. (2018) examined evapotranspiration (ET) for forests, wetlands, and the integrated landscape within the Scotty Creek watershed between 2013 and 2016. Daily ET values (mm day^{-1}) reported by Warren et al. (2018) were converted to annual ET (mm $year^{-1}$) for the purpose of the conceptual framework water balance in the present work (Table 2-1). The different land covers monitored by Warren et al. (2018) are representative of the

land cover end-members identified in our conceptual framework. Therefore, the annual ET values based on the data collected by Warren et al. (2018) for the *P. mariana*-dominated forests, open collapse scar wetlands and the integrated landscape were associated with the appropriate stage along our proposed trajectory of change. Stages of the trajectory for which representative measurements were not collected are interpolated between the land cover end-members for which ET was measured.

Given the insignificant changes in annual precipitation over the period of measurement (Connon et al., 2014; Haynes et al., 2018), annual storage was calculated as the residual of annual precipitation inputs, and annual evapotranspiration and runoff outputs for the conceptual framework water balance (Table 2-1).

2.3.4 Radiation Fluxes

A total of four meteorological stations at Scotty Creek were selected for use in this study (Figure 2-3). This included a station installed in a collapse scar wetland in 2004 (hereafter "wetland station") followed by a second station on a densely forested peat plateau in 2007 (hereafter "dense forest station"). The radiation flux data from these two stations are representative of the collapse scar wetland and permafrost plateau land cover types, respectively. Two additional stations located on forested plateaus were also used to represent tree canopy densities different from that of the dense forest station. These stations were installed on a sparsely forested peat plateau in 2015 (hereafter "sparse forest station") and a forested plateau with a canopy of intermediate density between that of the dense and sparse stations in 2014 (hereafter "intermediate forest station"). All radiation measurements were made below the tree canopy at a height of 2 m above the ground surface. Four component radiation data were

collected at the dense forest, sparse forest, and wetland meteorological stations, while only shortwave radiation was collected at the intermediate forest station. The reader is directed to Haynes et al. (2019) for full descriptions of the radiation instrumentation within the Scotty Creek basin. Radiation was measured every minute, and averaged and recorded every 30 minutes from which daily (24 hourly) averages were computed. The daily averages were then used to compute annual average radiation for each station. While these computations defined some of the variability of radiation fluxes among land cover types, they do not account for flux variations over short temporal and spatial scales (Webster et al., 2016). To address these, the daily average four component radiation data from each station were compared on a monthly time step. The monthly averages were calculated and compared across the land covers represented by each of the four meteorological stations using a one-way analysis of variance (ANOVA) with Tukey post-hoc test ($\alpha = 0.05$), thereby testing the effect of land cover on monthly shortwave and longwave incoming and outgoing radiation.

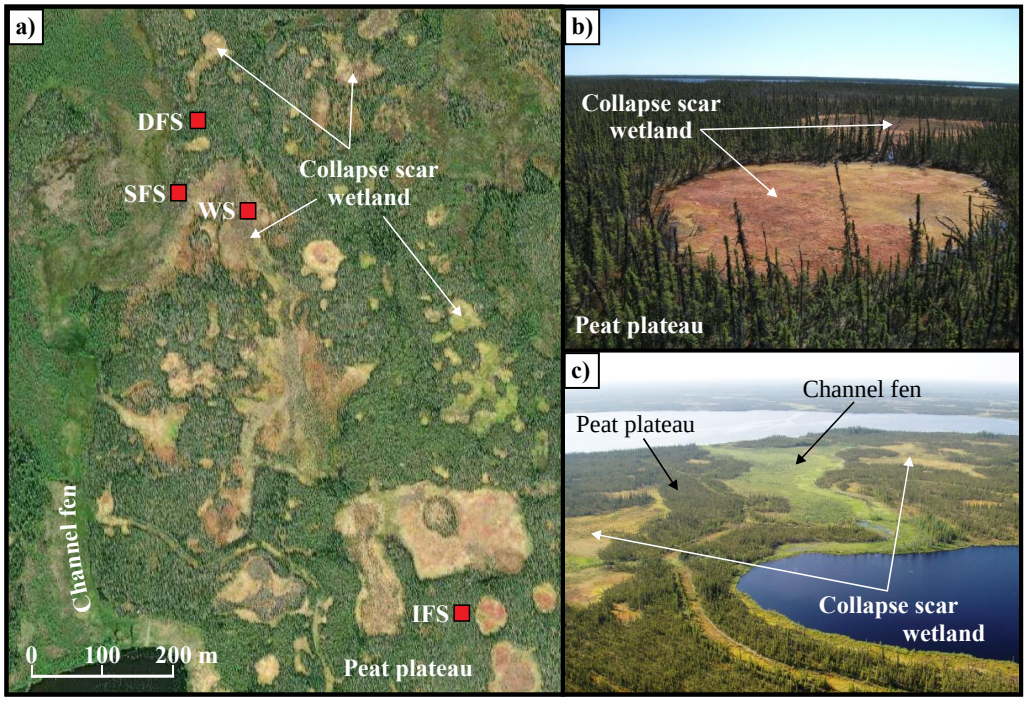

Figure 2-3: Worldview 2 satellite image (a) and oblique aerial photographs (b, c) over Scotty Creek, Northwest Territories. The satellite image also shows the locations of the Dense Forest Station (DFS), Sparse Forest Station (SFS), Wetland Station (WS) and Intermediate Forest Station (IFS) micrometeorological stations. The oblique aerial photographs show the land cover types that dominate lowlands with discontinuous permafrost in the Taiga Plains including peat plateau (permafrost), collapse scar wetland, and channel fen.

2.4 Results and Discussion

2.4.1 Peatland and Forest Occurrence

The type of peatland-dominated terrain composed of peat plateau-wetland complexes separated by channel fens as described for Scotty Creek, occupy approximately 35% of the discontinuous permafrost zones of the Taiga Plains (Figure 2-4a). Large peatland clusters are located in lowland areas with high histel or histosol soil percentages. In the extensive-discontinuous permafrost zone, peatlands are clustered to the west near to the Mackenzie River,

and are largely absent from the eastern portion of the study area in the region bounded by Great Bear Lake to the north and the Taiga Shield to the east. In the sporadic-discontinuous zone however, the peatland clusters are more longitudinally dispersed.

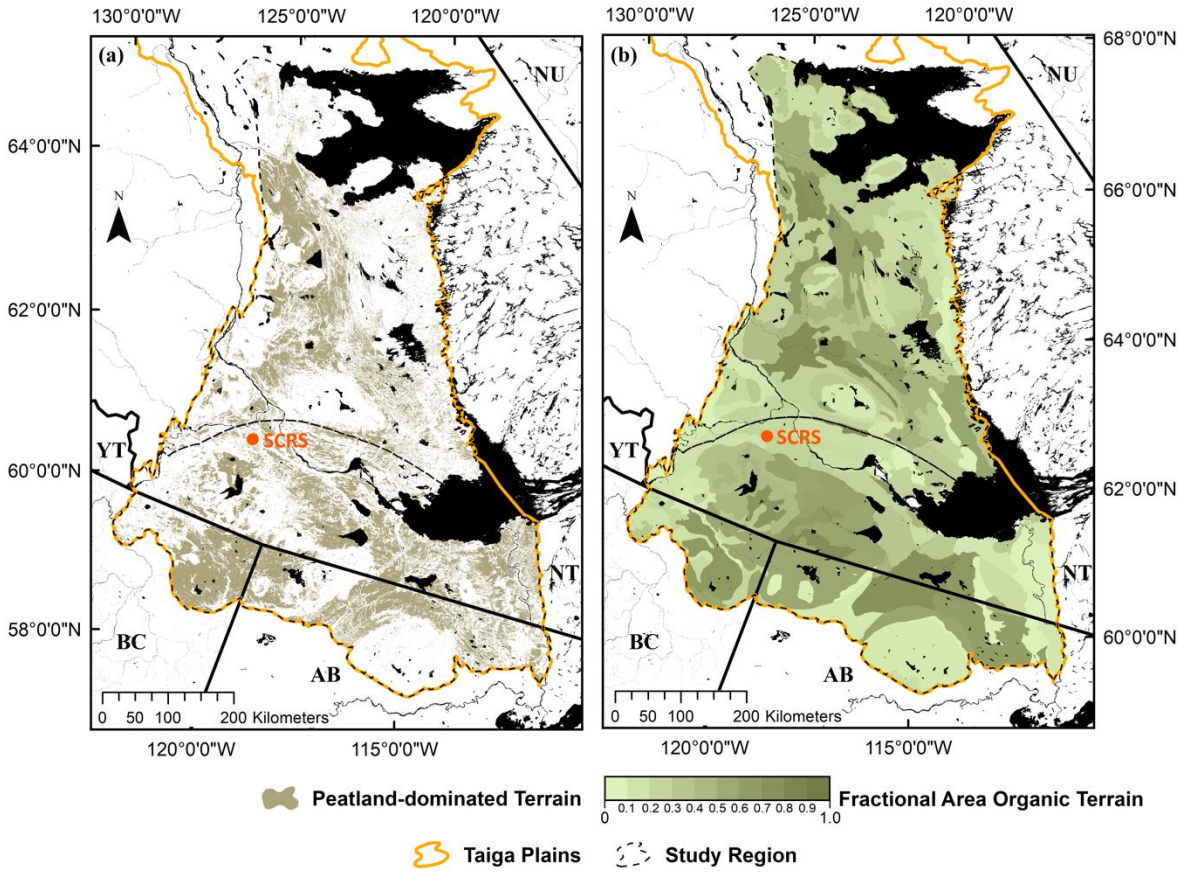

Figure 2-4: Predicted distribution of peatland-dominated terrain in the discontinuous permafrost zone of the Taiga Plains (a). Peatland-dominated terrain was mapped using a saturated soils dataset (Natural Resources Canada 2017) (a) and compared to the NCSCD (Bolin Centre for Climate Research 2013) (b). Contains information licensed under the Open Government Licence – Canada.

Comparing the fractional areas of probable peatland terrain from the saturated soils dataset to the NCSCD showed the saturated soils dataset was more likely to overstate the

distribution of probable peatland terrain compared to the NCSCD maps. Approximately 20% of the fractional areas were exact matches between the two datasets, 20% were lower in the saturated soils dataset, and 60% were higher in the saturated soils dataset. However, despite these disagreements, 79% of the fractional areas determined using the saturated soils dataset were within 15% of the fractional areas in the NCSCD. This suggests that using the Natural Resources Canada saturated soils dataset may be an appropriate method of mapping probable peatland terrain in the Taiga Plains on a finer scale (Figure 2-4a) compared to the broad zones presented by the NCSCD (Figure 2-4b). Only 11 of the 572 NCSCD zones (~2%) had disagreements over 25% when comparing the fractional areas between both datasets. The majority of these zones of disagreement were located along the Slave River, in the far southeast of the Taiga Plains study region.

A latitudinal trend in land cover percentage was found for the mapped peatland-dominated terrain (Figure 2-5). Along the boundary between the extensive-discontinuous and sporadic-discontinuous permafrost zones near the centre of the study region, collapse scar wetland features are most prevalent. Median fractional forest cover in peatlands (*i.e.* peat plateaus or treed wetlands) reaches its minimum value of 33% within the 61º N bin, near the latitude of Scotty Creek. The proportion of forested peatlands remains relatively low throughout the transitional zone between sporadic and extensive discontinuous permafrost (approximately 61º to 62º N) where the median forest cover does not exceed 34%. The widespread occurrence of collapse scars suggest that permafrost thaw and the resulting processes of ground surface subsidence and inundation are particularly active in this zone compared to the extensive

discontinuous permafrost zone to the north and the sporadic discontinuous permafrost zone to the south, where the fractional forested areas are higher.

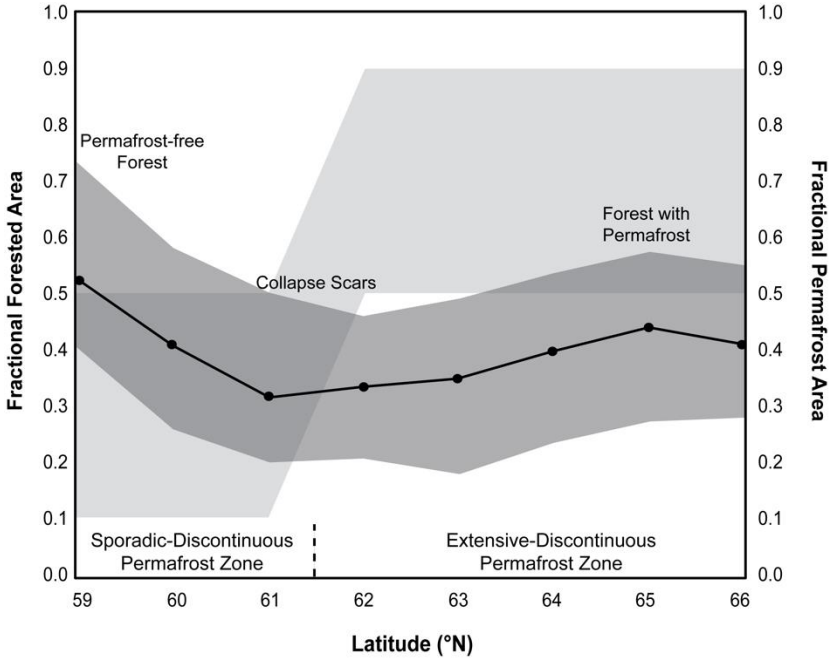

Figure 2-5: Median forested peatland area expressed as a fraction of the total peatland area and plotted as a function of latitude. The dark grey area represents the range in the proportion of the landscape occupied by forested peatland (*i.e.* fractional forested area) between the 25th percentile and 75th percentile. The lighter grey area indicates the range in the proportion of landscape underlain by permafrost (*i.e.* fractional permafrost area) as indicated by Brown et al. (2002).

The median proportion of forested peatlands in the extensive-discontinuous zone (63º to 66º N) ranges from approximately 35 to 45%, indicating that permafrost thaw is less prevalent over the landscape than in the transition zone immediately to the south. However, the median fractional forested area is at its greatest (52%) south of the transition in the sporadic-discontinuous zone (59º to 60º N), where about half of the peatland area is forest covered. Expansion of forest cover in this zone, especially in the areas of north-eastern British Columbia and north-western Alberta, has been reported by others (*e.g.* Zoltai, 1993; Carpino et al., 2018).

A pattern of forest expansion over permafrost-free terrain is consistent with the observation of a northward-moving southern limit of permafrost reported by Kwong and Gan (1994) and with the process of tree re-establishment following permafrost thaw-induced partial drainage of wetlands described by Haynes et al. (2020).

2.4.2 Conceptual Framework of Land Cover Change

From the remote sensing and field-based hydrological studies at Scotty Creek since the mid-1990s, key insights into incremental land cover changes initiated by permafrost thaw have emerged. Using this knowledge as a foundation, the present study examines both the hydrological and radiation regimes of each incremental stage and the land cover changes over the larger region in which permafrost thaw is known to be widely occurring and within which the southern edge of permafrost is migrating northward (Kwong & Gan, 1994). From this approach, a new conceptual framework is presented (Figure 2-6), which describes permafrost thaw-induced land cover change in the peatland-dominated regions of the discontinuous permafrost zone. The land cover change occurring simultaneously (to varying degrees) at Scotty Creek and latitudinally across the wider Taiga Plains region can be categorized into seven distinct land cover stages, the first and last of which are forest cover, with the difference being that the former overlies permafrost and the latter does not. The stages are as follows: (I) Forested permafrost plateaus; (II) Forested permafrost plateaus with small, isolated collapse scars; (III) Forested permafrost plateaus with larger, interconnected wetlands; (IV) Wetland complexes with small plateau islands; (V) Wetland complexes with hummock development and tree establishment; (VI) Hummock growth with forest establishment; and (VII) Forested peatlands (Figure 2-6). In

the following sections, the biophysical, hydrological and radiation regimes of each of these stages are presented and discussed, drawing on several investigations in the region.

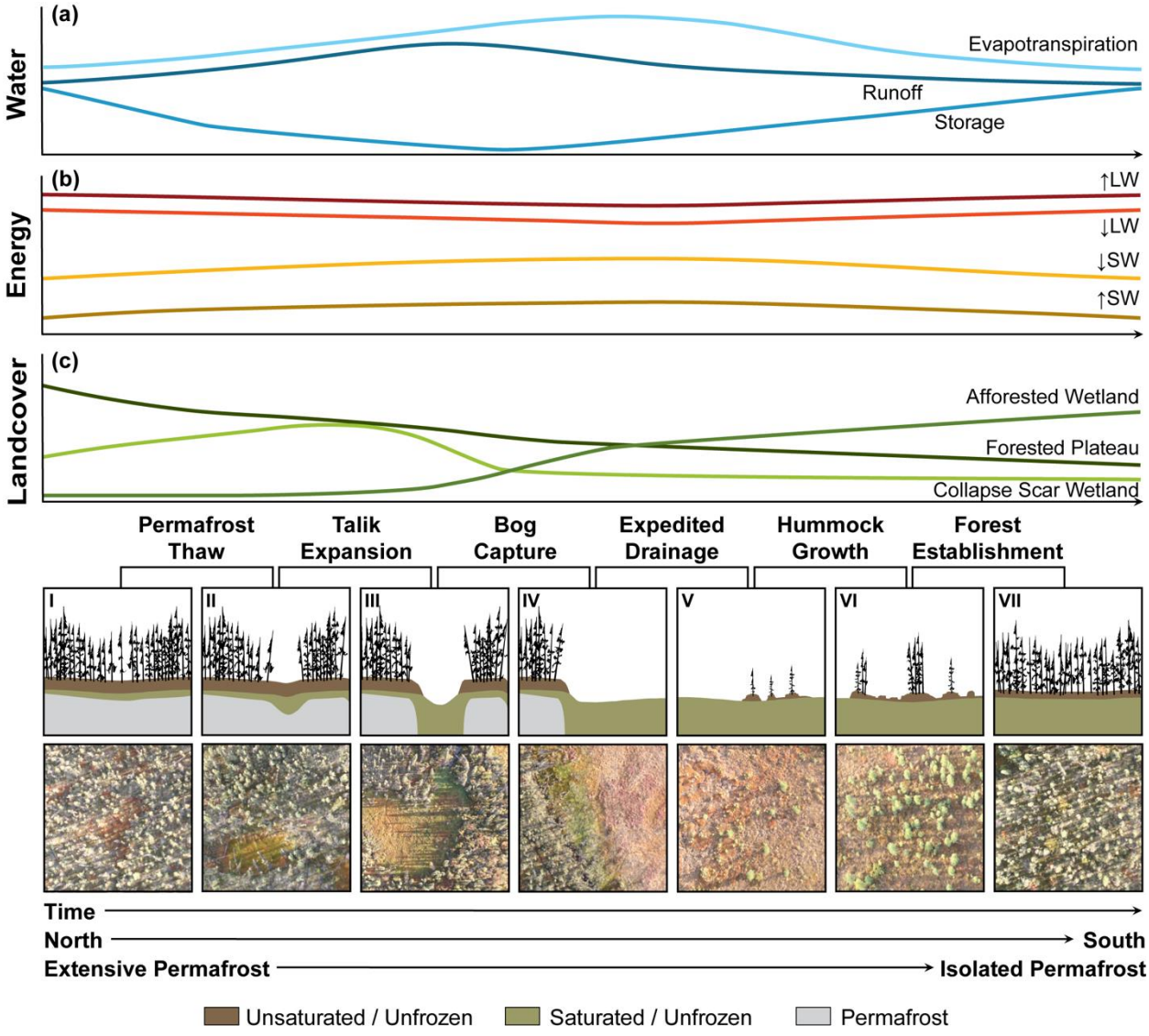

Figure 2-6: (Bottom) Proposed conceptual framework of landscape trajectory including a space-for-time substitution for changes to both permafrost and land cover. A conceptual model is presented to illustrate landscape change with the support of RPAS imagery collected in the Scotty Creek basin. The conceptual framework is presented alongside the processes that initiate the trajectory's progression. (a) Relative changes to local water balances of measured Scotty Creek basin runoff, evapotranspiration and residual storage with unchanging precipitation are summarized and presented over the trajectory of landscape change based on the proportion of forested vs. wetland area. (b) Relative changes to local energy balances are presented using data collected from sub-canopy

meteorological stations installed at Scotty Creek. (c) Changes to relative land cover proportions are presented using historical aerial photographs and recent acquisitions of satellite imagery over the Scotty Creek basin.

2.4.3 Biophysical Characteristics

The present study found that the early land cover stages presented in Figure 2-6 are more prevalent at the higher latitudes of the study region and the later stages at the lower latitudes. Considering that permafrost thaw is more advanced in the lower latitudes and that the southern limit of permafrost is advancing northward (Kwong & Gan, 1994), it is reasonable to expect that the more advanced stages presently characterising the lower latitudes will, in the future, characterise the higher latitudes, assuming a continuation of climate warming induced permafrost thaw. Approaching a change in latitude through the study region as analogous to a change in land cover stage, or more specifically, to a change in time, is supported by studies that examined land cover change over the last half-century at Scotty Creek (Chasmer & Hopkinson, 2017; Quinton et al., 2019) and along a north to south transect extending from Scotty Creek to northeastern British Columbia (Carpino et al., 2018).

The Scotty Creek basin, located near the northern limit of sporadic discontinuous permafrost (Figure 2-1) is characterised mainly by stages III and IV. However, examples of all seven stages can be found in local areas at Scotty Creek. For this reason, the long-term monitoring and research programs at Scotty Creek involving each of these land cover types contributes detailed information on their form and functioning, and on their transition from one to another. For example, permafrost thaw changes a landscape dominated by forested plateaus (Figure 2-6I) to one with small, suprapermafrost taliks (Connon et al., 2018) and isolated collapse scars (Figure 2-6II; Quinton et al., 2011). Continued thaw expands isolated collapse

scars (Figure 2-6III; Devoie et al., 2019) enabling them to coalesce to form interconnected wetlands (Connon et al., 2015), a process that then leads to a landscape of expansive wetlands dotted with isolated plateau "islands" (Figure 2-6IV; Baltzer et al., 2014; Chasmer & Hopkinson 2017). Since the process of wetland expansion removes peat plateaus, a land cover type that impounds wetlands and obstructs drainage (Connon et al., 2014), this process enables the landscape to drain more efficiently (Haynes et al., 2018). As wetlands drain, hummock micro-topography develops in their relatively drier interiors (Figure 2-6V; Haynes et al., 2020), which allows *P. mariana* to colonise the wetlands on the relatively dry hummock surfaces (Figure 2-6VI; Iversen et al., 2018; Dymond et al., 2019). Continued drainage and drying of wetlands enables the expansion of their hummocky terrain and therefore of their tree cover (Eppinga et al., 2009; Iversen et al., 2018) until the landscape returns to a more continuous forest cover (Figure 2-6VII; Carpino et al., 2018). However, the forest cover in this final stage is permafrost-free and for that reason, the conceptual framework presented in Figure 2-6 stands in contrast to those presented by Zoltai (1993) and Camill (1999) in which the re-emergence of a forest cover relies on the re-emergence of the underlying permafrost. According to Zoltai (1993), forest re-emerges because permafrost displaces the overlying ground surface upward, resulting in the development of an unsaturated layer suitable for tree establishment. By contrast, the tree establishment described in Figure 2-6 results not from the re-emergence of permafrost, but from its continued thaw over the landscape, a process that dewaters wetlands (Connon et al., 2014; Haynes et al., 2018) to the extent suitable for tree establishment (Haynes et al., 2020).

The land cover transition depicted in Figure 2-6 involving wetland drainage and forest re-establishment occurs in less than half a century as indicated by analysis of historical imagery for

Scotty Creek. By contrast, the process of forest re-growth enabled by the re-establishment of permafrost occurs over a much longer time frame of several centuries (Zoltai, 1993; Treat and Jones, 2018). At Scotty Creek, the early stages of Figure 2-6 (*i.e.* stages I, II) represent the predominant changes observed between 1947 and 2000 over which time the tree-covered area decreased from approximately 70% to approximately 50% (Quinton et al., 2011). The fraction of forested land above permafrost-free terrain cover is unknown for this period but assumed to be negligible based on land cover descriptions for this region (*e.g.* NWWG, 1988; Zoltai 1993; Robinson & Moore, 2000). This period therefore generated a concomitant rise in the cover of wetlands over the landscape (*i.e.* 30 to 50%) since permafrost thaw transitions the tree covered plateaus to collapse scars and channel fens, as confirmed by analysis of archived imagery (Chasmer et al., 2010). By 2018, tree-covered peat plateaus decreased to 40%, and treeless wetlands occupied 45% of the land cover (13% collapse scars and 32% channel fens) (Disher 2020). These studies indicate that permafrost thaw and the resulting processes have both removed forest as a result of thaw-induced subsidence and inundation of plateau surfaces, and more recently, enabled forest re-establishment in the form of treed wetlands (Haynes et al., 2020; Disher et al., 2021). However, the dominant land cover transition at Scotty Creek is still from forest (peat plateau) to wetland as a result of permafrost thaw, resulting in a net forest loss, a process that will continue until the later stages of Figure 2-6 are reached (*i.e.* stages VI, VII), at which point there will be a net forest gain.

The sequence of land cover stages following permafrost thaw observed at Scotty Creek and depicted in Figure 2-6 is supported by vegetation successional changes described in the literature for wetlands as they age. For example, aquatic *Sphagnum* species, notably *S. riparium*,

are the first to occupy the inundated margins between thawing permafrost plateaus and developing collapse scars (Garon-Labrecque et al., 2016; Pelletier et al., 2017). Such recent areas of collapse are easily identified on high-resolution RPAS imagery by the distinct bright green colour of *S. riparium* (Figure 2-6II, III, IV; Gibson et al., 2018; Haynes et al., 2020). These wetland-plateau edges may also be identified by bare peat or moats of water (Zoltai 1993). As collapse scars expand, lawn species, such as *S. angustifolium,* and hummock species, such as *S. fuscum,* emerge, particularly in the drier interior of wetlands (Zoltai 1993; Camill 1999; Pelletier et al., 2017). Hummock species, mainly *S. fuscum,* first emerge near the centre of collapse scars, and expand outward over time (Camill, 1999; Loisel & Yu, 2013). Much like *S. riparium, S. fuscum* is also easily identified in high-resolution imagery, where *S. fuscum* is distinguished by its russet colour (Figure 2-6V) (Haynes et al., 2020). As the density of the *S. fuscum* hummocks increases, imagery and ground-based observations indicate the presence of young *P. mariana* trees (Liefers & Rothwell 1987; Haynes et al., 2020), first on isolated hummocks (Figure 2-6VI) but eventually as widespread afforestation (Figure 2-6VII; Camill 2000; Ketteridge et al., 2013).

2.4.4 Radiation Flux Characteristics

The Scotty Creek basin is a microcosm of its larger regional setting since it contains each of the land cover stages of the conceptual framework in Figure 2-6. As such, the micro-meteorological measurements made at Scotty Creek for different land cover types provide insight into how energy regimes change as one land cover stage transitions to the next. Both incoming and outgoing shortwave radiation peak at the middle stages (IV, V), where treeless collapse scars predominate. Annual incoming and outgoing shortwave radiation is lowest at the dense forest station, which represents the initial stage (I). Likewise, incoming and outgoing annual longwave

radiation are greatest in the early (I, II) and late stages (VI, VII) and lowest in the wetland-dominated middle stages (IV, V).

Statistically significant differences were found between stations for incoming (Figure 2-7a) and outgoing (Figure 2-7b) shortwave and incoming longwave radiation (Figure 2-7c), while there was no statistical differences between stations for outgoing longwave (Figure 2-7d). However, Tukey post-hoc tests revealed variability between the two shortwave components in terms of which groups showed these significant differences. As the four meteorological stations fall along a gradient of forest density from treeless wetland to a densely forested plateau, no significant differences in incoming shortwave radiation were ever found between stations only one rank apart on that gradient. As such, measurements indicate average monthly incoming shortwave radiation is significantly greater at the wetland compared to both the intermediate forest ($p < 0.05$) and the dense forest ($p < 0.05$), while no significant difference exists between wetland and the sparse forest. However, the dense forest receives significantly less incoming shortwave radiation than both the wetland ($p < 0.05$) and the sparse forest ($p < 0.05$), but this station is not significantly different from the intermediate forest.

No significant differences in outgoing shortwave radiation exist between any of the forested plateau stations but all are significantly different from the wetland. Specifically, outgoing shortwave radiation recorded at the wetland station is significantly greater than the sparse forest ($p < 0.05$), intermediate forest ($p < 0.05$), and dense forest stations ($p < 0.05$). The differences between the wetland station and the forested plateau stations are also increasingly significant with increasing tree density. There was a statistically significant difference between the three stations (intermediate forest omitted due to lack of measurements) for incoming

longwave radiation, while no statistically significant differences were observed in the outgoing longwave radiation component. The only significant difference in incoming longwave was observed between the wetland and dense forest ($p < 0.05$). No significant differences exist between the sparse forest and the wetland or dense forest.

The comparison among the plateau stations of contrasting tree canopy densities provides insight into the permafrost thaw-induced progression of radiation regimes as plateaus transition to wetlands, a process involving the gradual thinning and eventual loss of the tree canopy. Wright et al. (2009) demonstrated that small-scale changes to the tree canopy density can increase insolation to the ground in localized areas leading to thaw depressions in the active layer and water flows toward such depressions from their surroundings. Such areas of preferential thaw therefore develop elevated soil moisture contents, and since soil thermal conductivity increases with its moisture content, the preferential thaw process is reinforced. This is suggested as the mechanism driving the transition from stage I to II in the trajectory (Quinton et al., 2019). This feedback is present in the initial stages of the trajectory, and is often associated with talik formation and expansion into collapse scars due to localized permafrost loss (Chasmer & Hopkinson 2017; Connon et al., 2018). Such thaw can extend to the base of the active layer in which case further thaw results in permafrost loss, ground surface subsidence, waterlogging of the ground surface, local tree mortality, and therefore further thinning of the overlying tree canopy and consequently more insolation at the ground surface. These processes and feedback mechanisms are critical in the generation of collapse scars in stage III.

Differing ground surface properties, particularly albedo, can amplify the differences in incoming shortwave radiation among the land covers. However, the difference in mean albedo

during the snow-free season (May-September) below the plateau canopies is less than 5% and displays a small increasing gradient as the canopy becomes more dense (sparse: 0.111, intermediate: 0.127, dense: 0.147). The mean wetland albedo (0.145) during the snow-free season is also similar to the plateau surfaces and most closely resembles the surface albedo of the dense plateau. The greatest contrast in albedo occurs during the period of several weeks while snow still covers the plateaus but is absent on the adjacent wetlands (Connon et al., 2021). This contrast in albedo is also evident in Figure 2-7b, which shows that following winter, outgoing shortwave radiation from the wetland increases before the forested stations. Helbig, Wischnewski, et al. (2016) attributed their observed increase in landscape albedo in this late winter/spring period to the permafrost thaw-induced conversion of forest (lower albedo) to wetland (higher albedo), and suggested that this could lead to a regional cooling effect during this time of the year. However, that study implicitly assumed that the wetlands were a final land cover stage rather than an incremental step toward the re-establishment of forest as depicted in the conceptual framework presented in Figure 2-6.

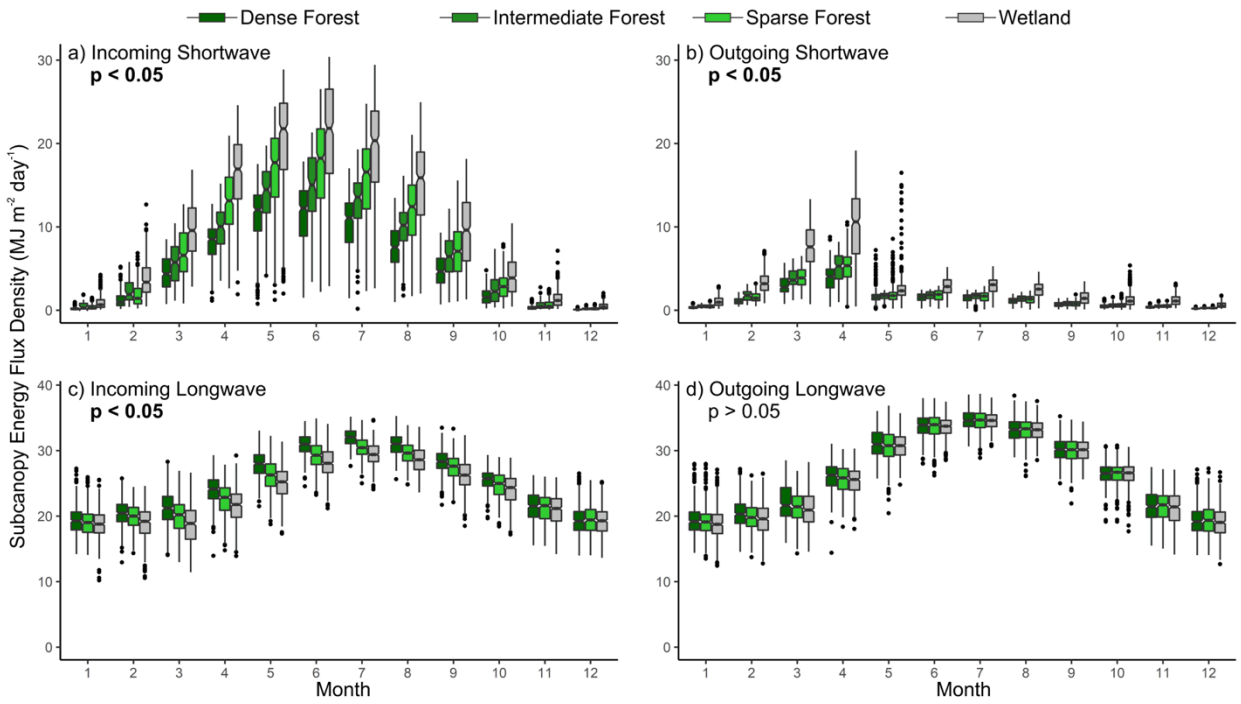

Figure 2-7: Sub-canopy daily total (MJ/m2/day) incoming shortwave (a), outgoing shortwave (b), incoming longwave (c), and outgoing longwave (d) at the four meteorological stations. Each station represents a distinct land cover: dense forest (2007-2019), intermediate forest (2014-2019), sparse forest (2015-2018), and treeless wetland (2004-2019). The boxes represent the 25th and 75th percentile, while the whiskers represent the range of the data. The notches on each box indicate the confidence interval (a = 0.05) around the mean while the statistical differences between meteorological stations have been presented in the upper left of each plot as determined by one-way ANOVA. Significant p values have been highlighted with bold text.

2.4.5 Hydrological Characteristics

As the land covers presented in the conceptual framework transition from one to the next, hydrological processes also change (Figure 2-6a). In the early stages (I, II), a relatively large proportion of hydrological inputs from the atmosphere are stored in collapse scars due to their impoundment by the permafrost on their margins (Connon et al., 2014). Evapotranspiration from the landscape is relatively low given the high proportion of forest and relatively low transpiration by the *P. mariana* that dominates the plateau canopies (Warren et al., 2018). In the early land cover stages (I, II) when forests predominate, understorey vegetation provide the pathway for

evapotranspiration (Chasmer et al., 2011). The incremental change in land covers presented in Figure 2-6 involves biophysical changes that affect the partitioning of precipitation into storage or runoff. By stage III to IV wetlands are interconnected and rapidly expanding, the storage of water on the landscape reaches its minimum level while runoff from the landscape is maximized (Figure 2-6a). This increased runoff is enabled by the removal of permafrost barriers (Haynes et al., 2018) and areal expansion of runoff contributing areas resulting in greater hydrological connectivity and therefore drainage of the landscape (Connon et al., 2014). These observations coincide with a period of steady, unchanging annual precipitation; therefore, precipitation does not account for elevated basin runoff (Connon et al., 2014). A decrease in landscape drainage then follows in the subsequent stages as the transient runoff contributions from "captured" collapse scars diminishes as the importance of evapotranspiration increases as the wetlands become the predominant land cover (IV, V). The increase in evapotranspiration is due to increases in evaporation from areas occupied by standing water and saturated or near-saturated wetland vegetation, including *Sphagnum* mosses, with losses due to transpiration driven by shrub vegetation (Warren et al., 2018). In the advanced stages (VI, VII) evapotranspiration would decrease as a result of the drier wetland surfaces as hummock microtopography replaces saturated *Sphagnum* lawns. The treed (afforested) wetlands (VII) have not been studied to the same degree as peat plateaus or collapse scar wetlands (Haynes et al., 2020; Disher et al., 2021) and therefore ground based hydrological data specific to these features are lacking.

2.5 Conclusions

The discontinuous permafrost zone of the Taiga Plains exemplifies a landscape in transition. Coupling a broad-scale mapping initiative with the detail of site-specific data

collected in the Scotty Creek basin demonstrates a permafrost thaw-induced land cover transition. This transition is incremental and involves distinct land cover stages. The first and last of these is a continuous forest cover, although in the first stage the forest is underlain by permafrost while in the last stage it is not. Unlike traditional concepts of land cover change in peatland dominated regions of discontinuous permafrost in which forest re-establishment occurs over centuries and is constrained by the rate of permafrost re-development, the concept presented here described forest re-establishment within decades and resulting from continued permafrost thaw, a process which allows wetlands to de-water sufficiently for tree growth. Each land cover stage has characteristic biophysical, hydrological and micro-meteorological features.

The proposed conceptual framework of landscape evolution describes the transitions occurring across the Taiga Plains in peat plateau-collapse scar wetland complexes like Scotty Creek. This study also identifies the applicability of this conceptual framework across a large region of the Canadian north. We establish the likely pattern of change across these peat plateau-collapse scar wetland complexes and project their future trajectory by combining long-term field observations with analyses of contemporary and historical imagery. It is proposed that, while permafrost thaw-induced land cover changes have previously been dominated by a transition from forest to wetland, this transition is not permanent and forested land covers are likely to return over time, although unlikely to be underlain by permafrost. This research improves the understanding of how peat plateau-collapse scar wetland complexes in the Taiga Plains may be impacted by ongoing permafrost thaw and these results may also be of relevance to other peatland-rich permafrost environments across the circumpolar north.

CHAPTER 3: Detecting forest-wetland changes in northwestern Canada's discontinuous permafrost region using Landsat trend analysis

3.1 Introduction

Northwestern Canada's discontinuous permafrost zone is among the most rapidly warming regions on Earth (Box et al., 2019; Vincent et al., 2015) and the impacts of climate change, particularly permafrost thaw, are increasingly apparent (Olefeldt et al., 2016). Permafrost thaw is especially pronounced where permafrost is relatively thin (<10 m) and warm (*i.e.* -2°C to -0.2°C) (Biskaborn et al., 2019; Kwong & Gan, 1994; Robinson & Moore, 2000; Smith et al., 2005). A decrease of ~10-50% in permafrost areal extent has already been recorded across the southern portion of the discontinuous permafrost zone over the last 50 years (Beilman & Robinson, 2003; Chasmer & Hopkinson, 2017; Quinton et al., 2011).

The majority of boreal forest is located in permafrost environments (Helbig, Pappas, et al., 2016; Hinzman et al., 2005), where permafrost thaw can result in pronounced landscape changes (Rowland et al., 2010). In northwestern Canada, permafrost thaw-induced landscape transformations are readily observed in the peatland-dominated regions between 59°N and 62°N (Gibson et al., 2021; Quinton et al., 2019; Quinton et al., 2011). Here, permafrost occurs preferentially below forested peatlands, such as peat plateaus, while adjacent peatlands occupying lower topographic positions, mainly collapse scars and channel fens are permafrost-free (Hayashi et al., 2004; Zoltai & Tarnocai, 1975). Peat plateaus are underlain by ice-rich permafrost and are topographically elevated by approximately 0.5 to 1.5 m above these surrounding permafrost-free features, which are at or near the water table (Vitt et al., 1994; Wright et al., 2009). The ground surface of the plateaus is sufficiently dry to support a tree cover

dominated by *Picea mariana* while the permafrost-free wetlands that comprise the rest of the landscape are saturated for most of the year (Iwata et al., 2012; Lieffers & Rothwell, 1987). When the permafrost underlying plateaus thaws, the plateaus are destabilized and their ground surface subsides and is eventually inundated by the surrounding wetlands (Baltzer et al., 2014; Beilman et al., 2001; Helbig, Pappas, et al., 2016; Quinton et al., 2011). As such, permafrost thaw in this environment largely transforms a forest-dominated landscape to one that is primarily comprised of treeless, permafrost-free wetlands (Baltzer et al., 2014; Quinton et al., 2011; Robinson & Moore, 2000).

Peatland landscape transition has been defined by distinct long-term cycles of permafrost aggradation and degradation (Robinson and Moore, 2000; Tarnocai, 2009). In a stable climate, the transition between permafrost and permafrost-free landcovers is continuous on the scale of hundreds (Zoltai, 1993) to thousands (Treat & Jones, 2018) of years, over which time the relative proportions of permafrost and permafrost-free terrains remain relatively constant. However, warming-induced permafrost thaw has disrupted the balance between permafrost aggradation and degradation (Beilman et al., 2001; Jorgenson et al., 2010; Schuur & Abbott, 2011), and greatly accelerated the rates of permafrost thaw and the resulting landcover transformations (Chasmer et al., 2011; Kurylyk et al., 2016). The current rates and patterns of permafrost thaw-induced landcover change (Carpino et al., 2021) are not accounted for by the cycle described above.

In peatland-dominated regions of sporadic-discontinuous permafrost, permafrost thaw alters the landscape in ways that are readily discernable. As such, the field of remote sensing offers novel and powerful tools to monitor permafrost thaw. Remote sensing is a cost-effective means of monitoring remote and large-scale environments that are spatially and temporally

heterogenous. Previous studies that have focused on changes to peatlands over time have largely used aerial photographs and/or high-resolution satellite images. While these studies have benefited from high spatial resolution, they typically used lower temporal resolution with imagery only at end nodes, multi-decadal, or decadal intervals (*e.g.* Baltzer et al., 2014; Carpino et al., 2018; Chasmer & Hopkinson, 2017; Gibson et al., 2018; Haynes et al., 2020; Quinton et al., 2011).

This study uses a dense near-annual resolution of mosaicked Landsat imagery to detect changes to peatland landscapes. The high temporal resolution provided by this analysis, is an important complement to studies that have previously used high spatial resolution but low temporal resolution methods across the same area. A major advantage of using temporally dense image stacks compared to conventional two-date remote sensing analyses is an improved ability to detect long-term changes that may be more subtle (Fraser et al., 2014), such as those associated with climate change and the resultant permafrost thaw. Landsat trend analysis of a dense image stack can reveal changes at near-annual time steps (Fraser et al., 2012; Fraser et al., 2011) and this study uses the three Tasseled Cap (TC) transformations (brightness, greenness, and wetness) to identify permafrost thaw-induced changes at the pixel level.

This study explores the differing landcover change trajectories of forested peat plateaus, collapse scar wetlands, and channel fens in a thawing landscape. This will be accomplished by:

1) relating previously identified permafrost thaw-induced landscape changes to TC changes in brightness, greenness, and wetness; and
2) comparing the brightness, greenness, and wetness trends between forested plateau and wetland landscapes.

3.2 Methods

3.2.1 Study Area

The discontinuous permafrost zone of the Taiga Plains contains a patchwork of mineral and organic terrain. This study examines the peatland complexes that dominate the lowlands of this ecozone (Wright et al., 2009). While air temperature is the predominant control on permafrost distribution in the southern discontinuous permafrost zone, permafrost is also strongly linked to peatlands with dry ground surfaces (*e.g.* peat plateaus) (Camill & Clark, 1998; Vitt et al., 1994). Peatlands across this landscape are represented by a patchwork of peat plateaus, which are forested and underlain by permafrost, and permafrost-free wetland features such as channel fens and collapse scars (Quinton et al., 2009; Wright et al., 2009; Zoltai & Tarnocai, 1975), the latter of which is developed from thermokarst erosion of the plateaus (Robinson & Moore, 2000). As the permafrost underlying peat plateaus thaws, the overlying plateau ground surface subsides and becomes saturated (Beilman et al., 2001; Quinton et al., 2011; Zoltai, 1993). Collapse scar wetlands can be small, isolated features within a peat plateau or connected features that drain into channel fens that then convey water to the basin outlet (Connon et al., 2014; Quinton et al., 2009; Vitt et al., 1994).

Ten study sites were selected for this study (Figure 3-8), which correspond with the areas of interest selected by Carpino et al. (2018). The 10 mapped study sites cover a latitudinal transect of 59.96°N to 61.30°N between northeastern British Columbia (BC) and the southern Northwest Territories (NWT) within the discontinuous permafrost zone of the Taiga Plains. This latitudinal range is particularly useful to study as most peatlands in this region that are south of 62°N exhibit a high degree of thaw based on the area covered by collapse scars (Gibson et al.,

2021). The ten sites were originally selected by Carpino et al. (2018) by targeting peatlands (*i.e.* lowlands) containing forested peat plateaus, collapse scar wetlands, and channel fens and were also confirmed to have sufficient remote sensing coverage for the purposes of that study. The study area is located near the isothermal boundary between the extensive-discontinuous and sporadic-discontinuous zones where the presence of peat-rich organic soils is largely responsible for any permafrost found in this zone (Halsey et al., 1995; Helbig, Pappas, et al., 2016; Vitt et al., 1994; Wright et al., 2009). This region is characterized by a dry continental climate and much like the documented panarctic warming trend (Box et al., 2019), this region has experienced warming by as much as 2°C over the past 50 years (Vincent et al. 2012). This is largely due to increases in average winter and spring temperatures of approximately 3°C over the same time period (Vincent et al. 2012). Mean annual precipitation has largely been consistent in this region over the past 50 years (Mekis & Vincent, 2011).

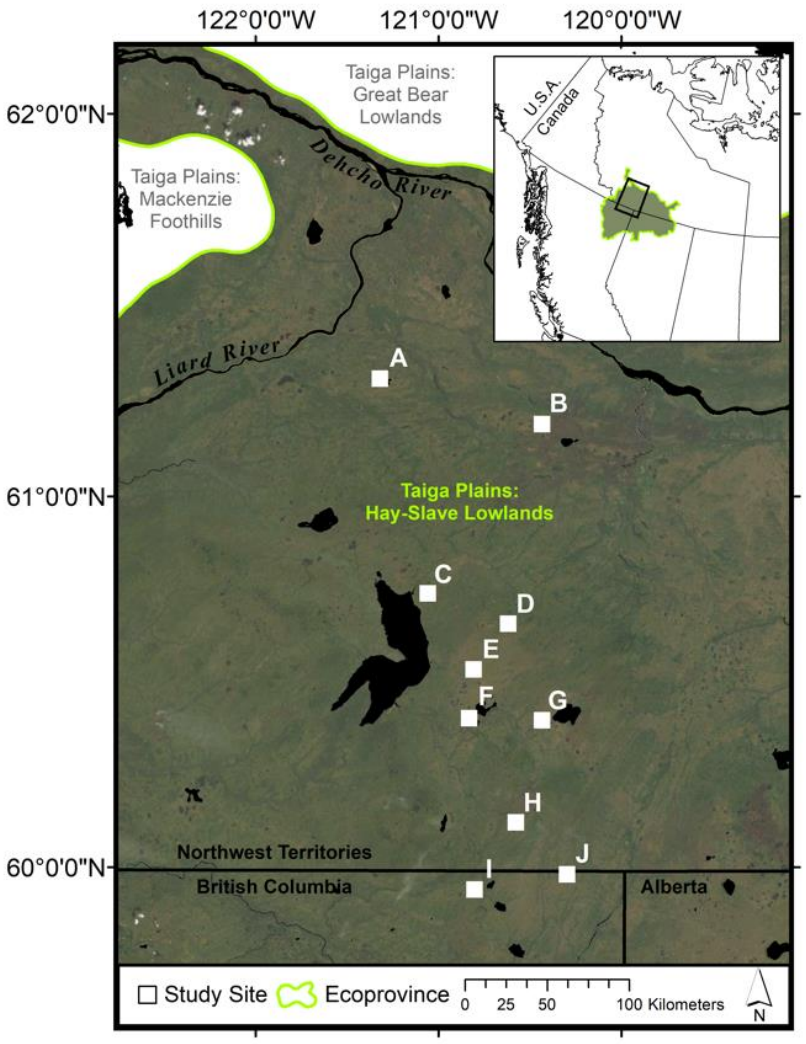

Figure 3-8: Mapped locations of 10 study sites (A-J) in the southernmost ecoprovince of the Taiga Plains, the Hay-Slave Lowlands. Study sites are located in the Northwest Territories (A-H) and British Columbia (I-J), Canada. Inset map shows location of study area (black extent indicator) and ecoprovince relative to northwestern North America.

3.2.2 Remote Sensing Analysis

The remote sensing methods used in this study are based on the work by Fraser et al. (2012) and Fraser et al. (2011), which uses multi-year cloud-free mosaics of Landsat images and trend analysis to monitor temporal changes at high latitude. Landsat 5, 7 and 8 top-of-atmosphere

(TOA) reflectance products acquired from the United States Geological Survey (USGS) and hosted on Google Earth Engine (GEE) (Gorelick et al., 2017; Wulder et al., 2019) were accessed programmatically for this work. Landsat TOA reflectance products were all pre-calibrated radiometrically (Chander et al., 2009) and all have the ground sample size of 30 m resolution. Landsat TOA image collections for a 37-year period (1984-2021) were filtered by multitemporal cloud and cloud shadow masks whereby cloud-free pixels for the Julian date range 153 to 244 (June, July, August, or early September) were retained. Due to cloud coverage none of the 10 sites had annual image coverage for all 37 years, yet for linear trend analysis this was not required. There was an average of 31 cloud-free, usable years at each site, with a minimum of 28 years, and a maximum of 35 years. Some years yielded multiple reflectance measurements during the growing season, which were not averaged. Prior to trend analysis, the Canadian Digital Elevation Model (CDEM) (NRCan, 2017) was then used for topographic correction to reduce the effects of sun-sensor illumination geometry throughout the growing season (Soenen et al., 2005). The final Landsat reflectance stack was generated for the entire NWT (NWT Centre for Geomatics, 2021) yet for this study only the southernmost ecoprovince of the Taiga Plains, the Hay-Slave Lowlands, was retained (Marshall et al., 1999) (Figure 3-8).

The three TC transformations (brightness, greenness, wetness; Kauth & Thomas, 1976) were calculated in GEE with corresponding coefficients for Landsat 5, 7, and 8, respectively (Baig et al., 2014; Crist & Cicone, 1984). TC transformations use coefficients in specific band channels to yield brightness, greenness, and wetness values. The brightness transformation monitors surface changes related to soil and albedo; the greenness transformation is associated with changes to the densities of green, healthy vegetation; and the wetness transformation

responds to changes in soil moisture, surface water (Baig et al., 2014), and plant canopy moisture associated with vegetation shifts (Fraser et al., 2011). After brightness, greenness, and wetness were calculated across all pixels in the Landsat stack in GEE, linear trends for each pixel were then computed across the 1984-2021 period using the Theil-Sen regression (Kendall & Stuart, 1967), which robustly fits a line to a series of points by calculating the median of all possible slopes between all pairwise points. The Theil-Sen regression is a beneficial approach for large temporal datasets as it is relatively insensitive to outliers, which may occur due to transient factors such as precipitation or snowmelt. A 3-band RGB colour-composite mosaic was then created after converting the 16-bit values to an 8-bit (255 values) radiometric conversion, with the respective Theil-Sen slopes (red=brightness, green=greenness, blue=wetness) to visually represent the TC trend trajectory between 1984-2021 (Figure 3-9).

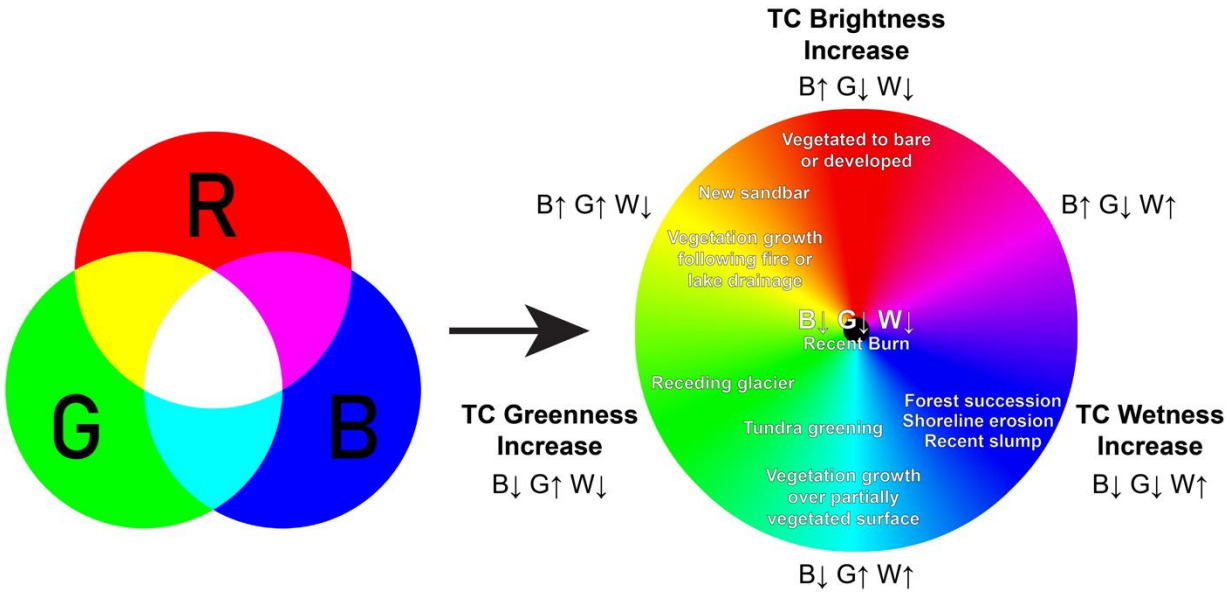

Figure 3-9: Tasseled Cap (TC) transformations displayed as RGB colour wheel legend. TC changes are displayed as increases or decreases to each transformation. Results of previous TC landscape change studies have been plotted on the colour wheel. Adapted from Fraser et al. 2014.

The high resolution panchromatic Worldview 1 and 2 imagery (0.3 m resolution) and aerial photographs (~1 – 1.5 m resolution) (from Carpino et al. (2018)) were used to help corroborate the TC transformation trajectories. Carpino et al. (2018) completed manual landcover classifications at each of the 10 sites across a 2.5 km by 4 km area. Classifications representing the landcovers that represent permafrost and permafrost-free ground and the changes to each of these landcover classes were mapped and reported for a 40-year time period (~1970 – 2010; Carpino et al. 2018). For this study, 300 m transects (*i.e.*, 10 Landsat pixels) were generated at each of the 10 sites (Figure 3-10). The specific locations of the transect were determined by ensuring they crossed at least one peat plateau-wetland boundary within the larger site and also ran in a cardinal direction to ensure evenly distributed transect points and pixels. These transects were used to sample the brightness, greenness, and wetness time series values as well as the calculated trends for each pixel along the transect. To focus on changes to landcover that could be attributed to permafrost-related landcover transitions, areas that experienced forest-fires during the study period (as per the Canadian National Fire Database) were not included in any of the 10 transects.

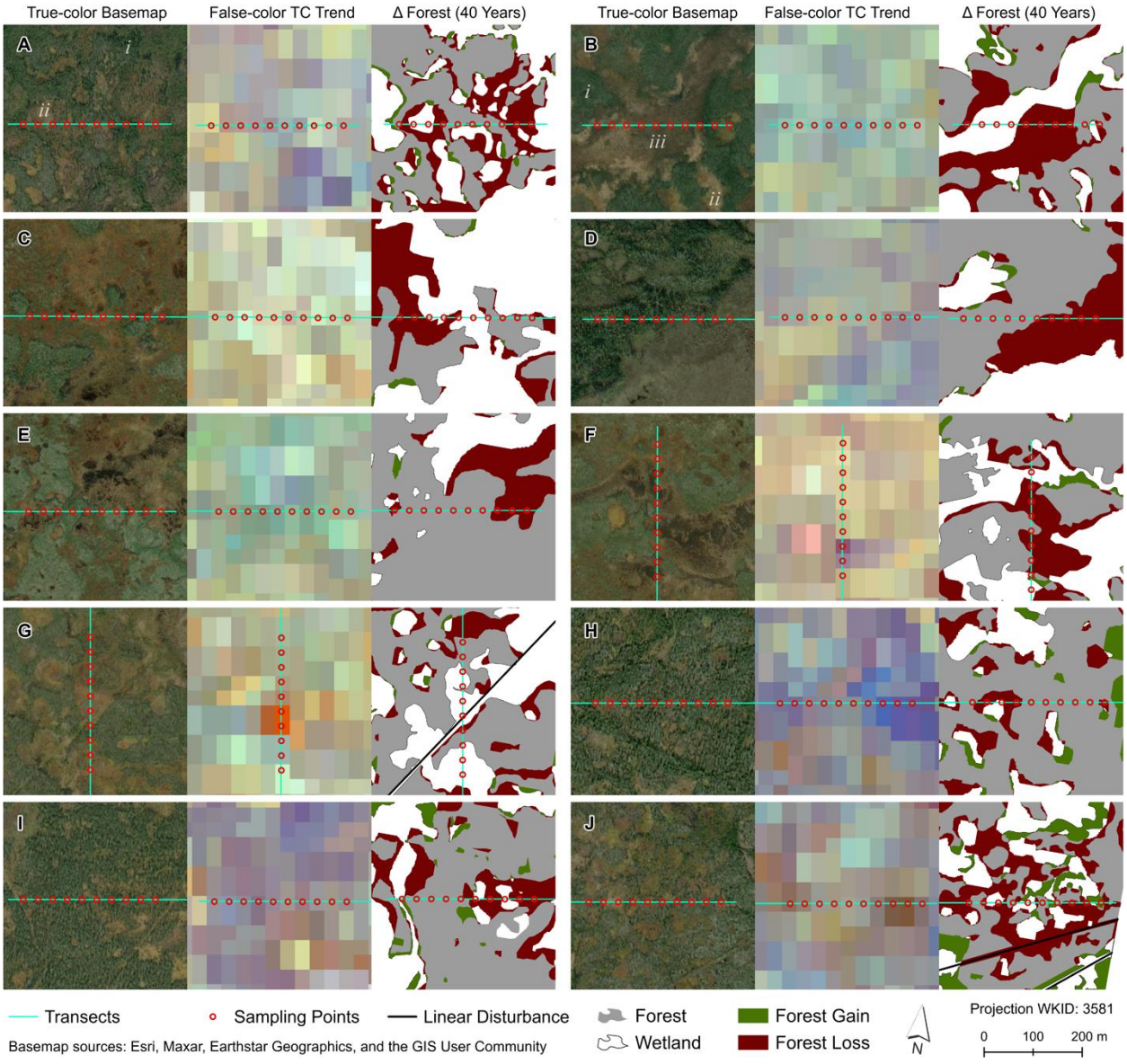

Figure 3-10: Study transects covering 300 m (10 Landsat pixels) for Sites A-J are shown against present-day satellite imagery (left), 3-band Tasseled Cap (TC) trend trajectory (1984-2021) mosaic (centre), and changes to forest (1970-2010) from Carpino et al. (2018) (right). The satellite imagery panels show distinct landcovers present in boreal peatlands including (i) forested plateaus, (ii) collapse scar wetlands, and (iii) channel fens. which have been labeled for sites A and B. The TC trend panels show brightness (red), greenness (green), and wetness (blue) trends for each pixel (see Figure 3-9). The changes to forest panels show unchanging areas of forest and wetland (both collapse scars and fens) as well as areas that have experienced tree mortality (forest loss) or tree re-establishment (forest gain). Linear disturbances (seismic lines) are also delineated but were not included in forest change calculations or mapped as forest loss for the purposes of Carpino et al. (2018).

3.2.3 Statistical Analysis

Two main datasets were created using TC transformations: the pixel trends (*i.e.*, brightness, greenness, wetness Theil-Sen slopes) and the pixel time series (*i.e.*, brightness, greenness, wetness values). Each point in the transect was manually classified based on the predominant landcover of the pixel (*i.e.* forested peat plateau, collapse scar wetland, or channel fen). The brightness, greenness, and wetness trends were compared across the 10 sites using an analysis of variance (ANOVA) with Tukey post-hoc ($\alpha = 0.05$) to test whether there were significant differences in trends between circa 2010 landcovers (forest or wetland) and landcover change (forest loss, forest gain, no change). These analyses were selected to help determine whether peat plateaus and wetlands have differing trajectories. Pearson correlations were also run on the trend data, which were used to determine if there were correlations between the brightness, greenness, and wetness values and distance from plateau-wetland boundary (*i.e.* Euclidian distance to nearest plateau boundary and Euclidian distance to nearest wetland boundary). The brightness, greenness, and wetness trends were plotted across the transect, highlighting the permafrost and permafrost-free landcovers (originally classified by Carpino et al. (2018) using 2010 and 2011 satellite imagery).

For the time series data, each point in the transect was also manually classified as peat plateau, collapse scar wetland, or channel fen based on the predominant landcover within the Landsat pixel. The brightness, greenness, and wetness values were plotted as a time series across the 1984-2021 period. Linear regressions were performed to compare values between landcovers. For sites where there was more than one transect point classified as a landcover, the

median brightness/greenness/wetness value for the class was calculated for all available years for the site.

3.3 Results

Permafrost thaw-induced landscape change was quantified as changes to brightness, greenness, and wetness. The results of the ANOVA indicated there were significant differences between the brightness, greenness, and wetness trends between sites for present-day landcover classes (Figure 3-11) and for recorded landcover change scenarios (1970-2010; Carpino et al. 2018). The results of the Tukey post-hoc indicated brightness trends were significantly greater ($p < 0.05$) in present-day wetlands (both collapse scars and fens) compared to plateaus (Figure 3-11) and significantly greater ($p < 0.05$) when examining areas that had experienced forest loss compared to areas that had undergone no change. There were no significant differences between brightness trends across areas that had experienced forest loss compared to forest gain. Greenness trends were also significantly greater ($p < 0.05$) in present-day wetlands (both collapse scars and fens) compared to plateaus (Figure 3-11). Greenness trends were similarly greater across pixels that had experienced forest gain compared to forest loss or no change but these differences were not statistically significant. There were no significant differences between wetness trends and present-day landcover class or observed landcover change. When comparing landcovers, there were no significant differences for brightness, wetness or greenness between the two wetland landcovers (*i.e.* collapse scars and fens), only between the wetland landcovers and forest. As such, when brightness, greenness, and wetness trends were plotted across each of

the 10 transects (*i.e.* 10 pixels) at all 10 sites, each point was identified as forest or wetland (Figure 3-12).

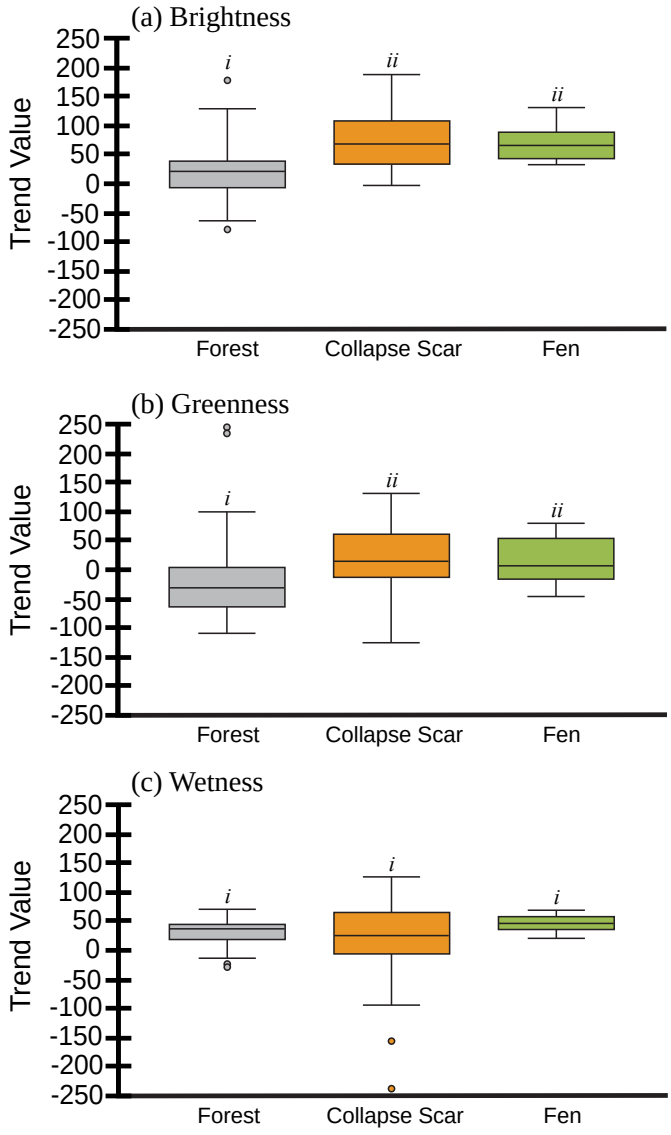

Figure 3-11: Brightness (a), greenness (b), and wetness (c) trend values measured for pixels classified as forested plateau (grey), collapse scar wetland (orange), and channel fen (green). Letters 'i' and 'ii' denote statistically similar groups. The bottom and top of the boxes represent the 25th and 75th quartiles, respectively. The whiskers represent the range of the data while points represent any outliers.

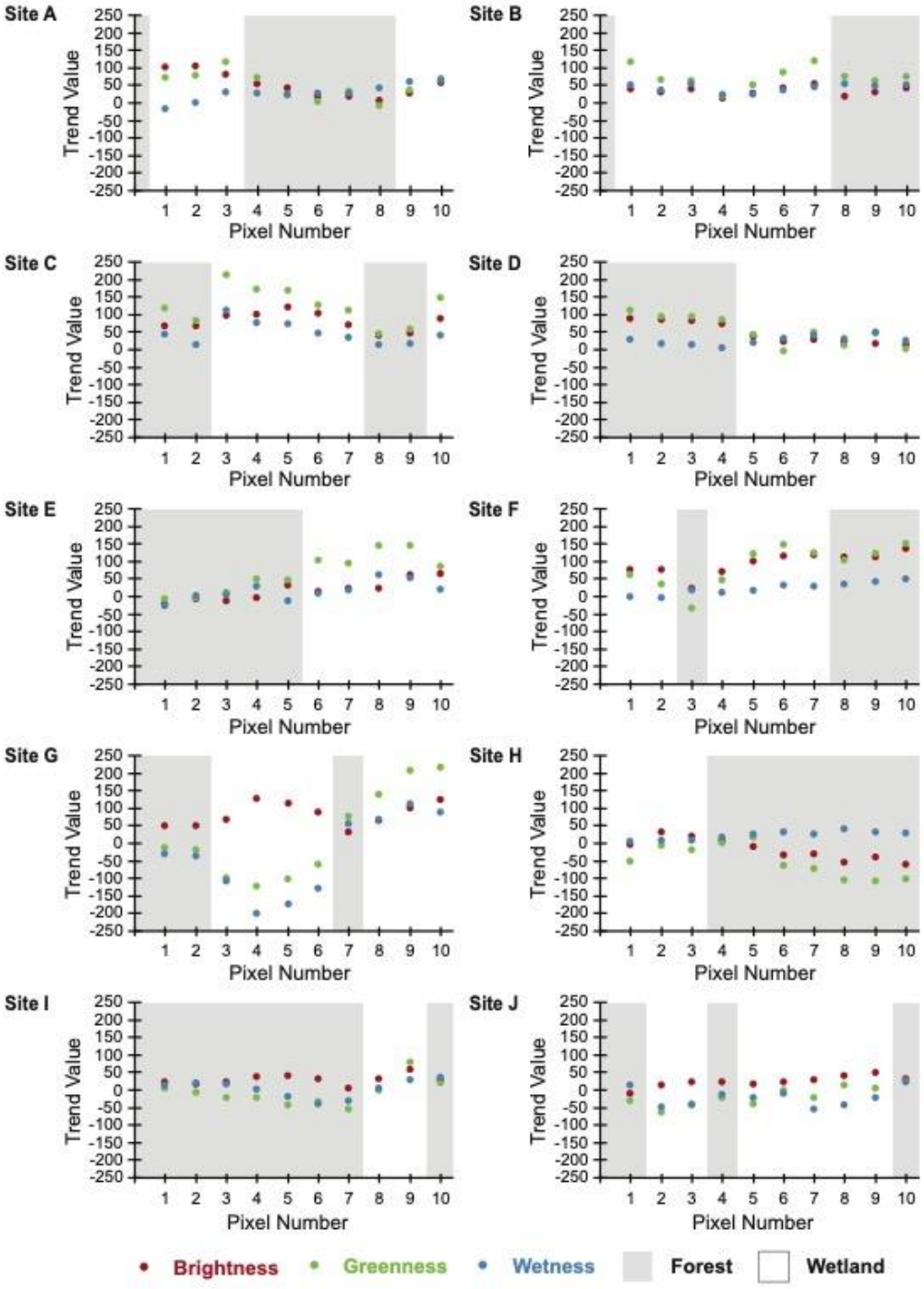

Figure 3-12: Brightness, greenness and wetness trends across a 300 m (10 pixel) transect at 10 sites. Forest and wetland landcover classes along the transect have been identified to represent the landcovers most likely to represent permafrost and permafrost-free ground, respectively.

The trends for brightness, greenness, and wetness were assessed for strength of correlation with landcover class, landcover change (1970-2010), and proximity to the boundary between plateau and wetland. A highly significant positive correlation (*i.e.* $p < 0.01$) emerged between wetness trend values and distance to present-day forested plateaus. This suggests that wetland areas further from forested plateaus have experienced the greatest wetting trend. There were highly significant negative correlations (*i.e.* $p < 0.01$) between brightness and greenness trends with distance to present-day wetlands. A further significant positive correlation (*i.e.* $p < 0.05$) between greenness trends and proximity to present-day forests was also present. Together, these significant correlations suggest that brightness and greenness trends have shown the greatest increases for pixels in or near-to wetland landcovers whereas forested areas and nearby pixels showed lower greenness trend values.

Brightness, greenness, and wetness values for each transect pixel were also plotted as a time series across the 1984-2021 study period. Linear regressions were performed on the time series datasets for each landcover class present along the transect. Brightness values across the study period (Figure 3-13) were greatest for pixels overlying wetland landcovers at eight of ten sites. Of the linear regressions performed on the brightness time series, seven R-squared values emerged as significant at five different sites (three forested plateau best-fit lines & four collapse scar wetland best-fit lines). Across all significant regressions, increasing brightness was observed.

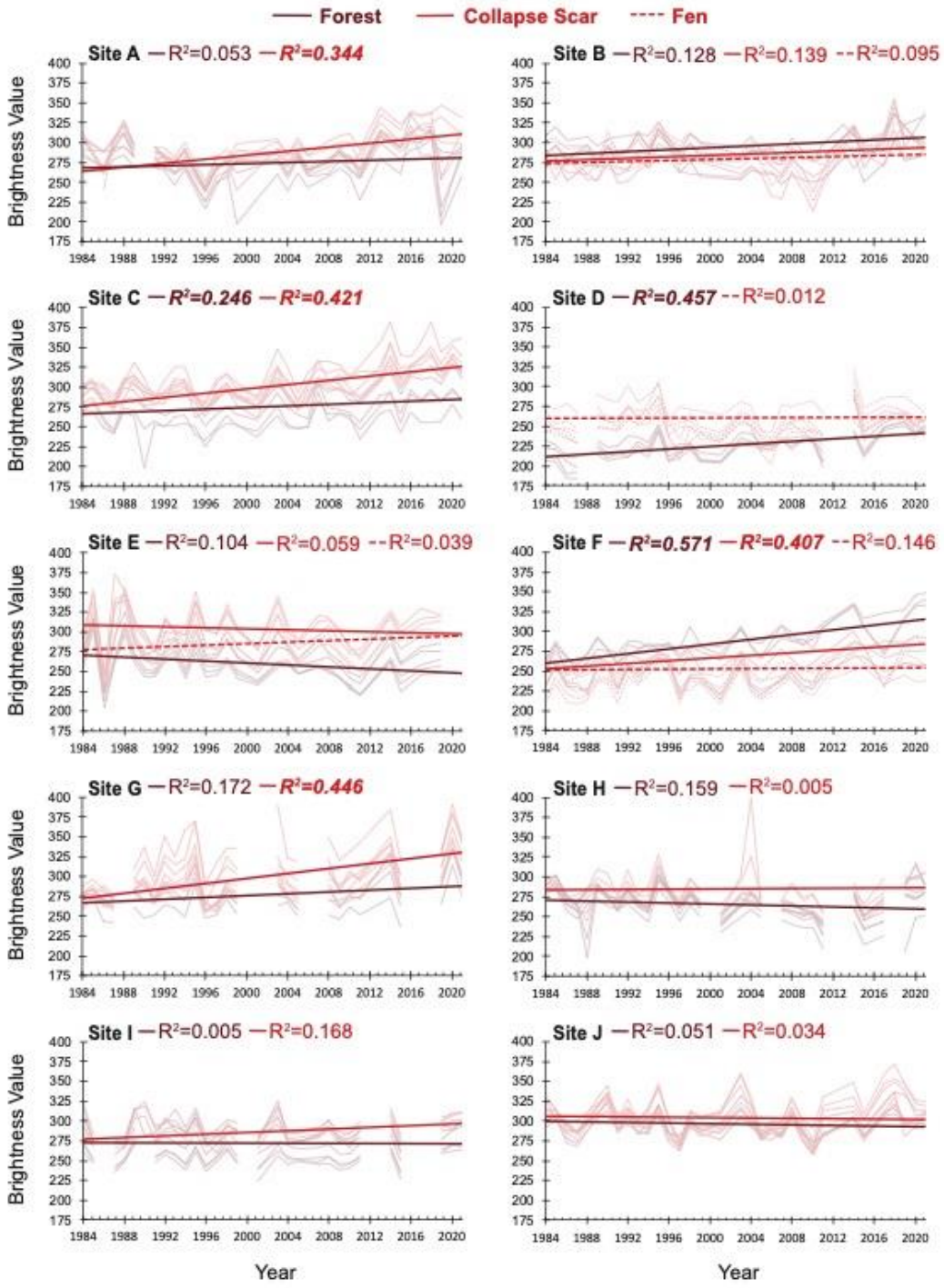

Figure 3-13: Annual brightness time series of 300 m transect (10 pixels) extending across plateau-wetland boundaries at 10 sites. Linear best-fit lines are presented and significant R-squared values have been bolded and italicized.

Greenness values across the study period (Figure 3-14) were also greatest for wetland pixels at nine of 10 sites. For the greenness time series, 13 linear regressions emerged as significant across eight sites (five forested plateau best-fit lines, seven collapse scar wetland best-fit lines and one channel fen best-fit line). Of the significant results, all best-fit lines showed increasing greenness.

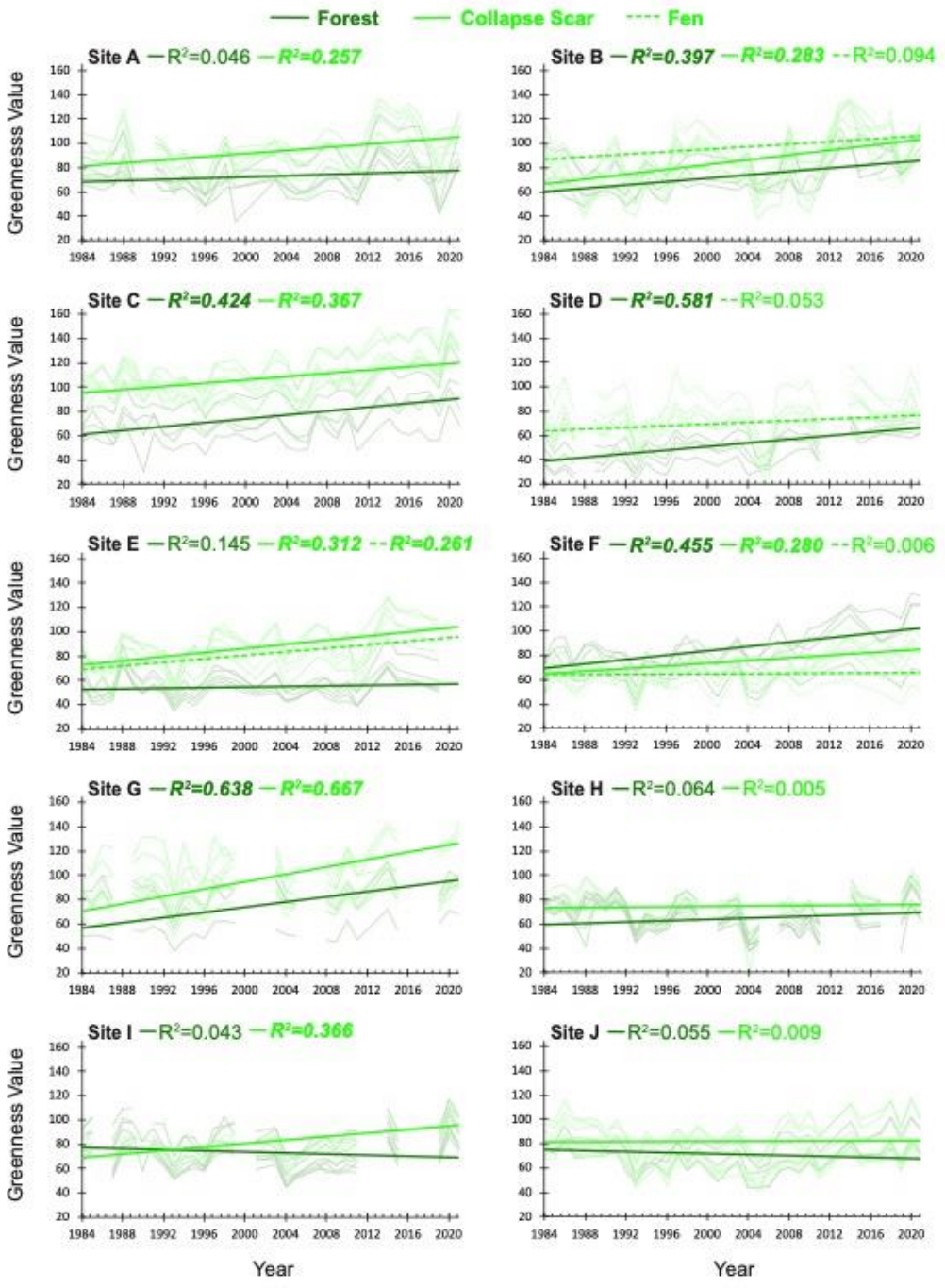

Figure 3-14: Annual greenness time series of 300 m transect (10 pixels) extending across plateau-wetland boundaries at 10 sites. Linear best-fit lines are presented and significant R-squared values have been bolded and italicized.

While wetlands appeared to have greater brightness and greenness pixel values overall, wetness values (Figure 3-15) were largely similar between forested plateaus, collapse scar wetlands, and channel fens. Wetness appeared to be largely unchanged outside of four significant R-squared results at two sites (two forested plateau best-fit lines & two collapse scar wetland best-fit lines), both of which showed decreasing wetness for forests and collapse scars.

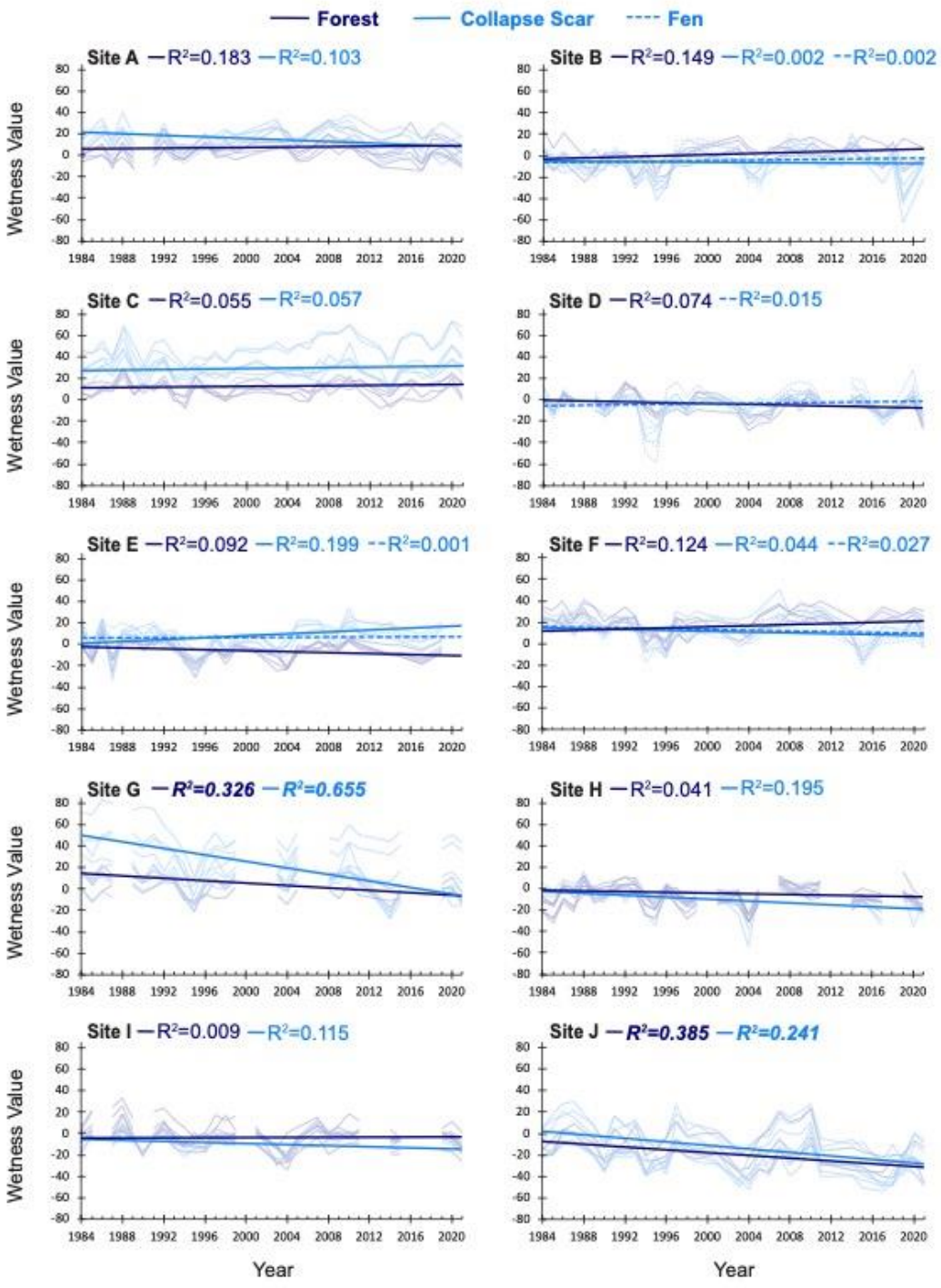

Figure 3-15: Annual wetness time series of 300 m transect (10 pixels) extending across plateau-wetland boundaries at 10 sites. Linear best-fit lines are presented and significant R-squared values have been bolded and italicized.

3.4 Discussion

3.4.1 Brightness

The brightness transformation is indicative of changes to the ground surface and vegetation canopies, particularly with respect to albedo. Wetland brightness values were greater compared to forested areas (Figure 3-11), although both showed increasing brightness trends (Figure 3-13). Brightness trends were also found to be greatest in areas closest to wetlands. While wetlands do generally have higher albedos, there is little variation in ground surface albedo between peat plateaus and wetlands (Connon et al., 2021). Mean wetland albedo (0.15) during the snow-free period (period used in this study) is similar to plateau surfaces (0.11-0.15, dependent on canopy density). The only substantial divergence of albedo between the landcovers is during the late snowmelt period once wetlands have already undergone snowmelt while plateaus are still snow covered (Connon et al., 2021).

Although albedo is similar between landcovers, the amount of incoming solar radiation incident to the ground is dependent on canopy coverage. Permafrost thaw is driven not only by vertical conduction from the ground surface, but also horizontal conduction and advection from adjacent wetlands (Devoie et al., 2021; Walvoord & Kurylyk, 2016). As permafrost thaws, the forested plateau surface subsides and is engulfed by the expanding neighbouring wetlands (Beilman et al., 2001; Helbig, Pappas, et al., 2016; Quinton et al., 2011), possibly explaining why wetland areas as well as the areas nearest to wetlands experienced the greatest brightness trends. Localized decreases of the canopy can increase insolation to the ground (Wright et al., 2009) which drives a thermal and hydrologic feedback that thaws permafrost from above and forms higher albedo collapse scar wetlands on the peat plateau (Quinton et al., 2019; Wright et

al., 2009). This process would explain why forest areas are also increasing in brightness. Continued permafrost thaw leads to widespread surface subsidence, waterlogging of the ground surface, tree mortality, canopy thinning, and thus the complete conversion of forest (lower albedo) to wetland (higher albedo).

The reduction in the areal cover of forested plateaus and the concomitant increase in the coverage of treeless wetlands indicates a transition from areas with a lower albedo and relatively low insolation to one with higher albedo and higher insolation (Devoie et al., 2019; Kurylyk et al., 2016). While this permafrost-thaw induced transition, as well as the associated changes to surface brightness and shortwave radiation, occurs over a number of years to decades (Chasmer et al., 2011), anthropogenic disturbances such as seismic lines, winter roads, or pipelines can have drastic impacts almost immediately. Such disturbances remove tree cover, which leads to permafrost thaw and ground surface subsidence, much like a natural disturbance and the resultant thaw depression. This promotes the accumulation of water in linear disturbances, which cannot regenerate permafrost and instead much more closely resemble a fen (Williams et al., 2013). This instantaneous removal of tree cover may be responsible for the notably different TC trends, including increases in brightness, observed at Site G, where a seismic line intersects the transect.

3.4.2 Wetness

The wetness transformation characterizes changes to moisture and water content in both soil and vegetation. Wetness trends were largely not significant in this study (Figure 3-11). Only two sites showed significant decreases in wetness across the time series for both forest and wetland landcovers (Figure 3-15) and wetland areas furthest from plateaus experienced the greatest wetting trends. While permafrost thaw in these environments transforms forest-

dominated areas to those that are dominated by permafrost-free wetlands (Robinson & Moore, 2000), this also changes the hydrological function of the transformed landscapes. Although not all of these changes appeared significant in this study, permafrost thaw-induced landscape change can have impacts on local drainage processes and pathways (Connon et al., 2014, 2015) as well as on regional-scale hydrology (Connon et al., 2018; Korosi et al., 2017; St. Jacques & Sauchyn, 2009). Many of the hydrologic changes occurring in these systems are also occurring in the subsurface, particularly in the summer season, and therefore may be less discernable using TC transformations compared to changes in surface water levels (Fraser et al., 2014), for example. Nevertheless, changes in brightness and greenness can be used to infer hydrologic change.

As permafrost thaw commences, a forest-dominated landscape underlain by permafrost transitions to one with taliks (Connon et al., 2018) and isolated collapse scar bogs (Quinton et al., 2011). At this stage in the landscape transition, the majority of precipitation inputs are stored in these isolated collapse scars due to the surrounding permafrost margins that prevent collapse scars from draining (Connon et al., 2014; Haynes et al., 2018). This is also the stage where areas towards the centre of wetlands and further from plateau edges would experience the greatest wetness trends. As permafrost thaws, the previously isolated wetlands coalesce, becoming more hydrologically connected (Connon et al., 2014, 2015; Devoie et al., 2019), thereby enabling wetlands to drain and dry (Haynes et al., 2018), which may explain the decreasing wetness trend observed at some sites. Site G is also unique due to the presence of a seismic line, which ultimately also increases hydrological connectivity like natural wetland features, moving water more efficiently off the landscape (Connon et al., 2014; Waddington et al., 2015; Williams et al.,

2013). Eventually, wetlands proliferate and become increasingly connected, creating a landscape dominated by widespread wetland complexes with only isolated plateau islands (Baltzer et al., 2014; Chasmer & Hopkinson, 2017). As these wetlands become more connected they start to drain into channel fens and ultimately experience decreases in wetness over time (Connon et al., 2015). Hydrology in these landscapes has been documented to vary spatially and temporally depending on the degree of thaw and forest fragmentation observed (Baltzer et al., 2014; Connon et al., 2015; Haynes et al., 2018). This variation may impact the TC trends observed in this study.

3.4.3 Greenness

The greenness transformation represents changes to green, healthy vegetation and vegetation density. Greenness trends were greater in wetlands compared to forested plateaus (Figure 3-11). Both wetlands and forests experienced increases in greenness over the study period (Figure 3-14), with the greatest increases occurring for areas in or near wetlands. While the predominant permafrost thaw-induced transition is from forest to wetland (Baltzer et al., 2014; Chasmer & Hopkinson, 2017; Quinton et al., 2011), forest expansion has also been observed (Baltzer et al., 2014; Carpino et al., 2018; Disher et al., 2021). Increases in drainage density (Connon et al., 2014, 2015) and evapotranspiration (Warren et al., 2018), gradually dewater and dry collapse scar wetlands so that they may be suitable for forest reestablishment (Baltzer et al., 2014). Permafrost thaw in plateau-wetland complexes has led to changes in community composition as tree species that are better suited to these new environments begin to establish (Dearborn et al., 2021; Dearborn & Baltzer, 2021). Climate warming has also been proposed as a potential mechanism for forest expansion due to increased primary productivity (Baltzer et al., 2014; Soja et al., 2007).

Forest cover has decreased over recent decades as plateaus become increasingly fragmented (Baltzer et al., 2014). Canopy height and vegetation cover are greatest in the center of plateaus while plateau edges show reduced heights and reduced canopy cover, both indicative of tree mortality (Chasmer et al., 2011). Tree mortality or stunted growth are particularly prominent on southeast to westerly facing plateau edge slopes as well as in areas with lower elevation and closer to the water table (Chasmer et al., 2011). As such, most tree mortality occurs along the boundaries of plateaus and in the saturated margins of surrounding wetlands (Baltzer et al., 2014; Chasmer et al., 2011). Much like permafrost thaw-induced landcover change, anthropogenic developments such as seismic lines, winter roads and drill pads can also initiate the transformation from forested plateaus to treeless, permafrost-free. However, the increased hydrological connectivity and dewatering that accompany wetland expansion appear to enable forest re-establishment and greening.

Expanding hydrological flowpaths that connect collapse scar wetlands to the basin drainage network allow for partial drainage of wetlands and set in motion a sequence of ecohydrological changes (Connon et al., 2014; Haynes et al., 2018, 2020). Forest growth enabled by wetland drainage occurs in less than half a century (Carpino et al., 2021), much quicker than the process of forest regrowth driven by permafrost reestablishment (Treat & Jones, 2018; Zoltai, 1993). The landcover evolution that follows permafrost thaw is also visible in the vegetation succession. As plateaus thaw and collapse scars develop, the thawing margins are occupied by aquatic *Sphagnum* species, notably *S. riparium* (Pelletier et al., 2017), which is easily identified as it is bright green (Gibson et al., 2018; Haynes et al., 2020). As permafrost thaw continues and collapse scars expand, lawn species, such as *S. angustifolium*, and hummock species, such as *S.*

fuscum, begin to establish in the drier wetland interiors (Camill, 1999; Pelletier et al., 2017; Zoltai, 1993), the latter of which is also easily identified due to its russet colour (Haynes et al., 2020). With continued dewatering, *S. fuscum* continues to increase and the density of hummocks expands, allowing young *P. mariana* trees to establish on the relatively dry hummock (Dymond et al., 2019; Iversen et al., 2018) before widespread forest reestablishment is observed (Camill, 2000; Kettridge et al., 2013).

In addition to forest regrowth due to the emergence of hummocky wetland terrain, coupled greening and forest loss can be driven by changes in tree species composition. For example, Dearborn et al (2021) and Dearborn & Baltzer (2021) found NDVI values to be almost exclusively positive despite widespread loss of *P. mariana*. Wang & Friedl (2019) also reported NDVI increases despite coniferous forest loss. Dearborn & Baltzer (2021) note that unlike *P. mariana* and *Betula*, recruitment of *Larix laricina* corresponded positively with NDVI trends. Increasing abundance of *L. laricina* may be responsible for some of the greening trends observed in plateau-wetland complexes as it is more tolerant of the waterlogging that follows permafrost thaw and plateau subsidence compared to *P. mariana* (Islam & Macdonald, 2004). This suggests that *P. mariana*-dominated plateaus may transition to *L. laricina*-dominated wetlands with on-going permafrost thaw. This transition may be concomitant to the forest reestablishment by *P. mariana* in hummocky wetlands (Camill, 2000; Disher et al., 2021; Haynes et al., 2020) or *L. laricina* may be responsible for more of the current boreal greening observed (Dearborn et al., 2021; Dearborn & Baltzer, 2021; Wang & Friedl, 2019).

3.5 Conclusions

Landscape evolution following permafrost thaw appears to be cyclical and northwestern Canada's discontinuous permafrost zone exemplifies a landscape in transition. As this landscape evolves, ground surface energy balances, hydrological regimes, and biophysical characteristics are changing too. The three TC transformations, brightness, greenness, and wetness can be used to monitor these changes. Permafrost thaw transforms forest-covered peat plateaus through several stages of wetland cover culminating in a permafrost-free forest. Identification of the transitional stages and the time taken to re-establish forest has helped to clarify the rate and trajectory of permafrost thaw induced changes to landcovers in the study region. We suggest the initial stages of permafrost thaw-induced forest loss are best described by increases to brightness and wetness, although forest loss due to anthropogenic disturbance is dominated by brightness increase. As the landscape continues to evolve following permafrost thaw, wetness remains steady while greenness increases. The exact mechanisms for peatland greening may be dependent on local factors including soil moisture trajectory.

CHAPTER 4: Permafrost distribution in northwestern Canada's sporadic-discontinuous permafrost zone

4.1 Introduction

Permafrost is a critical foundation for much of Canada's boreal landscape as it exerts a primary control on surface geomorphology (Olefeldt et al., 2016), surface and subsurface hydrological processes (Hinzman et al., 2005; Quinton et al., 2011), and landscape ecology (Baltzer et al., 2014). As a result, permafrost thaw and degradation can have profound implications on these landscapes at both local and regional scales. As such, the significance of permafrost to Canada's north provides strong justification for comprehensive mapping. However, the discontinuous permafrost zone is inherently defined by variability when it comes to permafrost presence or absence across the landscape, emphasizing the complexities of this environment as well as the importance of ongoing mapping efforts.

Canada's northwestern boreal region largely falls within the discontinuous permafrost zone, which is vulnerable to climate change-induced permafrost thaw (Box et al., 2019). This vulnerability is largely due to warming air temperature, increased rain-on-snow events, and a shift towards earlier spring snowmelt – all of which have the potential to increase permafrost degradation (Hinzman et al., 2005; Smith & Riseborough, 2010). Additionally, permafrost across Canada's southern discontinuous permafrost zone is already relatively thin and warm (*i.e.* near to 0ºC) (Holloway & Lewkowicz, 2020; Smith et al., 2005). As a result, permafrost thaw-induced changes are disrupting the discontinuous permafrost zone's land and water as well as the human activities that depend on them. Not only do these factors present meaningful challenges to current investigations of how climate warming might affect the permafrost in these regions, but

they also provide strong justification for improving the existing understanding of permafrost distribution and evaluating permafrost condition on a continual basis.

Permafrost maps typically rely on an existing understanding of the conditions that contribute to permafrost distribution (Bonnaventure & Lamoureux, 2013; Bonnaventure & Lewkowicz, 2011) and there are an increasing number of geomatics products that relate to permafrost at a national or circumpolar level. However, the fine-scale data that would be most helpful in studying permafrost distribution and used for producing detailed maps is mostly isolated to a narrow subset of the region such as communities, infrastructure corridors, or research stations. While these datasets are geographically restricted due to the remoteness and size of the region, data availability is significantly enhanced with geomatics products combined with GIS platforms, which can be used to estimate broad-scale distributions of permafrost landscapes. When used in combination with existing knowledge of permafrost landscapes, such methods can determine the spatial distribution of a variety of factors that contribute to permafrost presence or absence.

High resolution permafrost distribution maps and models have been created for a number of Canadian regions over a range of scales and climatic zones (*e.g.* Bonnaventure et al., 2012; Bonnaventure & Lewkowicz, 2011; Lewkowicz & Bonnaventure, 2008; Lewkowicz & Ednie, 2004). It is critical to develop higher resolution permafrost mapping products compared to the coarse resolution, broad-scale maps that are most readily available. Northern communities rely on permafrost maps as an essential element in development and infrastructure planning, resource management, and climate change adaptation. Additionally, it is also important to develop products using data and methods that are approachable and easily and fully accessible by

researchers and these communities, as is the case with freely available geomatics products and GIS platforms. Importantly, these approaches can help with uptake and also helps ensure methods are transferrable across similar circumpolar regions.

This paper aims to develop an improved understanding of permafrost distribution across the discontinuous permafrost zone. While permafrost zone delineations (*e.g.* Brown et al., 2002; Heginbottom & Dubreuil, 1993) are very useful at coarse scales, such maps are at a disadvantage as they can supress the heterogeneity that is present at finer scales, particularly in the discontinuous permafrost zone (Spence et al., 2020). The goal of this study is to develop and apply a conceptual framework for permafrost distribution using the factors responsible for permafrost distribution in this environment that are also readily available through geomatics datasets. The overall objective of this paper is to improve the understanding of the surface conditions governing the occurrence and distribution of permafrost, an important step toward producing a high resolution product needed by northern communities and other stakeholders for their resource planning and management needs. Specifically, this paper will a) identify the key factors that determine permafrost presence in a landscape; b) use these factors to develop a permafrost map for the southern discontinuous permafrost zone in the Hay-Slave Lowlands ecoprovince of northwestern Canada; and c) present a conceptual approach to help guide permafrost map development according to its intended use.

4.2 Study Region

The Taiga Plains ecozone is an area of low-lying plains with poor drainage and thick organic deposits in northwestern Canada and is bounded by the Taiga Cordillera ecozone to the west and Taiga Shield ecozone to the east. The Taiga Plains developed with the recession of the

Laurentide Ice Sheet and the region is characterized as a dry continental climate with short summers and long, cold winters. Permafrost in the Taiga Plains is relatively thin and warm (Holloway & Lewkowicz, 2020; Smith et al., 2005) and therefore, permafrost is predominantly found in peatlands (*e.g.*, peat plateaus and palsas) due to the insulating properties of unsaturated peat (Brown, 1964; Quinton & Baltzer, 2013; Woo, 2012). As such, this is a particularly important factor for maintaining permafrost in the warmer and more southerly portions of the Taiga plains. Peatlands cover almost half of the total Taiga Plains area (McClymont et al., 2013; Tarnocai, 2009), largely within a central corridor along the Dehcho River (Gibson et al., 2021; Wright et al., 2022).

This study is focused on the 230,000 km^2 Hay-Slave Lowlands, an ecoprovince of the Taiga Plains which is predominantly within the sporadic-discontinuous permafrost zone (10-50% areal coverage of permafrost), with smaller areas in the extensive-discontinuous zone (50-90%) to the north and isolated zone (<10%) to the south (Figure 4-16). This ecoprovince is central to where the borders of the Northwest Territories, British Columbia, and Alberta meet. The Hay-Slave Lowlands extends between 57º N and 63º N, and has a mean annual air temperature (MAAT) range between 2.0°C in the southernmost areas to approximately −3.0°C in the north (Vincent et al., 2020). This latitudinal span is of particular note as it has been experiencing significant climate warming, largely due to observed increases during winter and spring months (Vincent et al. 2012). Additionally, Gibson et al. (2021) noted that peatlands south of 62°N exhibit characteristics that indicate a high degree of thaw.

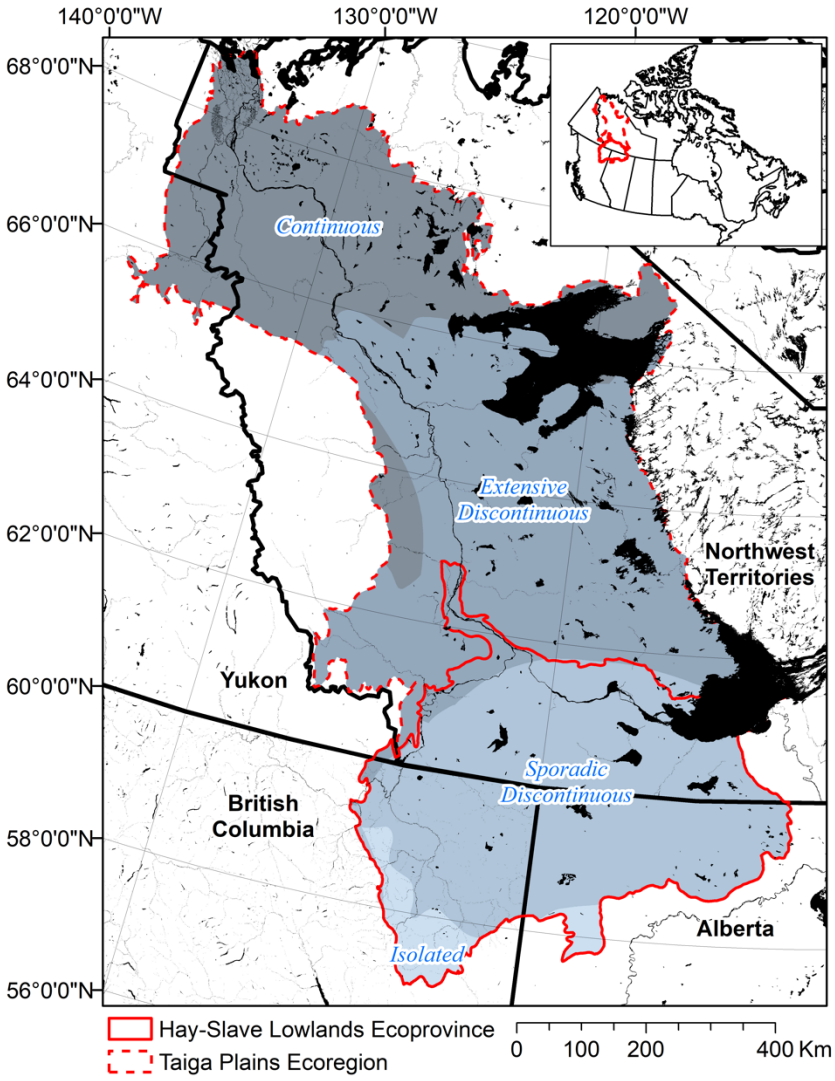

Figure 4-16: Hay-Slave Lowlands ecoprovince (solid red) across the southern extent of the Taiga Plains ecoregion (dashed red). Permafrost zones are displayed within the Taiga Plains: Isolated (<10%), Sporadic-Discontinuous (10-50%), Extensive-Discontinuous (50-90%) and Continuous (>90%). Inset shows Hay-Slave Lowlands and Taiga Plains relative to Canada.

Forested peat plateaus are the most common permafrost landform in the southern Taiga Plains, though palsas are also found in smaller numbers (Wright et al., 2022). Peat plateaus are most commonly found in wetland environments and are comprised of frozen peat that is elevated

above the surrounding wetland surface (Brown, 1964; Zoltai & Tarnocai, 1975). Peat plateaus typically have 1.5 – 8 m of vertical peat depth overlying fine grained mineral sediments such as silts and clays (Zoltai & Tarnocai, 1975). As these features are elevated above surrounding wetlands, peat plateaus are also distinguishable as they maintain a cover of black spruce (*Picea mariana*) as the peat is sufficiently dry to support the black spruce forest's shallow root systems (Islam & Macdonald, 2004).

The surrounding wetlands include channel fens and collapse scar wetlands, the latter of which is a thermokarst feature that develops following the thaw of the permafrost underlying the plateau features (Robinson & Moore, 2000). As the permafrost thaws, the plateaus collapse along their margins causing the ground to subside and become inundated by the surrounding wetlands (Zoltai, 1993). As such, permafrost thaw in this environment transforms forests to treeless, permafrost-free wetlands (Robinson & Moore, 2000). These collapse scar wetlands can be isolated and found within plateaus where they are relatively small features or can be larger and interconnected features that drain to the channel fens, which move water off the landscape towards the basin outlet (Connon et al., 2014; Quinton et al., 2009; Vitt et al., 1994). While peat plateaus throughout the lowland areas of this region are the predominant permafrost landform, permafrost can also be found in upland areas with fine-grained mineral sediment with an organic layer no shallower than 0.3 m (Holloway & Lewkowicz, 2020). These areas are distinguishable as they have a mixed forest-cover and are areas elevated above the low-lying plains that dominate much of the region (Holloway & Lewkowicz, 2020). Ultimately, beyond temperature, thick organic layers are the most significant control on permafrost presence in this region,

followed by fine-grained soil types, which also commonly maintain permafrost (Wright et al., 2022).

As evidenced by the forest covers that dominate the lowlands and uplands of the region, the Hay-Slave Lowlands are predominantly covered by boreal forest with needleleaf trees interspersed with more contained areas of broadleaf trees (Wright et al., 2022). Both broadleaf forest and mixed-forest types appear to be increasingly common with decreasing latitude. There are also isolated areas of shrubland, grassland, and lichen-moss-dominated environments, the latter of which is most common across elevated terrain types. Elevations in the Hay-Slave Lowlands range from approximately 150 m above sea level (asl) along the shores of Great Slave Lake to greater than 1500 m asl in the foothills of the Northern Rocky Mountains. Other terrain features that are distinctly elevated above the surrounding region include the Cameron Hills (~600-850 m asl) and the Caribou Mountains (~700-900 m asl).

4.3 Methods

4.3.1 Data Sources

The permafrost distribution map was developed using a combination of factors. Each factor was selected based on two main criteria. Firstly, that the factor has a significant impact on distribution in the Hay-Slave Lowlands and secondly, that a pan-Canadian spatial data set was publicly available at a resolution that was appropriate for this study (≤ 100 x 100 m) (Table 4-2). The latter criterion eliminated some potential factors, including any measure of ground temperature that would be appropriate for this study. All datasets were used at or aggregated to a resolution of 100 m in a NAD 1983 coordinate system with a Lambert Conformal Conic projection before being masked to the boundaries of the Hay-Slave Lowlands.

Table 4-2: Data sources for each factor.

Factor	Dataset	Source
Air Temperature	- Mean Annual Air Temperature (MAAT)	- https://climate-change.canada.ca/climate-data/#/adjusted-station-data
Elevation	- Canadian Digital Elevation Model (CDEM)	- https://open.canada.ca/data/en/dataset/7f245e4d-76c2-4caa-951a-45d1d2051333
Soil Condition	- Soil Organic Carbon Content - Soil Taxa - Saturated Soils	- https://bolin.su.se/data/ncscd/shape.php - https://bolin.su.se/data/ncscd/shape.php - https://open.canada.ca/data/en/dataset/80aa8ec6-4947-48de-bc9c-7d09d48b4cad
Landcover	- Landcover (2020) - Landcover (2015)	- https://open.canada.ca/data/en/dataset/ee1580ab-a23d-4f86-a09b-79763677eb47 - https://open.canada.ca/data/en/dataset/4e615eae-b90c-420b-adee-2ca35896caf6

The air temperature dataset is a homogenized and statistically adjusted product created by Vincent et al. (2020). Mean annual air temperature (MAAT) was downloaded for all stations located within the Hay-Slave Lowlands study region boundaries as well as stations within 100 km of the study region boundary. Stations were also selected based on time frame of data collection, with a target of MAAT data collected between 2010-2019. The total number of selected stations used for this study was 42. For each station MAAT was averaged across the available annual data, with a minimum record length of 2010-2014. As this data is point-form, an interpolated raster dataset was created using the Inverse Distance Weighted tool in ArcGIS (ESRI, Redlands, California). The Spline with Barriers tool was also used along the western boundary of the Hay-Slave Lowlands so as not to falsely relate temperatures collected in nearby mountainous terrain with the temperatures across the lowland-dominated terrain that is more typical of the study region.

The digital elevation model used for this study was the Canada Digital Elevation Model (CDEM; NRCan, 2015). While higher resolution elevation data exists such as the ArcticDEM

(Porter et al., 2018) and the High Resolution Digital Elevation Model (HRDEM; NRCan, 2022), the CDEM is continuous across the study extent. The ArcticDEM is only available north of 60° N and gaps still exist within the study region. The HRDEM also relies on the ArcticDEM across northern Canada and similarly, gaps exist within the study region as this product is still being developed across the rest of the country. To avoid patching or potential issues with integration or edge-matching, the CDEM was selected for this study. The CDEM was also used to create two additional datasets: aspect and potential incoming solar radiation (PISR). Both were created in ArcGIS. The former was done using the Aspect tool while the latter used the Area Solar Radiation Toolset in 1° latitude increments before merging the resultant rasters together.

Three different factors related to soil condition were selected for this study. The Soil Organic Carbon Content and Soil Taxa datasets are different attributes within the Northern Circumpolar Soil Carbon Database (NCSCD; Bolin Centre for Climate Research, 2013). The NCSCD is based on polygons from regional soil maps across the north. Soil Organic Carbon (SOC) content is expressed as kg/m^2 between 0 – 3 m depth within each polygon and Soil Taxa is expressed as fractional areal coverage for each soil within the polygons. The saturated soils dataset (NRCan, 2017) is similarly a polygon dataset and outlines areas that are likely wetland-dominated terrain. All soil condition datasets were converted to rasters using ArcGIS.

The landcover datasets (NRCan, 2020; NRCan 2015) were created by the Canadian Centre for Remote Sensing for Natural Resources Canada using observation from the Operational Land Imager Landsat sensor (30 m resolution). An accuracy assessment of the products based on randomly distributed samples showed ~ 87% accuracy for 2020 and ~ 80% accuracy for 2015 (NRCan, 2020; NRCan 2015). The 2015 and 2020 products were created

using different methodologies, and while NRCan (2020) note that the 2020 product is an improvement over the 2015 product, there are differences in the landcover classes used including in landscapes that are particularly relevant to permafrost distribution in this region. For the purposes of this study, the 2015 product provided useful delineation beyond the 2020 product within areas thought to be peatland-dominated terrain based on agreement with manual classifications completed on some of these areas within the study region (Carpino et al., 2018). As such, both landcover datasets were used in this study. The 2020 dataset was used for general landcover across the study region while landcover was also combined with the saturated soils dataset (using 2015 product) and the digital elevation model dataset (using 2020 product) to more wholly account for the landcovers that contribute to permafrost likelihood across these differing circumstances. Waterbodies were masked out from the study region and displayed as "NoData" so that they were automatically excluded from the map.

4.3.2 Permafrost Map

The permafrost map was created by summing the values of each factor listed in Table 4-2 for each 100 m x 100 m cell in the Hay-Slave Lowlands. This additive index therefore represents the combined effects of air temperature, elevation, soil condition, and landcover. Each factor included multiple datasets that were ranked from 0-1.0 based on the likelihood that condition was to individually contribute to permafrost presence, with 0 being very unlikely to 1.0 being very likely (Table 4-3). Ranks were also in some cases based on the variability within each factor including across classifications and the range of values present.

Table 4-3: Ranked values for each dataset. Ranks range from 0-1.0 with larger values indicating greater likelihood of that factor contributing to permafrost presence. Units, when relevant, are included as part of the dataset information column.

Factor	Dataset	Ranked Value										
		0	0.1	0.2	0.3	0.4	0.5	0.6	0.7	0.8	0.9	1.0
Air Temperature	- MAAT (°C)	>0	0- -0.5		-0.5- -1		-1- -1.5		-1.5- -2		-2- -3	<-3
	- MAAT >0 (°C)	>0										<0
Elevation	- CDEM (m asl)	<500	500-600			600-700				700-800		>800
	- Aspect	S	SE, SW		W	E				NE, NW		N
	- PISR (WH/m^2 $x10^5$)						>7.0					1.9-7.0
Soil Condition	- SOC (kg/m^2)	0	0-1	1-3	3-5	5-10	10-15	15-20	20-25	25-30	30-40	>40
	- Gelisol (%)	<5	5-10	10-20	20-30	30-40	40-50	50-60	60-70	70-80	80-90	>90
	- Histosol (%)	<5	5-10	10-20	20-30	30-40	40-50	50-60	60-70	70-80	80-90	>90
	- Histel (%)	<5	5-10	10-20	20-30	30-40	40-50	50-60	60-70	70-80	80-90	>90
	- Saturated Soils	No										Yes
Landcover	- Landcover (2020)	Crop, Urban		Broadleaf Forest,		Barren	Grass	Shrub	Mixed Forest, Lichen-Moss	Needleleaf Forest		Wetland
	- Elevated Terrain Landcover (2020)	Crop, Urban		Broadleaf Forest,			Grass, Barren		Shrub	Needleleaf Forest	Mixed Forest, Lichen-Moss	Wetland
	- Saturated Soils Landcover (2015)	Crop, Urban, Broadleaf Forest, Grass, Barren	Wetland		Mixed Forest		Shrub, Lichen-Moss					Needleleaf Forest

Due to the difficulty of objectively deciding the importance of each factor, no weights were assigned to the factors in this study. Instead, each factor was included by averaging the ranks of each dataset in hopes of minimizing any bias associated with an individual factor. As this map was created using an additive index, each factor was treated as an arithmetic mean of the individual datasets to ensure each factor was assigned a single value (Alessa et al., 2008). The resultant means of each of the four factors: Temperature (F_T), Elevation (F_E), Soil (F_S) and Landcover (F_L) were then summed:

[Eqn. 4-1] $$Permafrost\ Index = F_T + F_E + F_S + F_L$$

This method was largely based on Spence et al. (2020) and Alessa et al. (2008). While those works used the method to assess an environment's vulnerability to permafrost thaw, many similar datasets were used and many other mapping methods specific to permafrost probability (*e.g.* Bonnaventure et al. 2012) rely heavily on field-collected ground temperature data, which is not readily available across this region at a scale that would be appropriate for the objectives of this study. While ground temperature would be most appropriate and recent increases in air temperature have introduced uncertainty to permafrost mapping (Spence et al., 2020), air temperature has been used to map permafrost condition (Gruber, 2012). The air temperature factor included two ranks of the same dataset, first ranking MAAT at intervals across the entire MAAT range within the study boundaries, and second ranking MAAT as a binary of above or below 0°C. The temperature factor was calculated as:

[Eqn. 4-2] $$F_T = \frac{MAAT_{range} + MAAT_{binary}}{2}$$

The elevation factor is also made up of multiple datasets. The first component uses the CDEM to highlight areas of high elevation relative to the surrounding region as areas that contribute to permafrost likelihood. The second component uses aspect to rank directions with the understanding that north-facing slopes will receive significantly less solar insolation, and thus a higher rank, than south-facing slopes given the northern location of this study region. The third elevational component is PISR, which was ranked based on the potential incoming solar radiation that a cell would receive annually with lower values receiving a higher rank and higher values receiving a lower rank. The elevation factor was calculated as:

[Eqn. 4-3] $$F_E = \frac{CDEM + Aspect + PISR}{3}$$

Soil conditions similarly contribute to the likelihood of finding permafrost in a given cell. While no pan-Canadian database of organic layer thickness exists, SOC content from the Northern Circumpolar Soil Carbon Database (Hugelius, Bockheim, et al., 2013) was used. Areas with high SOC were ranked higher than areas with low SOC due to the insulating properties of deep peat (Zoltai & Tarnocai, 1975). Similarly, areas with high areal cover of Gelisols, Histosols, or Histels were also ranked highly. The three soil taxa included were already in percentage form, which was directly paired with the corresponding rank number. The saturated soils dataset was ranked as a binary of either 0 or 1, with the latter representing the targeted wetland-dominated terrain. The soil condition factor was calculated as:

[Eqn. 4-4] $$F_S = \frac{SOC+Gelisol+Histosol+Histel+SaturatedSoils}{5}$$

Finally, three different components were included in the landcover factor. The first was the 2020 landcover classification across the entire study region, which targeted landcovers that may correspond with possible permafrost terrain. The second was created using the 2020 landcover dataset but only covered areas identified as high-elevation terrain. The third was created using the 2015 landcover dataset across only the areas identified as wetland-dominated per the saturated soils dataset. In all instances, landcovers that were most likely to be associated with underlying permafrost were ranked highest while landcovers that were less likely to be associated with permafrost were ranked lower. In addition to landcovers that have a moderate chance of being underlain by permafrost, landcovers that have no distinct or consistent relationship with permafrost were also ranked as a moderate value. The landcover factor was calculated as:

[Eqn. 4-5] $$F_L = \frac{Landcover_{regional} + Landcover_{elevation} + Landcover_{saturated}}{3}$$

All rankings were applied in ArcGIS using the Reclassify tool and the subsequent calculations for the factors as well as the overall permafrost index were completed using Raster Calculator.

4.3.3 Validation

The permafrost map was validated in two ways (Table 4-4). Firstly, the map was compared with the Brown et al. (2002) permafrost map and the corresponding areal extent percentages. Brown et al. (2002) was selected as it is a commonly referenced permafrost zone map in Canadian research. The comparison was completed using Zonal Statistics in ArcGIS with the average values for the map in this study across the Brown et al. (2002) permafrost zones. Secondly, 1464 validation points in the form of borehole point data were collected from five sources (Table 4-4).

Table 4-4: Data sources for map validation.

Validation Method	Category	Spatial Summary	Source
Permafrost Zones	- Isolated (<10%)	- ~20,000 km^2 (British Columbia & Alberta)	- https://nsidc.org/data/ggd318/versions/2
	- Sporadic (10-50%)	- ~197,000 km^2 (Northwest Territories, British Columbia, Alberta & Yukon)	- https://nsidc.org/data/ggd318/versions/2
	- Extensive (50-90%)	- ~15,000 km^2 (Northwest Territories)	- https://nsidc.org/data/ggd318/versions/2
Permafrost Point-Data	- Thermistors & Frost Table (Carpino et al.)	- 11 points (Northwest Territories & British Columbia)	- Data in prep.
	- Seismic Shothole	- 514 points (Northwest Territories & Yukon)	- https://doi.org/10.4095/290974
	- Permafrost Information Network (PIN)	- 850 points (Northwest Territories & Alberta)	- https://gin.gw-info.net/service/api_ngwds:gin2/en/data/standard.download.html?ID=249

- Holloway & Lewkowicz (2020)	- 65 points (Northwest Territories & Alberta)	- https://doi.org/10.1002/ppp.2017
- Global Terrestrial Network for Permafrost (GTNP)	- 24 points (Northwest Territories & Alberta)	- http://gtnpdatabase.org/boreholes

Despite the large number of validation points, the vast majority are located in the northern half of the study region in the Northwest Territories (Figure 4-17). There are very few validation points in British Columbia, which is a clear information gap and acquiring or collecting such data will be a future step needed for this work. The validation points are also predominantly along highways and waterways, leaving large swaths with no validation points (including all elevated terrain areas) due to limited data availability and the remoteness of the region. In addition to falling within the study region, these 1464 permafrost borehole data points were also selected with the following criteria. Any data that was last collected before 1970 was removed and any recorded permafrost thicknesses less than 10 m was removed if the data were collected before 2000 or if the data was undated. This was largely done to improve confidence in the validation points based on conservative estimated thaw rates (Devoie et al., 2021). Permafrost borehole data were converted from subsurface temperatures to a binary of permafrost present or absent for this study's purposes. Of the 1464 permafrost borehole validation points, permafrost was present at 801 versus absent at 663.

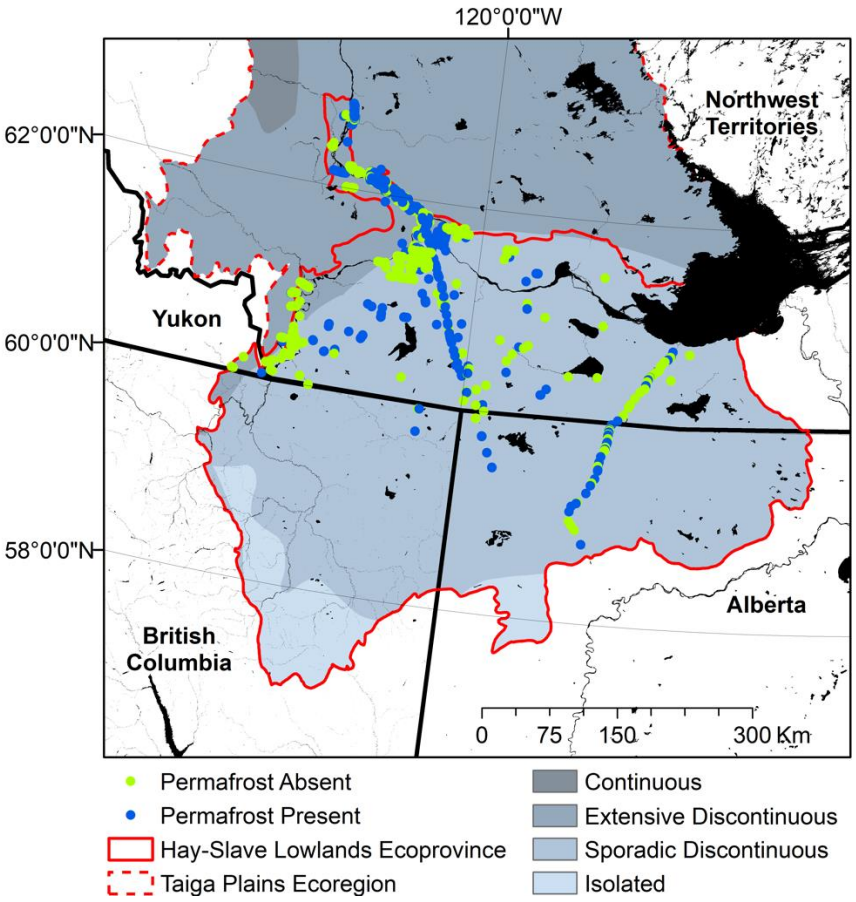

Figure 4-17: Distribution of validation points across Hay-Slave Lowlands. Permafrost zones are also displayed.

4.4 Results and Discussion

The permafrost index was mapped across the Hay-Slave Lowlands for a possible range of 0.0-1.0 (Figure 4-18). The mean index value for all cells within the study area was 0.43 and the median was 0.40, while the range of values extended from 0.0 to 1.0. The standard deviation was 0.23, indicating high variability across the study region.

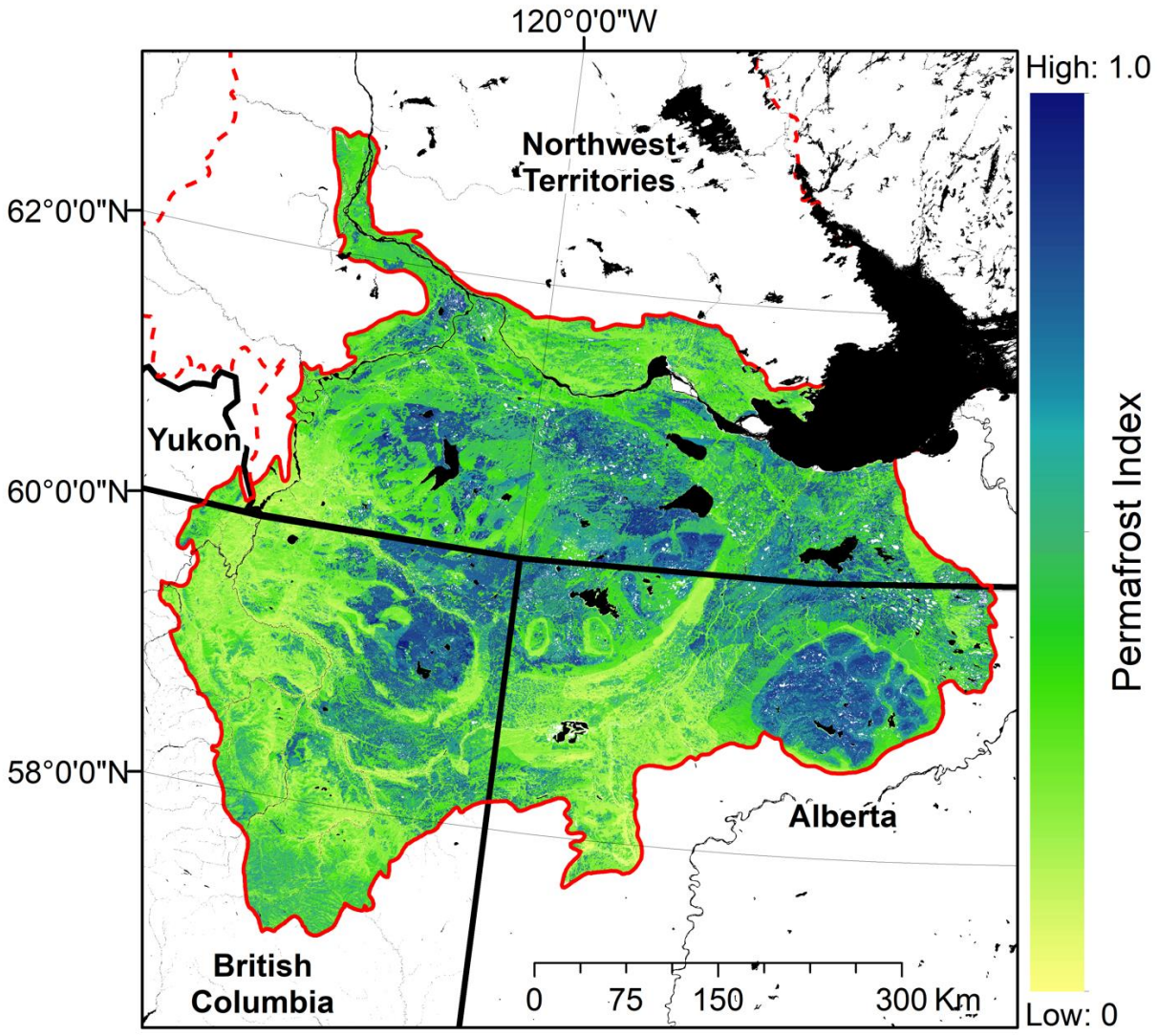

Figure 4-18: Permafrost index map for Hay-Slave Lowlands. White areas represent "NoData" areas outside the study region or small water bodies that were masked out of the map. Large water bodies continue to be displayed in black for legibility and to help orient the reader.

The highest index values were found in the region's peatland-dominated environments and areas of high elevation. The highest index values required the additive contributions of many factors. In the case of peatland-dominated areas, the relationship between the saturated soils and

landcover datasets is particularly evident (Figure 4-19a & b). One such area is the well-studied drainage basin of Scotty Creek (Figure 4-19a; 61.3ºN, 121.3ºW) south of the confluence of the Liard and Mackenzie rivers. Here, only tree-covered peatlands (*i.e.* peat plateaus) have index values that indicate a high likelihood of permafrost (0.78-0.85). The surrounding treeless wetlands (*i.e.* collapse scars and channel fens) have much lower permafrost index values (0.35-0.54). Similar patterns were found in the peatland-dominated area further south (Figure 4-19b; 59.7ºN, 120.8ºW), where the tree-covered peatlands had values ranging from 0.71-0.81 while the values of the surrounding treeless wetlands ranged between 0.30-0.58. Areas identified by the binary saturated soils dataset also corresponded with highly ranked characteristics in the other soil condition datasets, contributing to the high index values across these peatland-dominated regions. The variability within the forest cover of the peat plateaus and within the wetlands are likely due to the cumulative impacts of the other factors, particularly the datasets associated with aspect and PISR (Jorgenson et al., 2010; Shur & Jorgenson, 2007).

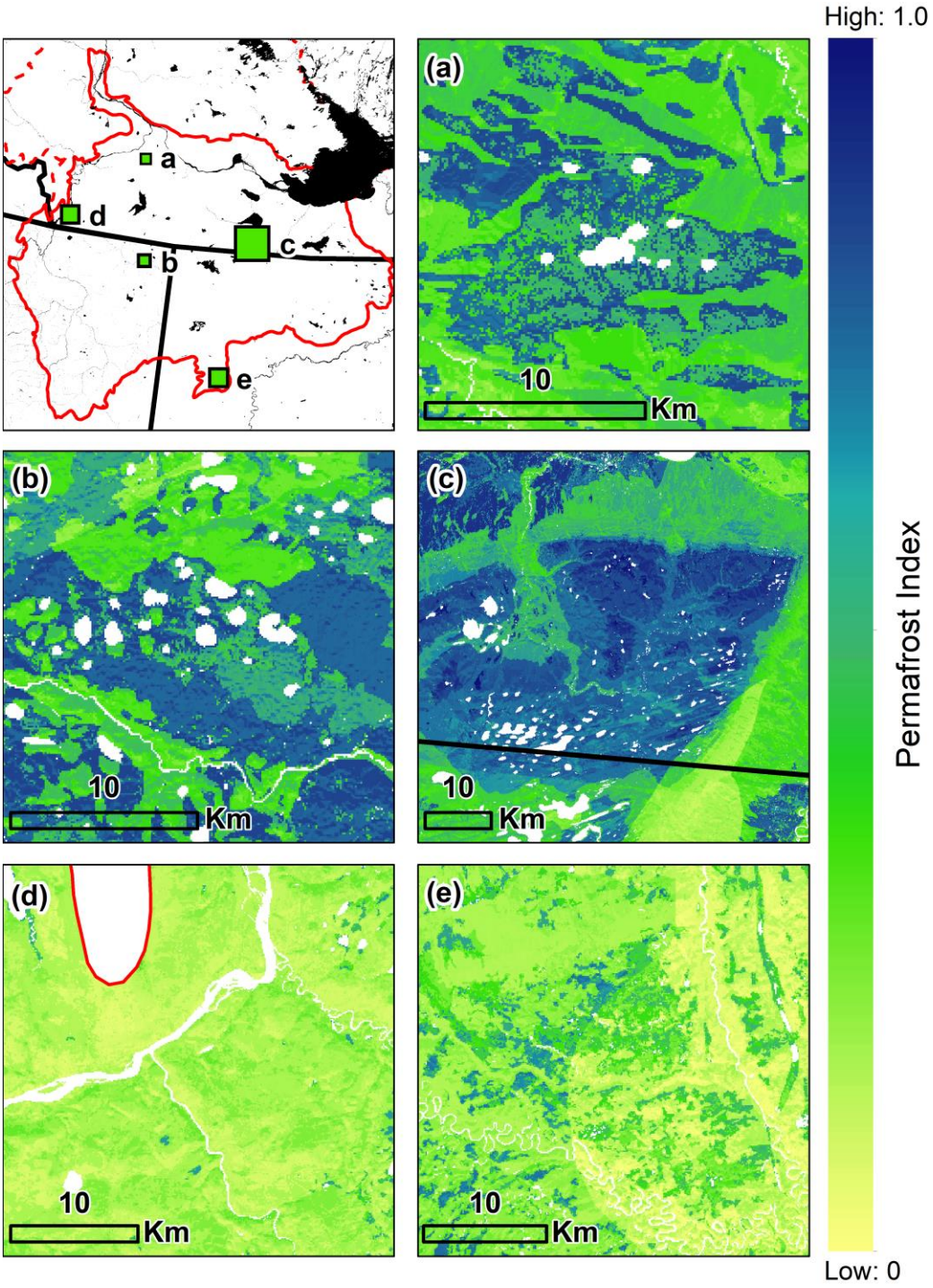

Figure 4-19: Areas of interest displaying high and/or low permafrost index values. The top left shows locations of areas of interest within the Hay-Slave Lowlands. Permafrost index values for peatland-dominated terrain (a & b), elevated terrain (c), and mid-boreal plain (d & e). Scotty Creek basin, a well-studied research site, is present in (a).

In addition to the peatland-dominated terrain, which is largely highlighted by the soil condition factors, elevated terrain is also highlighted as having high permafrost likelihood, most notably parts of the Cameron Hills and the Caribou Mountains. While the greatest elevations occur in the southwestern corner of the Hay-Slave Lowlands, the effect of elevation on the permafrost index there is countered by its relatively high MAAT owing to its relatively low latitude. The northwestern portion of the Cameron Hills is just north of the Northwest Territories-Alberta border (Figure 4-19c; 60.1ºN, 117.6ºW). This area has notably higher permafrost index values than the surrounding region due to its elevation but small-scale variability within the elevated area is also present. Within this area, cell values range from 0.60-1.0, with values of 0.84-1.0 reflected in the highest elevations with north-facing slopes that also have organic or fine-grained soils and wetland, needleleaf forest, or moss-lichen landcovers. The more moderate values across this elevated area are mostly located on south-facing slopes with more diverse soil types.

Despite having similar latitudes, just beyond the boundaries of the highlighted elevated areas are two areas with notably lower permafrost index values (Figure 4-19c). One such region is to the north of the Cameron Hills along the deeply incised Cameron River valley (0.26-0.48). In combination with the lower elevation, the lower values are largely due to the predominance of well-drained soil types on the valley slopes as well as broadleaf or mixed forest types. On the opposite, south-facing side of the Cameron Hills slopes, there is another area of low permafrost index values (0.09-0.25). This low value area is largely due to its south and southeast aspect, coarse grained soil type (*e.g.* sands and rocks), and broadleaf or mixed forest paired with areas of barren ground in areas of recent mass movements. Other low index value regions occur in more

mid-boreal areas along the western edge of the Hay-Slave Lowlands (Figure 4-19d) and in the southernmost isolated permafrost area in Alberta (Figure 4-19e). The low index values along the western portion of the region (0.05-0.22) correspond with a relatively low-lying area that does not have the same degree of wetlands and peatland-dominated terrain as is present throughout the centre of the Hay Slave Lowlands. As such, vegetation here is very mixed with varied forest types, shrublands, and grasslands. Soils here are similarly mixed along the eastern banks of the Liard River. At some of the most southerly latitudes of the Hay-Slave Lowlands in Alberta, temperature, elevation, landcover, and soil types all contribute to some of the lowest permafrost index values found within the map (0.0-0.43). Here, there are more developed areas and cropland as well as a mixed vegetation assemblages including all forest types, shrubland, and grassland. The ranked values associated with the soil factor were correspondingly not conducive to permafrost.

The results of this map were validated by comparing the average permafrost index within commonly referenced permafrost zones delineations such as Brown et al. (2002). The areas of isolated permafrost (<10% areal coverage) at the southernmost tips of the Hay-Slave Lowlands had a mean permafrost index of nearly 0.30. However, when the two areas of isolated permafrost are treated separately, the vast majority of the higher permafrost index values are present in the isolated area of British Columbia compared to Alberta. The mode for this area was 0.15 with a median value of 0.26. The vast majority of the study region falls within the sporadic discontinuous permafrost zone (10-50% areal coverage), which had a mean mapped permafrost index of 0.45. The mode for the sporadic discontinuous permafrost zone was 0.34 and the median was 0.26. Finally, the extensive-discontinuous permafrost zone (50-90% areal coverage)

had a mean value of 0.46. The mode was 0.40 and the median was 0.34. Based on this validation method, the variability between the three zones appears to be dampened as the averaged permafrost index values are largely similar. Additionally, it appears that the greatest discrepancy is along the southernmost portion in the isolated patches where permafrost index values are much greater than expected, especially since the permafrost zone delineations are based on 2002 information (Brown et al., 2002).

The map was also validated using point-form borehole data. The borehole data was converted to a binary of permafrost present and permafrost absent. Across the study region, the validation points where permafrost was present corresponded with a mean map index value of 0.55 while the validation points where permafrost was absent corresponded with a mean map index value of 0.34. The median index for points where permafrost was present versus absent were 0.51 and 0.31, respectively. The range of index values between the points where permafrost was present compared to where permafrost was absent was largely similar and both encompassed much of the total possible range. While the average values are distinctly different between boreholes with and without permafrost, some of the same dampening between areas with higher or lower permafrost index values appears to be occurring just as seen within the permafrost zones. There is an area of poor agreement between the borehole data and the permafrost index along the Dehcho River within the extensive-discontinuous permafrost zone, which may be responsible for some of this. Nevertheless, there are no borehole validation points within the isolated permafrost zone, in British Columbia, or in areas classified as elevated terrain making it more challenging to draw conclusions about map performance from the point validation.

The general trends (*i.e.* greater or lesser permafrost likelihood) appear to be mostly accurate across the study region. However, the index values do not appear to have enough contrast between the cells that have greater or lesser permafrost values nor does there appear to be enough contrast across the latitudinal span of the region.

This paper identifies the major environmental factors known to control the presence of permafrost, and through an additive process, derives for each 100 m x 100 m cell within the 230,000 km^2 Hay-Slave Lowlands, a permafrost index. Since each factor can positively or negatively influence the occurrence of permafrost, the additive process accounts for instances where each factor may reinforce or compensate other factors. For example, high elevation would be reinforced by dry, organic soils, while high elevation would be compensated by high soil moisture content given the high thermal conductivity of soils with high moisture contents.

At the largest scale of the overall Hay-Slave Lowlands, the additive process produced a permafrost index (Figure 4-18) that reflects the expected regional distribution of permafrost considering the distribution of environmental factors. However, at the finer scale (Figure 4-19), some inconsistencies were noted. For example, in some areas, a higher index value was given to channels fens, the linear features draining into and from the lakes and ponds in Figure 4-19b than to the peat plateaus that dominate the landscape separating the fens. Extensive field studies at Scotty Creek clearly demonstrate the opposite, namely a near-absence of permafrost below channel fens while permafrost is a defining feature of the plateaus (Quinton et al., 2019). Upon further investigation into the landcover datasets, this error was due to a combination of two main factors. Firstly, the resolution of the raster used here was much coarser compared to prior classifications of the Scotty Creek basin (*e.g.* Baltzer et al., 2014; Carpino et al., 2018; Chasmer

& Hopkinson, 2017; Quinton et al., 2011). As peatlands in this region, including Scotty Creek, are a patchwork landscape and often highly fragmented, raster datasets do not always accurately reflect pixels that represent a mix of landcovers (*e.g.* forested plateau and channel fen). Secondly, when compared to collapse scar wetlands that are dominated by *Sphagnum* mosses, channel fens can appear much more similar to forested features due to their high shrub cover (Bauer & Vitt, 2011; Beilman et al., 2001). There were some notable misclassifications, largely concerning fens and plateaus, in the landcover datasets used. However, errors of this nature are to be expected in a landcover dataset with national spatial coverage. On the regional map (Figure 4-18), this error is undetectable. Even at the finer scale shown on Figure 4-19b it could easily be missed by observers not familiar with this landscape since the cover of plateaus and channel fens at Scotty Creek are roughly equal in proportion (Baltzer et al., 2014; Quinton et al., 2011), and so the relative proportion of high and low value terrains on the image are not greatly affected. Similar errors are likely to be present in other datasets or throughout the study region and across the other areas of interest identified in Figure 4-19. However, these areas, and much of northern Canada, do not have the benefit of decades of intensive research (Quinton et al., 2019) to recognize related shortcomings. This error noted at Scotty Creek also demonstrates limitations on the transposability of a single methodology which may produce favourable results in some locations but not in others, and therefore the need for validation of mapping products by field measurements.

Errors in estimating permafrost occurrence or likelihood which are not apparent at one scale, but which, to an informed observer, are easily recognised at another, identifies the need for a method to help guide the development of permafrost maps so that their utility is maximised.

Considering that errors of attribution can be masked by increasing the spatial scale as demonstrated above, a key recommendation of this work is to initiate map development at the local scale to couple the development with field validation. The mapper should then decide on an optimal grid size appropriate for the landscape and suitable to the intended use of the map. This decision process can be demonstrated with reference to a hypothetical 1 km^2 area of interest (AOI) within the Scotty Creek basin (Figure 4-19b). The AOI is then rasterized into cells of equal size with each cell indicating whether or not it overlies permafrost. The question of the optimal cell size is then decided upon recognizing that cell size can range from infinitely small to an upper size equal to that of the AOI (*i.e.* a single large cell). The cells containing permafrost (C_p) can then be expressed as a fraction of the total number of cells in the AOI (C_t). For any landscape, the cell size has a lower limit below which any further decrease in cell size would have no further effect on the resulting map (Figure 4-20).

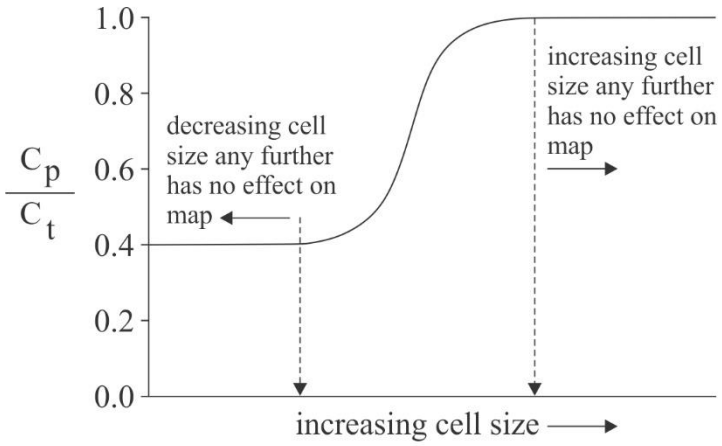

Figure 4-20: A conceptual diagram depicting the influence of cell size on how the presence of permafrost is represented on a map.

Considering the size of peat plateaus at Scotty Creek, the lower limit there would be on the order of 10 m grid cells and the resulting map for this grid size would essentially depict the distribution of permafrost within the AOI, with the total permafrost area being approximately 40% of the AOI (*i.e.* $C_p/C_t = 0.4$). However, this amount of detail and computation may not suit other uses. For example, if the map is intended to indicate whether or not permafrost is present within the AOI, then the cell size can be increased to the point where all cells overly permafrost such (*i.e.* $C_p/C_t = 1.0$), and any further increase in cell size yields no further information (Figure 4-20). As such, this optimal upper cell size is a representative elemental area for the landscape considered. This upper cell size is too coarse to distinguish permafrost from permafrost-free terrain within the AOI but would be useful to distinguish terrains containing permafrost from those that do not in larger, regional permafrost maps. Unlike the lower limit of cell size, the upper limit has greater applicability for permafrost mapping than for detailed mapping of permafrost distribution.

The lower and upper and optimal cell sizes could vary for other AOIs within Figure 4-19b and certainly among five frames presented in Figure 4-19. For example, two AOIs of equal area and equal permafrost cover (*e.g.* 40%) may have contrasting permafrost distributions. For example, if the permafrost of one is distributed into a large number of small permafrost bodies, while the permafrost of the other is distributed into a small number of large bodies, the former AOI would require a lower minimum cell size to capture the permafrost distribution, and a lower maximum cell size to identify the AOI as containing permafrost. As a result, it is expected that the curve depicted in Figure 4-20 is a unique characteristic of the landscape under consideration and that such characteristic curve could be transposable to other like landscapes in other regions.

As such, defining such curves has the potential to aid the development of regional maps of permafrost.

4.5 Conclusions

This research represents an initial step in mapping permafrost distribution in an area with discontinuous permafrost and is several orders of magnitude more detailed than previous Canadian maps that are still widely used, such as Brown et al. (2002). This mapping effort covered approximately 230,000 km^2 with an average permafrost index value of approximately 0.43. Permafrost distribution was largely limited to forested peatland landcovers and elevated areas but even within such regions, small-scale variability was also present due to the additive index of factors used. The lowest values were found predominantly at lower latitudes particularly with coarse mineral soils and broadleaf vegetation. The broad trends in permafrost distribution appeared largely accurate and as expected across the study region however the difference in index values between higher and lower value areas appeared diminished by the methods used. Ultimately, permafrost is a binary condition where it is either present or absent but this map struggled to wholly reflect those contrasting conditions. Additionally, inaccuracies were present in the mapping efforts due to a combination of dataset limitations, scale, and the subjectivity of the assigned rank values. Despite these challenges, this work presents the groundwork for determining permafrost likelihood using an accessible methodology.

CHAPTER 5: Conclusion

5.1 Summary

Canada's subarctic and its peatlands are becoming increasingly transitional as they are impacted by the dynamic factors reshaping this landscape. Understanding permafrost thaw and its effects on landcover and hydrology provides insight into the future trends and issues expected across this rapidly changing and vulnerable landscape, making research in this environment an important yet challenging task. Studying peatland-dominated regions with discontinuous permafrost is challenging as these environments are increasingly in disequilibrium with current climatic conditions. The remoteness and size of the region can limit the depth of understanding of these environments as well as the scope of the locations where research can be conducted. Additionally, the remoteness and inaccessibility of this region also increases the reliance on remote sensing methods. However, the effectiveness of remote sensing methods can also be impacted by the rapid successional changes observed here and the state of disequilibrium currently afflicting much of the discontinuous permafrost zone. Against this backdrop, understanding permafrost distribution and the associated permafrost thaw-induced changes in peatland-dominated discontinuous permafrost regions is best achieved through a combination of remote sensing methodologies coupled with finely-resolved field campaigns.

Monitoring large-scale landscape changes in Canada's increasingly vulnerable cold regions is one of the most critical contributions of this research. Much of the previous research in this field has largely been limited to specific sites and localized areas but less work has been done to expand such research across broader regions of a vast environment. Similarly, little work has been completed to better determine the applicability of such research across these

environments, now with an enhanced knowledge of the heterogeneity of these landscapes. The research presented in this dissertation aimed to develop an improved understanding of permafrost distribution in the discontinuous permafrost zone, identify terrain types underlain by both permafrost and permafrost-free ground, more holistically present the impacts of permafrost thaw on landcover change, and determine the landcover trajectory of permafrost environments under the impacts of climate change.

Chapter 2 first provides a broad-scale review of how recent climate warming has led to significant permafrost thaw, which has resulted in significant landscape transition across the peatland complexes of the Taiga Plains. While the transition from forest-dominated permafrost landscapes to wetland-dominated landscapes that are permafrost-free has been well established (Baltzer et al., 2014; Quinton et al., 2011; Tarnocai, 2009; Zoltai, 1993; Zoltai & Tarnocai, 1975), the more advanced stages of the landscape transition has not been as well studied. This chapter also explores the hydrological, ecological and thermal changes that accompany these landscape changes. In turn, this chapter aimed to more wholly explore landcover change by presenting a conceptual framework of landscape trajectory following permafrost thaw. This was completed by combining field data from a well-studied research site, Scotty Creek Research Station, with extensive geomatics data across the discontinuous portion of the Taiga Plains.

Chapter 3 explores how boreal peatlands across the sporadic-discontinuous permafrost zone of the Taiga Plains have changed over recent decades. These areas have experienced widespread changes to landcover due to the effects of initial permafrost thaw and the following landscape succession. While most studies in this region that have looked at permafrost thaw-induced landscape transition (*e.g.* Baltzer et al., 2014; Carpino et al., 2018; Chasmer &

Hopkinson, 2017; Quinton et al., 2011) have used historical aerial photographs and/or high-resolution satellite images collected at decadal time intervals, the work presented here uses a near-annual time step for Landsat imagery. Tasseled cap transformations (brightness, greenness, and wetness) were applied to the Landsat time series. The brightness, greenness, and wetness trends were used to assess landcover change across the study period for peat plateaus, collapse scar wetlands, and channel fens, which indicated that each landcover class had a different trajectory.

Chapter 4 presents a permafrost map across the southern boundary of the Taiga Plains, in the Hay-Slave Lowlands. The map of the Hay-Slave Lowlands had a resolution of 100 m, with each cell assigned a permafrost index value between 0-1.0. The permafrost index values across the cells were created via an additive index of the factors selected due to their influence on permafrost distribution. The factors included were also selected based on data availability criteria. Such factors included those related to air temperature, soil condition, landcover and elevation based on available data highlighted in previous works (Bonnaventure et al., 2012; Bonnaventure & Lewkowicz, 2011; Gibson et al., 2021; Lewkowicz & Ednie, 2004; Olefeldt et al., 2016; Spence et al., 2020). The results presented in this chapter indicate that peatland-dominated areas and areas of high elevation had the highest permafrost likelihood within the Hay-Slave Lowlands. In addition to producing a relatively high resolution map, the work in this chapter is advantageous as both the datasets and methods are widely accessible.

Northern environments are dynamic and increasingly transitional so understanding permafrost distribution, condition, and the impacts of thaw are increasingly important. The peatland-dominated regions of northwestern Canada's discontinuous permafrost zone are

urgently at risk to changes in climate, which may also impact the land and water resources northern communities rely on. The need to develop efficient and predictive methods to better determine permafrost condition and change on all spatial scales is essential given the pressing need to improve the monitoring and conservation of these environments. The work presented in this dissertation highlights the need to develop effective approaches that combine remote and field methods to balance the ability to study a broad and remote region while maintaining an accurate understanding of the finer scale processes and feedbacks. Understanding the impacts of permafrost thaw-induced landcover change is particularly timely and relevant given the vulnerability of these landscapes. Additionally, the discontinuous permafrost zone is an inherently variable landscape, which highlights the need for increased confidence in the applicability of local findings across the broader region.

5.2 Limitations

While this research enhances the understanding of permafrost environments of peatland-dominated terrain under the impacts of climate change, some limitations of the work have also been identified. Firstly, there was some bias in site selection and site analysis. In Chapter 3, beyond having suitable remote sensing coverage, sites were only selected if they could confidently be characterized as boreal peatlands based on their similar appearance to Scotty Creek basin. Scotty Creek was also relied on heavily for Chapters 2 and 4. In Chapter 2 all fieldwork data used to determine the trajectory of landcover, water, and energy fluxes following initial permafrost thaw was collected at Scotty Creek despite also making conclusions about the broader discontinuous permafrost zone of the Taiga Plains. In Chapter 4, much of the discussion on map applicability relied on shortcomings noted throughout Scotty Creek basin.

Additionally, classification errors have the potential to skew results as both automated and manual classification methods are used throughout this research. Outlining the surface conditions that are prerequisite to classifying each landcover type can help limit these errors but, in the case of Chapter 3, classifications relied on previous work (Carpino et al. 2018), which had not been completed with the purposes of this new work in mind. Furthermore, the tasseled cap analysis may be picking up elements of peatland post-thaw evolution that are not directly related to permafrost thaw, including long-term landscape succession. This is also partially exacerbated by the small sample size used in the pixel transects. Additionally, the presented Chapter 3 results do not cover trend direction or magnitude in relation to the latitudinal transect or related site attributes such as elevation. Finally, pixels with mixed classifications are potentially a relevant limitation in all three research chapters. As much of the broad-scale geomatics work was completed at resolutions of 30-100 m, raster pixels may not always accurately represent the environment when multiple landcovers are present within each pixel. This issue of scale is particularly relevant when monitoring changes in Chapter 3 and also discussed in detail as part of Chapter 4. Potential classification issues were also noted in the landcover dataset used in Chapter 4, as identified by the misclassifications at Scotty Creek.

5.3 Future Research

While this work contributes to the understanding of peatlands with discontinuous permafrost and their landcover trajectory following initial permafrost thaw, a framework and direction for future research can also be proposed. One such example of future research is to improve the understanding of the treed wetland features that appear to be a late-stage successional landcover type. While it is currently proposed that these treed wetlands form

following the dewatering of treeless wetlands and the formation of hummocky terrain, further work should be completed to determine whether this is the only pathway or if these features can also be formed following plateau subsidence if the canopy is able to persist. Additionally, further work needs to be completed to determine the species composition of these treed wetlands given that both *Picea mariana* and *Larix laricina* have been observed as the dominant species in treed wetlands.

Although permafrost does not appear to be found beneath treed wetland features, further monitoring should take place to better understand the cyclic nature of landcover change as well as the permanence or impermanence of treed wetlands as a major landcover type. This may be particularly relevant as peatland landscapes are currently understood as becoming increasingly fragmented following initial permafrost thaw and the impacts of further thaw should also be explored. In a highly thawed landscape, where forested plateaus are small and permafrost is patchy, the hydrological response to further thaw may differ from what has previously been observed. This may have an impact on observed runoff as well as further landcover succession depending on these changes.

Another avenue for further research is related to the mineral soil landscapes that make up large portions of both Scotty Creek as well as the broader Taiga Plains. Very little work has been done to explore the ecohydrological processes at play across these upland regions. As such, the understanding of these regions is lacking and increasingly apparent when compared to the more thorough work completed in neighbouring peatland-dominated environments. While the focus of this dissertation is largely on peatland areas, it is worthwhile to explore these upland regions in greater detail. Permafrost can also be found in fine-grained mineral soils throughout the Taiga

Plains but uplands adjacent to peatlands are largely generalized as only permafrost-free features. Common exploratory methods for permafrost presence or absence sampling, such as frost probing, are not well suited to mineral soils so broader geophysical surveys may be useful. Improved knowledge of non-peatland environments in terms of permafrost distribution and impacts of climate change, both related and unrelated to permafrost thaw, are of particular importance.

CHAPTER 6: References

Alessa, L., Kliskey, A., Lammers, R., Arp, C., White, D., Hinzman, L., & Busey, R. (2008). The Arctic Water Resource Vulnerability Index: An Integrated Assessment Tool for Community Resilience and Vulnerability with Respect to Freshwater. *Environmental Management*, *42*(3), 523–541. https://doi.org/10.1007/s00267-008-9152-0

Baig, M. H. A., Zhang, L., Shuai, T., & Tong, Q. (2014). Derivation of a tasselled cap transformation based on Landsat 8 at-satellite reflectance. *Remote Sensing Letters*, *5*(5), 423–431. https://doi.org/10.1080/2150704X.2014.915434

Baltzer, J. L., Veness, T., Chasmer, L. E., Sniderhan, A. E., & Quinton, W. L. (2014). Forests on thawing permafrost: Fragmentation, edge effects, and net forest loss. *Global Change Biology*, *20*(3), 824–834. https://doi.org/10.1111/gcb.12349

Bauer, I. E., & Vitt, D. H. (2011). Peatland dynamics in a complex landscape: Development of a fen-bog complex in the Sporadic Discontinuous Permafrost zone of northern Alberta, Canada: Development of peatland in the Sporadic Discontinuous Permafrost zone, Canada. *Boreas*, *40*(4), 714–726. https://doi.org/10.1111/j.1502-3885.2011.00210.x

Beilman, D. W., & Robinson, S. D. (2003). Peatland permafrost thaw and landform type along a climatic gradient. *Proceedings of the Eighth International Conference on Permafrost*, *1*, 61–65.

Beilman, D. W., Vitt, D. H., & Halsey, L. A. (2001). Localized Permafrost Peatlands in Western Canada: Definition, Distributions, and Degradation. *Arctic, Antarctic, and Alpine Research*, *33*(1), 70–77. https://doi.org/10.1080/15230430.2001.12003406

Biskaborn, B. K., Smith, S. L., Noetzli, J., Matthes, H., Vieira, G., Streletskiy, D. A., Schoeneich, P., Romanovsky, V. E., Lewkowicz, A. G., Abramov, A., Allard, M., Boike, J., Cable, W. L., Christiansen, H. H., Delaloye, R., Diekmann, B., Drozdov, D., Etzelmüller, B., Grosse, G., … Lantuit, H. (2019). Permafrost is warming at a global scale. *Nature Communications*, *10*(1), 264. https://doi.org/10.1038/s41467-018-08240-4

Bolin Centre for Climate Research (2013): The Northern Circumpolar Soil Carbon Database. Available at: https://bolin.su.se/data/ncscd/, Last Accessed March 20, 2019.

Bonnaventure, P. P., & Lamoureux, S. F. (2013). The active layer: A conceptual review of monitoring, modelling techniques and changes in a warming climate. *Progress in Physical Geography: Earth and Environment*, *37*(3), 352–376. https://doi.org/10.1177/0309133313478314

Bonnaventure, P. P., & Lewkowicz, A. G. (2011). Modelling climate change effects on the spatial distribution of mountain permafrost at three sites in northwest Canada. *Climatic Change*, *105*(1–2), 293–312. https://doi.org/10.1007/s10584-010-9818-5

Bonnaventure, P. P., Lewkowicz, A. G., Kremer, M., & Sawada, M. C. (2012). A Permafrost Probability Model for the Southern Yukon and Northern British Columbia, Canada: A Regional Permafrost Probability Model. *Permafrost and Periglacial Processes*, *23*(1), 52–68. https://doi.org/10.1002/ppp.1733

Box, J. E., Colgan, W. T., Christensen, T. R., Schmidt, N. M., Lund, M., Parmentier, F.-J. W., Brown, R., Bhatt, U. S., Euskirchen, E. S., Romanovsky, V. E., Walsh, J. E., Overland, J. E., Wang, M., Corell, R. W., Meier, W. N., Wouters, B., Mernild, S., Mård, J., Pawlak, J., & Olsen, M. S. (2019). Key indicators of Arctic climate change: 1971–2017.

Environmental Research Letters, *14*(4), 045010. https://doi.org/10.1088/1748-9326/aafc1b

Brown, J., O. Ferrians, J. A. Heginbottom, and E. Melnikov.: Circum-Arctic Map of Permafrost and Ground-Ice Conditions, Version 2. Permaice subset used. Boulder, Colorado USA. NSIDC: National Snow and Ice Data Center. Date accessed: Jan. 2020., 2002.

Brown, R. J. E. (1964). *Permafrost investigations on the MacKenzie Highway in Alberta and MacKenzie District* (p. 65 p.). National Research Council of Canada. https://doi.org/10.4224/20358861

Camill, P. (1999). Peat accumulation and succession following permafrost thaw in the boreal peatlands of Manitoba, Canada. *Écoscience*, *6*(4), 592–602. https://doi.org/10.1080/11956860.1999.11682561

Camill, P. (2000). How much do local factors matter for predicting transient ecosystem dynamics? Suggestions from permafrost formation in boreal peatlands. *Global Change Biology*, *6*(2), 169–182. https://doi.org/10.1046/j.1365-2486.2000.00293.x

Camill, P. (2005). Permafrost Thaw Accelerates in Boreal Peatlands During Late-20th Century Climate Warming. *Climatic Change*, *68*(1–2), 135–152. https://doi.org/10.1007/s10584-005-4785-y

Camill, P., & Clark, J. S. (1998). Climate Change Disequilibrium of Boreal Permafrost Peatlands Caused by Local Processes. *The American Naturalist*, *151*(3), 207–222. https://doi.org/10.1086/286112

Carpino, O. A., Berg, A. A., Quinton, W. L., & Adams, J. R. (2018). Climate change and permafrost thaw-induced boreal forest loss in northwestern Canada. *Environmental Research Letters*, *13*(8), 084018. https://doi.org/10.1088/1748-9326/aad74e

Carpino, O., Haynes, K., Connon, R., Craig, J., Devoie, É., & Quinton, W. (2021). Long-term climate-influenced land cover change in discontinuous permafrost peatland complexes. *Hydrology and Earth System Sciences*, *25*(6), 3301–3317. https://doi.org/10.5194/hess-25-3301-2021

Chander, G., Markham, B. L., & Helder, D. L. (2009). Chander, G., Markham, B.L., Helder, D.L. (2009). Summary of Current Radiometric Calibration Coefficients for Landsat MSS, TM, ETM+, and EO-1 ALI Sensors. (In Press, Remote. *Remote Sensing of Environment*, *1*(5), 1–24.

Chasmer, L., & Hopkinson, C. (2017). Threshold loss of discontinuous permafrost and landscape evolution. *Global Change Biology*, *23*(7), 2672–2686. https://doi.org/10.1111/gcb.13537

Chasmer, L., Hopkinson, C., & Quinton, W. (2010). Quantifying errors in discontinuous permafrost plateau change from optical data, Northwest Territories, Canada: 1947–2008. *Canadian Journal of Remote Sensing*, *36*(sup2), S211–S223. https://doi.org/10.5589/m10-058

Chasmer, L., Quinton, W., Hopkinson, C., Petrone, R., & Whittington, P. (2011). Vegetation Canopy and Radiation Controls on Permafrost Plateau Evolution within the Discontinuous Permafrost Zone, Northwest Territories, Canada: Vegetation and Radiation Controls on Permafrost Plateau Evolution. *Permafrost and Periglacial Processes*, n/a-n/a. https://doi.org/10.1002/ppp.724

Connon, R., Devoie, É., Hayashi, M., Veness, T., & Quinton, W. (2018). The Influence of Shallow Taliks on Permafrost Thaw and Active Layer Dynamics in Subarctic Canada. *Journal of Geophysical Research: Earth Surface*, *123*(2), 281–297. https://doi.org/10.1002/2017JF004469

Connon, R. F., Chasmer, L., Haughton, E., Helbig, M., Hopkinson, C., Sonnentag, O., & Quinton, W. L. (2021). The implications of permafrost thaw and land cover change on snow water equivalent accumulation, melt and runoff in discontinuous permafrost peatlands. *Hydrological Processes*, *35*(9). https://doi.org/10.1002/hyp.14363

Connon, R. F., Quinton, W. L., Craig, J. R., Hanisch, J., & Sonnentag, O. (2015). The hydrology of interconnected bog complexes in discontinuous permafrost terrains. *Hydrological Processes*, *29*(18), 3831–3847. https://doi.org/10.1002/hyp.10604

Connon, R. F., Quinton, W. L., Craig, J. R., & Hayashi, M. (2014). Changing hydrologic connectivity due to permafrost thaw in the lower Liard River valley, NWT, Canada. *Hydrological Processes*, *28*(14), 4163–4178. https://doi.org/10.1002/hyp.10206

Crist, E. P., & Cicone, R. C. (1984). A Physically-Based Transformation of Thematic Mapper Data—The TM Tasseled Cap. *IEEE Transactions on Geoscience and Remote Sensing*. https://doi.org/10.1109/TGRS.1984.350619

Dearborn, K. D., & Baltzer, J. L. (2021). Unexpected greening in a boreal permafrost peatland undergoing forest loss is partially attributable to tree species turnover. *Global Change Biology*, *27*(12), 2867–2882. https://doi.org/10.1111/gcb.15608

Dearborn, K. D., Wallace, C. A., Patankar, R., & Baltzer, J. L. (2021). Permafrost thaw in boreal peatlands is rapidly altering forest community composition. *Journal of Ecology*, *109*(3), 1452–1467. https://doi.org/10.1111/1365-2745.13569

Devoie, É. G., Craig, J. R., Connon, R. F., & Quinton, W. L. (2019). Taliks: A Tipping Point in Discontinuous Permafrost Degradation in Peatlands. *Water Resources Research*, *55*(11), 9838–9857. https://doi.org/10.1029/2018WR024488

Devoie, É. G., Craig, J. R., Dominico, M., Carpino, O., Connon, R. F., Rudy, A. C. A., & Quinton, W. L. (2021). Mechanisms of Discontinuous Permafrost Thaw in Peatlands. *Journal of Geophysical Research: Earth Surface*, *126*(11), e2021JF006204. https://doi.org/10.1029/2021JF006204

Disher, B. S., Connon, R. F., Haynes, K. M., Hopkinson, C., & Quinton, W. L. (2021). The hydrology of treed wetlands in thawing discontinuous permafrost regions. *Ecohydrology*, *14*(5). https://doi.org/10.1002/eco.2296

Disher, B.S.: Characterising the hydrological function of treed bogs in the zone of discontinuous permafrost, M.Sc. Thesis, Wilfrid Laurier University, Waterloo, 72 pp., 2020.

Dymond, S. F., D'Amato, A. W., Kolka, R. K., Bolstad, P. V., Sebestyen, S. D., Gill, K., & Curzon, M. T. (2019). Climatic controls on peatland black spruce growth in relation to water table variation and precipitation. *Ecohydrology*, *12*(7). https://doi.org/10.1002/eco.2137

Environment and Climate Change Canada. Adjusted and homogenized Canadian climate data. Available at: https://www.canada.ca/en/environment-climate-change/services/climate-

change/science-research-data/climate-trends-variability/adjusted-homogenized-canadian-data.html (Accessed June 1, 2020).

Eppinga, M. B., Rietkerk, M., Wassen, M. J., & De Ruiter, P. C. (2009). Linking habitat modification to catastrophic shifts and vegetation patterns in bogs. *Plant Ecology*, *200*(1), 53–68. https://doi.org/10.1007/s11258-007-9309-6

Fraser, R. H., Olthof, I., Carrière, M., Deschamps, A., & Pouliot, D. (2011). Detecting long-term changes to vegetation in northern Canada using the Landsat satellite image archive. *Environmental Research Letters*, *6*(4). https://doi.org/10.1088/1748-9326/6/4/045502

Fraser, R. H., Olthof, I., Kokelj, S. V., Lantz, T. C., Lacelle, D., Brooker, A., Wolfe, S., & Schwarz, S. (2014). Detecting landscape changes in high latitude environments using landsat trend analysis: 1. Visualization. *Remote Sensing*, *6*(11), 11533–11557. https://doi.org/10.3390/rs61111533

Fraser, R., Olthof, I., Carrière, M., Deschamps, A., & Pouliot, D. (2012). A method for trend-based change analysis in Arctic tundra using the 25-year Landsat archive. *Polar Record*, *48*(1), 83–93. https://doi.org/10.1017/S0032247411000477

Garon-Labrecque, M.-È., Léveillé-Bourret, É., Higgins, K., & Sonnentag, O. (2016). Additions to the boreal flora of the Northwest Territories with a preliminary vascular flora of Scotty Creek. *The Canadian Field-Naturalist*, *129*(4), 349. https://doi.org/10.22621/cfn.v129i4.1757

Gibson, C., Cottenie, K., Gingras-Hill, T., Kokelj, S. V., Baltzer, J. L., Chasmer, L., & Turetsky, M. R. (2021). Mapping and understanding the vulnerability of northern peatlands to

permafrost thaw at scales relevant to community adaptation planning. *Environmental Research Letters*, *16*(5), 055022. https://doi.org/10.1088/1748-9326/abe74b

Gibson, C. M., Chasmer, L. E., Thompson, D. K., Quinton, W. L., Flannigan, M. D., & Olefeldt, D. (2018). Wildfire as a major driver of recent permafrost thaw in boreal peatlands. *Nature Communications*, *9*(1), 3041. https://doi.org/10.1038/s41467-018-05457-1

Gorelick, N., Hancher, M., Dixon, M., Ilyushchenko, S., Thau, D., & Moore, R. (2017). Google Earth Engine: Planetary-scale geospatial analysis for everyone. *Remote Sensing of Environment*, *202*, 18–27. https://doi.org/10.1016/j.rse.2017.06.031

Gruber, S. (2012). Derivation and analysis of a high-resolution estimate of global permafrost zonation. *The Cryosphere*, *6*(1), 221–233. https://doi.org/10.5194/tc-6-221-2012

Halsey, L. A., Vitt, D. H., & Zoltai, S. C. (1995). Disequilibrium response of permafrost in boreal continental western Canada to climate change. *Climatic Change, 30*(1), 57–73. https://doi.org/10.1007/BF01093225

Hayashi, M., Quinton, W. L., Pietroniro, A., & Gibson, J. J. (2004). Hydrologic functions of wetlands in a discontinuous permafrost basin indicated by isotopic and chemical signatures. *Journal of Hydrology*, *296*(1–4), 81–97. https://doi.org/10.1016/j.jhydrol.2004.03.020

Haynes, K. M., Connon, R. F., & Quinton, W. L. (2018). Permafrost thaw induced drying of wetlands at Scotty Creek, NWT, Canada. *Environmental Research Letters*, *13*(11), 114001. https://doi.org/10.1088/1748-9326/aae46c

Haynes, K. M., Connon, R. F., & Quinton, W. L. (2019). Hydrometeorological measurements in peatland-dominated, discontinuous permafrost at Scotty Creek, Northwest Territories, Canada. *Geoscience Data Journal*, *6*(2), 85–96. https://doi.org/10.1002/gdj3.69

Haynes, K. M., Smart, J., Disher, B., Carpino, O., & Quinton, W. L. (2020). The role of hummocks in re-establishing black spruce forest following permafrost thaw. *Ecohydrology*, *14*(3). https://doi.org/10.1002/eco.2273

Heginbottom, J.A., and Dubreuil, M.A. 1993. A new permafrost and ground ice map for the National Atlas of Canada. In Proceedings of the Sixth International Conference on Permafrost, Beijing, China, 5–9July.Vol.1, pp. 255–260.

Helbig, M., Pappas, C., & Sonnentag, O. (2016). Permafrost thaw and wildfire: Equally important drivers of boreal tree cover changes in the Taiga Plains, Canada. *Geophysical Research Letters*, *43*(4), 1598–1606. https://doi.org/10.1002/2015GL067193

Helbig, M., Wischnewski, K., Kljun, N., Chasmer, L. E., Quinton, W. L., Detto, M., & Sonnentag, O. (2016). Regional atmospheric cooling and wetting effect of permafrost thaw-induced boreal forest loss. *Global Change Biology*, *22*(12), 4048–4066. https://doi.org/10.1111/gcb.13348

Hinzman, L. D., Bettez, N. D., Bolton, W. R., Chapin, F. S., Dyurgerov, M. B., Fastie, C. L., Griffith, B., Hollister, R. D., Hope, A., Huntington, H. P., Jensen, A. M., Jia, G. J., Jorgenson, T., Kane, D. L., Klein, D. R., Kofinas, G., Lynch, A. H., Lloyd, A. H., McGuire, A. D., … Yoshikawa, K. (2005). Evidence and Implications of Recent Climate Change in Northern Alaska and Other Arctic Regions. *Climatic Change*, *72*(3), 251–298. https://doi.org/10.1007/s10584-005-5352-2

Holloway, J. E., & Lewkowicz, A. G. (2020). Half a century of discontinuous permafrost persistence and degradation in western Canada. *Permafrost and Periglacial Processes*, *31*(1), 85–96. https://doi.org/10.1002/ppp.2017

Hugelius, G., Bockheim, J. G., Camill, P., Elberling, B., Grosse, G., Harden, J. W., Johnson, K., Jorgenson, T., Koven, C. D., Kuhry, P., Michaelson, G., Mishra, U., Palmtag, J., Ping, C.-L., O'Donnell, J., Schirrmeister, L., Schuur, E. A. G., Sheng, Y., Smith, L. C., … Yu, Z. (2013). A new data set for estimating organic carbon storage to 3 m depth in soils of the northern circumpolar permafrost region. *Earth System Science Data*, *5*(2), 393–402. https://doi.org/10.5194/essd-5-393-2013

Hugelius, G., Tarnocai, C., Broll, G., Canadell, J. G., Kuhry, P., & Swanson, D. K. (2013). *The Northern Circumpolar Soil Carbon Database: Spatially distributed datasets of soil coverage and soil carbon storage in the northern permafrost regions*.

Islam, M. A., & Macdonald, S. E. (2004). Ecophysiological adaptations of black spruce (Picea mariana) and tamarack (Larix laricina) seedlings to flooding. *Trees - Structure and Function*, *18*(1), 35–42. https://doi.org/10.1007/s00468-003-0276-9

Iversen, C. M., Childs, J., Norby, R. J., Ontl, T. A., Kolka, R. K., Brice, D. J., McFarlane, K. J., & Hanson, P. J. (2018). Fine-root growth in a forested bog is seasonally dynamic, but shallowly distributed in nutrient-poor peat. *Plant and Soil*, *424*(1–2), 123–143. https://doi.org/10.1007/s11104-017-3231-z

Iwata, H., Harazono, Y., & Ueyama, M. (2012). The role of permafrost in water exchange of a black spruce forest in Interior Alaska. *Agricultural and Forest Meteorology*, *161*, 107–115. https://doi.org/10.1016/j.agrformet.2012.03.017

Jorgenson, M. T., & Osterkamp, T. E. (2005). Response of boreal ecosystems to varying modes of permafrost degradation. *Canadian Journal of Forest Research, 35*, 12.

Jorgenson, M. T., Romanovsky, V., Harden, J., Shur, Y., O'Donnell, J., Schuur, E. A. G., Kanevskiy, M., & Marchenko, S. (2010). Resilience and vulnerability of permafrost to climate change. *Canadian Journal of Forest Research, 40*(7), 1219–1236. https://doi.org/10.1139/X10-060

Kauth, R. J., & Thomas, G. S. (1976). *Tasselled Cap—A Graphic Description of the Spectral-Temporal Development of Agricultural Crops As Seen By Landsat.* 41–51.

Kendall, M., & Stuart, A. (1967). *Advanced Theory of Statistics Volume 2*. Charles Griffin and Company.

Kettridge, N., Thompson, D. K., Bombonato, L., Turetsky, M. R., Benscoter, B. W., & Waddington, J. M. (2013). The ecohydrology of forested peatlands: Simulating the effects of tree shading on moss evaporation and species composition. *Journal of Geophysical Research: Biogeosciences, 118*(2), 422–435. https://doi.org/10.1002/jgrg.20043

Kokelj, S. V., Palmer, M. J., Lantz, T. C., & Burn, C. R. (2017). Ground Temperatures and Permafrost Warming from Forest to Tundra, Tuktoyaktuk Coastlands and Anderson Plain, NWT, Canada: Permafrost temperatures across tree line northwestern Canada. *Permafrost and Periglacial Processes, 28*(3), 543–551. https://doi.org/10.1002/ppp.1934

Korosi, J. B., Thienpont, J. R., Pisaric, M. F. J., deMontigny, P., Perreault, J. T., McDonald, J., Simpson, M. J., Armstrong, T., Kokelj, S. V., Smol, J. P., & Blais, J. M. (2017). Broad-

scale lake expansion and flooding inundates essential wood bison habitat. *Nature Communications*, *8*(1), 14510. https://doi.org/10.1038/ncomms14510

Kurylyk, B. L., Hayashi, M., Quinton, W. L., McKenzie, J. M., & Voss, C. I. (2016). Influence of vertical and lateral heat transfer on permafrost thaw, peatland landscape transition, and groundwater flow. *Water Resources Research*, *52*(2), 1286–1305. https://doi.org/10.1002/2015WR018057

Kwong, Y. T. J., & Gan, T. Y. (1994). Northward migration of permafrost along the Mackenzie highway and climatic warming. *Climatic Change*, *26*(4), 399–419. https://doi.org/10.1007/BF01094404

Lewkowicz, A. G., & Bonnaventure, P. P. (2008). Interchangeability of mountain permafrost probability models, northwest Canada: Interchangeability of Mountain Permafrost Probability Models. *Permafrost and Periglacial Processes*, *19*(1), 49–62. https://doi.org/10.1002/ppp.612

Lewkowicz, A. G., & Ednie, M. (2004). Probability mapping of mountain permafrost using the BTS method, Wolf Creek, Yukon Territory, Canada. *Permafrost and Periglacial Processes*, *15*(1), 67–80. https://doi.org/10.1002/ppp.480

Lieffers, V. J., & Rothwell, R. L. (1987). Rooting of peatland black spruce and tamarack in relation to depth of water table. *Canadian Journal of Botany*, *65*(5), 817–821. https://doi.org/10.1139/b87-111

Loisel, J., & Yu, Z. (2013). Surface vegetation patterning controls carbon accumulation in peatlands: peatland patterning controls carbon accumulation. *Geophysical Research Letters*, *40*(20), 5508–5513. https://doi.org/10.1002/grl.50744

Marshall, I. B., Schut, P. H., & Ballard, M. (1999). A National Ecological Framework for Canada: Attribute Data. In *Agriculture and Agri-Food Canada, Research Branch, Centre for Land and Biological Resources Research, and Environment Canada, State of the Environment Directorate, Ecozone Analysis Branch*. https://sis.agr.gc.ca/cansis/nsdb/ecostrat/1999report/index.html

McClymont, A. F., Hayashi, M., Bentley, L. R., & Christensen, B. S. (2013). Geophysical imaging and thermal modeling of subsurface morphology and thaw evolution of discontinuous permafrost. *Journal of Geophysical Research: Earth Surface, 118*(3), 1826–1837. https://doi.org/10.1002/jgrf.20114

McKenzie, J. M., & Voss, C. I. (2013). Permafrost thaw in a nested groundwater-flow system. *Hydrogeology Journal*, *21*(1), 299–316. https://doi.org/10.1007/s10040-012-0942-3

Mekis, É., & Vincent, L. A. (2011). An Overview of the Second Generation Adjusted Daily Precipitation Dataset for Trend Analysis in Canada. *Atmosphere-Ocean*, *49*(2), 163–177. https://doi.org/10.1080/07055900.2011.583910

Natural Resources Canada (2017): Wooded areas, saturated soils and landscape in Canada – CanVec series – Land features. Available at: https://open.canada.ca/data/en/dataset/80aa8ec6-4947-48de-bc9c-7d09d48b4cad, Last accessed July 10, 2019.

Natural Resources Canada (2020): 2020 Land Cover of Canada. Available at: https://open.canada.ca/data/en/dataset/ee1580ab-a23d-4f86-a09b-79763677eb47, last accessed January 3, 2023.

Natural Resources Canada (2015): 2015 Land Cover of Canada. Available at: https://open.canada.ca/data/en/dataset/4e615eae-b90c-420b-adee-2ca35896caf6, last accessed January 3, 2023.

Natural Resources Canada (2015): Canadian Digital Elevation Model, 1945-2011. Available at: https://open.canada.ca/data/en/dataset/7f245e4d-76c2-4caa-951a-45d1d2051333, last accessed January 3, 2023.

Natural Resources Canada (2022): High Resolution Digital Elevation Model (HRDEM) - CanElevation Series. Available at: https://open.canada.ca/data/en/dataset/957782bf-847c-4644-a757-e383c0057995, last accessed January 3, 2023.

NRCan. (2017). *Canadian Digital Elevation Model, 1945—2011*. Government of Canada; Natural Resources Canada; Strategic Policy and Innovation Sector. https://open.canada.ca/data/en/dataset/7f245e4d-76c2-4caa-951a-45d1d2051333

NWWG. : Wetlands of Canada. Ecological Land Classification Series, no. 24. Sustainable Development Branch, Environment Canada, Polyscience Publications Inc., Ottawa, Ontario Montreal, Quebec, 1988.

Olefeldt, D., Goswami, S., Grosse, G., Hayes, D., Hugelius, G., Kuhry, P., McGuire, A. D., Romanovsky, V. E., Sannel, A. B. K., Schuur, E. A. G., & Turetsky, M. R. (2016). Circumpolar distribution and carbon storage of thermokarst landscapes. *Nature Communications*, *7*(1), 13043. https://doi.org/10.1038/ncomms13043

Olefeldt, D., Persson, A., & Turetsky, M. R. (2014). Influence of the permafrost boundary on dissolved organic matter characteristics in rivers within the Boreal and Taiga plains of

western Canada. *Environmental Research Letters*, *9*(3), 035005. https://doi.org/10.1088/1748-9326/9/3/035005

Osterkamp, T. E. (2003). A thermal history of permafrost in Alaska. *Proceedings of the Eighth International Conference on Permafrost, Zurich, Switzerland*, *1*, 6.

Osterkamp, T. E., & Romanovsky, V. E. (1999). *Evidence for warming and thawing of discontinuous permafrost in Alaska*. 21.

Pellerin, S., & Lavoie, C. (2000). *Peatland fragments of southern Quebec: Recent evolution of their vegetation structure*. *78*, 11.

Pelletier, N., Talbot, J., Olefeldt, D., Turetsky, M., Blodau, C., Sonnentag, O., & Quinton, W. L. (2017). Influence of Holocene permafrost aggradation and thaw on the paleoecology and carbon storage of a peatland complex in northwestern Canada. *The Holocene*, *27*(9), 1391–1405. https://doi.org/10.1177/0959683617693899

Porter, Claire; Morin, Paul; Howat, Ian; Noh, Myoung-Jon; Bates, Brian; Peterman, Kenneth; Keesey, Scott; Schlenk, Matthew; Gardiner, Judith; Tomko, Karen; Willis, Michael; Kelleher, Cole; Cloutier, Michael; Husby, Eric; Foga, Steven; Nakamura, Hitomi; Platson, Melisa; Wethington, Michael, Jr.; Williamson, Cathleen; Bauer, Gregory; Enos, Jeremy; Arnold, Galen; Kramer, William; Becker, Peter; Doshi, Abhijit; D'Souza, Cristelle; Cummens, Pat; Laurier, Fabien; Bojesen, Mikkel, 2018, "ArcticDEM", https://doi.org/10.7910/DVN/OHHUKH, Harvard Dataverse, V1, last accessed January 3, 2023.

Porter, T. J., Schoenemann, S. W., Davies, L. J., Steig, E. J., Bandara, S., & Froese, D. G. (2019). Recent summer warming in northwestern Canada exceeds the Holocene thermal

maximum. *Nature Communications*, *10*(1), 1631. https://doi.org/10.1038/s41467-019-09622-y

Quinton, W., Berg, A., Braverman, M., Carpino, O., Chasmer, L., Connon, R., Craig, J., Devoie, É., Hayashi, M., Haynes, K., Olefeldt, D., Pietroniro, A., Rezanezhad, F., Schincariol, R., & Sonnentag, O. (2019). A synthesis of three decades of hydrological research at Scotty Creek, NWT, Canada. *Hydrology and Earth System Sciences*, *23*(4), 2015–2039. https://doi.org/10.5194/hess-23-2015-2019

Quinton, W. L., & Baltzer, J. L. (2013). The active-layer hydrology of a peat plateau with thawing permafrost (Scotty Creek, Canada). *Hydrogeology Journal*, *21*(1), 201–220. https://doi.org/10.1007/s10040-012-0935-2

Quinton, W. L., Hayashi, M., & Chasmer, L. E. (2009). Peatland Hydrology of Discontinuous Permafrost in the Northwest Territories: Overview and Synthesis. *Canadian Water Resources Journal*, *34*(4), 311–328. https://doi.org/10.4296/cwrj3404311

Quinton, W. L., Hayashi, M., & Chasmer, L. E. (2011). Permafrost-thaw-induced land-cover change in the Canadian subarctic: Implications for water resources. *Hydrological Processes*, *25*(1), 152–158. https://doi.org/10.1002/hyp.7894

Quinton, W. L., Hayashi, M., & Pietroniro, A. (2003). Connectivity and storage functions of channel fens and flat bogs in northern basins. *Hydrological Processes*, *17*(18), 3665–3684. https://doi.org/10.1002/hyp.1369

Robinson, S. D., & Moore, T. R. (2000). The Influence of Permafrost and Fire upon Carbon Accumulation in High Boreal Peatlands, Northwest Territories, Canada. *Arctic, Antarctic, and Alpine Research*, *32*(2), 155–166. https://doi.org/10.1080/15230430.2000.12003351

Rowland, J. C., Jones, C. E., Altmann, G., Bryan, R., Crosby, B. T., Hinzman, L. D., Kane, D. L., Lawrence, D. M., Mancino, A., Marsh, P., McNamara, J. P., Romanvosky, V. E., Toniolo, H., Travis, B. J., Trochim, E., Wilson, C. J., & Geernaert, G. L. (2010). Arctic Landscapes in Transition: Responses to Thawing Permafrost. *Eos, Transactions American Geophysical Union*, *91*(26), 229–230. https://doi.org/10.1029/2010EO260001

Schuur, E. A. G., & Abbott, B. (2011). High risk of permafrost thaw. *Nature*, *480*(7375), 32–33. https://doi.org/10.1038/480032a

Shur, Y. L., & Jorgenson, M. T. (2007). Patterns of permafrost formation and degradation in relation to climate and ecosystems. *Permafrost and Periglacial Processes*, *18*(1), 7–19. https://doi.org/10.1002/ppp.582

Smith, S. L., Burgess, M. M., Riseborough, D., & Mark Nixon, F. (2005). Recent trends from Canadian permafrost thermal monitoring network sites. *Permafrost and Periglacial Processes*, *16*(1), 19–30. https://doi.org/10.1002/ppp.511

Smith, S. L., & Riseborough, D. W. (2010). Modelling the thermal response of permafrost terrain to right-of-way disturbance and climate warming. *Cold Regions Science and Technology*, *60*(1), 92–103. https://doi.org/10.1016/j.coldregions.2009.08.009

Soenen, S. A., Peddle, D. R., & Coburn, C. A. (2005). SCS+C: A modified sun-canopy-sensor topographic correction in forested terrain. *IEEE Transactions on Geoscience and Remote Sensing*, *43*(9), 2148–2159. https://doi.org/10.1109/TGRS.2005.852480

Soja, A. J., Tchebakova, N. M., French, N. H. F., Flannigan, M. D., Shugart, H. H., Stocks, B. J., Sukhinin, A. I., Parfenova, E. I., Chapin, F. S., & Stackhouse, P. W. (2007). Climate-

induced boreal forest change: Predictions versus current observations. *Global and Planetary Change*, *56*(3–4), 274–296. https://doi.org/10.1016/j.gloplacha.2006.07.028

Spence, C., Norris, M., Bickerton, G., Bonsal, B. R., Brua, R., Culp, J. M., Dibike, Y., Gruber, S., Morse, P. D., Peters, D. L., Shrestha, R., & Wolfe, S. A. (2020). The Canadian Water Resource Vulnerability Index to Permafrost Thaw (CWRVI $_{PT}$). *Arctic Science*, *6*(4), 437–462. https://doi.org/10.1139/as-2019-0028

St. Jacques, J.-M., & Sauchyn, D. J. (2009). Increasing winter baseflow and mean annual streamflow from possible permafrost thawing in the Northwest Territories, Canada. *Geophysical Research Letters*, *36*(1), L01401. https://doi.org/10.1029/2008GL035822

Stofferahn, E., Fisher, J. B., Hayes, D. J., Schwalm, C. R., Huntzinger, D. N., Hantson, W., Poulter, B., & Zhang, Z. (2019). The Arctic-Boreal vulnerability experiment model benchmarking system. *Environmental Research Letters*, *14*(5), 055002. https://doi.org/10.1088/1748-9326/ab10fa

Tarnocai, C. (2009). The Impact of Climate Change on Canadian Peatlands. *Canadian Water Resources Journal*, *34*(4), 453–466. https://doi.org/10.4296/cwrj3404453

Thie, J. (1974). Distribution and Thawing of Permafrost in the Southern Part of the Discontinuous Permafrost Zone in Manitoba. *ARCTIC*, *27*(3), 189–200. https://doi.org/10.14430/arctic2873

Treat, C. C., & Jones, M. C. (2018). Near-surface permafrost aggradation in Northern Hemisphere peatlands shows regional and global trends during the past 6000 years. *The Holocene*, *28*(6), 998–1010. https://doi.org/10.1177/0959683617752858

Turetsky, M. R., Wieder, R. K., Vitt, D. H., Evans, R. J., & Scott, K. D. (2007). The disappearance of relict permafrost in boreal north America: Effects on peatland carbon storage and fluxes. *Global Change Biology*, *13*(9), 1922–1934. https://doi.org/10.1111/j.1365-2486.2007.01381.x

Vincent, L. A., Hartwell, M. M., & Wang, X. L. (2020). A Third Generation of Homogenized Temperature for Trend Analysis and Monitoring Changes in Canada's Climate. *Atmosphere-Ocean*, *58*(3), 173–191. https://doi.org/10.1080/07055900.2020.1765728

Vincent, L. A., Wang, X. L., Milewska, E. J., Wan, H., Yang, F., & Swail, V. (2012). A second generation of homogenized Canadian monthly surface air temperature for climate trend analysis: HOMOGENIZED CANADIAN TEMPERATURE. *Journal of Geophysical Research: Atmospheres*, *117*(D18), n/a-n/a. https://doi.org/10.1029/2012JD017859

Vincent, L. A., Zhang, X., Brown, R. D., Feng, Y., Mekis, E., Milewska, E. J., Wan, H., & Wang, X. L. (2015). Observed Trends in Canada's Climate and Influence of Low-Frequency Variability Modes. *Journal of Climate*, *28*(11), 4545–4560. https://doi.org/10.1175/JCLI-D-14-00697.1

Vitt, D. H., Halsey, L. A., & Zoltai, S. C. (1994). The Bog Landforms of Continental Western Canada in Relation to Climate and Permafrost Patterns. *Arctic and Alpine Research*, *26*(1), 1. https://doi.org/10.2307/1551870

Vonk, J. E., Tank, S. E., & Walvoord, M. A. (2019). Integrating hydrology and biogeochemistry across frozen landscapes. *Nature Communications*, *10*(1), 5377. https://doi.org/10.1038/s41467-019-13361-5

Waddington, J. M., Morris, P. J., Kettridge, N., Granath, G., Thompson, D. K., & Moore, P. A. (2015). Hydrological feedbacks in northern peatlands. *Ecohydrology*, *8*(1), 113–127. https://doi.org/10.1002/eco.1493

Walvoord, M. A., & Kurylyk, B. L. (2016). Hydrologic Impacts of Thawing Permafrost-A Review. *Vadose Zone Journal*, *15*(6), vzj2016.01.0010. https://doi.org/10.2136/vzj2016.01.0010

Wang, J. A., & Friedl, M. A. (2019). The role of land cover change in Arctic-Boreal greening and browning trends. *Environmental Research Letters*, *14*(12), 125007. https://doi.org/10.1088/1748-9326/ab5429

Warren, R. K., Pappas, C., Helbig, M., Chasmer, L. E., Berg, A. A., Baltzer, J. L., Quinton, W. L., & Sonnentag, O. (2018). Minor contribution of overstorey transpiration to landscape evapotranspiration in boreal permafrost peatlands: Contribution of overstory transpiration in a boreal permafrost peatland. *Ecohydrology*, *11*(5), e1975. https://doi.org/10.1002/eco.1975

Webster, C., Rutter, N., Zahner, F., & Jonas, T. (2016). Measurement of Incoming Radiation below Forest Canopies: A Comparison of Different Radiometer Configurations. *Journal of Hydrometeorology*, *17*(3), 853–864. https://doi.org/10.1175/JHM-D-15-0125.1

Williams, T. J., Quinton, W. L., & Baltzer, J. L. (2013). Linear disturbances on discontinuous permafrost: Implications for thaw-induced changes to land cover and drainage patterns. *Environmental Research Letters*, *8*(2), 025006. https://doi.org/10.1088/1748-9326/8/2/025006

Woo, M. (2012). *Permafrost Hydrology*. Springer Berlin Heidelberg. https://doi.org/10.1007/978-3-642-23462-0

Wright, N., Hayashi, M., & Quinton, W. L. (2009). Spatial and temporal variations in active layer thawing and their implication on runoff generation in peat-covered permafrost terrain. *Water Resources Research*, *45*(5). https://doi.org/10.1029/2008WR006880

Wright, S. N., Thompson, L. M., Olefeldt, D., Connon, R. F., Carpino, O. A., Beel, C. R., & Quinton, W. L. (2022). Thaw-induced impacts on land and water in discontinuous permafrost: A review of the Taiga Plains and Taiga Shield, northwestern Canada. *Earth-Science Reviews*, *232*, 104104. https://doi.org/10.1016/j.earscirev.2022.104104

Wulder, M. A., Loveland, T. R., Roy, D. P., Crawford, C. J., Masek, J. G., Woodcock, C. E., Allen, R. G., Anderson, M. C., Belward, A. S., Cohen, W. B., Dwyer, J., Erb, A., Gao, F., Griffiths, P., Helder, D., Hermosilla, T., Hipple, J. D., Hostert, P., Hughes, M. J., … Zhu, Z. (2019). Current status of Landsat program, science, and applications. *Remote Sensing of Environment*, *225*(February), 127–147. https://doi.org/10.1016/j.rse.2019.02.015

Zoltai, S. C. (1993). Cyclic Development of Permafrost in the Peatlands of Northwestern Alberta, Canada. *Arctic and Alpine Research*, *25*(3), 240. https://doi.org/10.2307/1551820

Zoltai, S. C., & Tarnocai, C. (1975). Perennially Frozen Peatlands in the Western Arctic and Subarctic of Canada. *Canadian Journal of Earth Sciences*, *12*(1), 28–43. https://doi.org/10.1139/e75-004